2005

Investigations of the kinetics of liquid droplets on soil substrates using a novel approach: Contact ratio

Abdelhafiz "Moh'd Adnan" Herbawi

United Arab Emirates University
Deanship of Graduate Studies

Investigations of the Kinetics of Liquid Droplets on Solid Substrates Using a Novel Approach: Contact Ratio

By

Abdelhafiz "Moh'd Adnan" Herbawi

A Thesis Submitted to the Deanship of Graduate Studies in Partial Fulfillment of the Requirements for Degree of Masters of Science in Materials Science and Engineering

2004 - 2005

GES/F11

United Arab Emirates University
Graduate Studies
M.S.c. Program in Materials Science and Engineering

THESIS EXAMINATION REPORT

Student ID : 200250409
Student Name : Abdelhafiz (Moh'd Adnan) Herbawi

Title of The Thesis : Investigations of the Kinetics of Liquid Droplets on Solid Substrates Using a Novel Approach: Contact Ratio.

The Thesis Examination as A Partial Fulfillment of M. Sc. Degree in Materilas Science and Engineering Was conducted on ..... Based on Examining the Thesis and the Students Presentation and the Subsequent Discussion, The Committee Recommends:

☐ Thesis is Satisfactory as is.

☑ Thesis is Satisfactory After Minor Modifications.

☐ Thesis should be Re-Evaluated After Major Modifications.

☐ Thesis is Rejected.

Examining Committee Members:

Thesis Supervisor: Name: Dr. A. Alterait Signature: Date: 9/1/2005

Thesis Co-Advisor: Name: ..... Signature: ..... Date:

Member : Name: A. Amirfazli Signature: Date: Jan. 9, 2005

Name: Prof. Rachid Chebbi Signature: Date: Jan. 9, 2005

Approval of Program Coordinator:

Dr. Yousef Haik ..... Date : 9/1/05

Materials Science & Engineering Program
Dean of Graduate Studies
United Arab Emirates University

APPROVAL:
Dean of Graduate Studies ..... Date :.....

Dean of Graduate Studies
U A E UNIVERSITY

Dedication

This thesis and all my future success are dedicated to very special people

To my beloved parents

Without their endless love, wisdom, and guidance

None of this could have been possible

Abstract

In view of Young's equation, in which the contact angle "θ" and the liquid surface tension γ_{lv} are the only measurable parameters, the contact angle has been widely conceived as a thermodynamic quantity. Accordingly "θ" has been the main focus of most theoretical and experimental investigations. The rate of change in the contact angle has been commonly used as the relevant parameter of spreading dynamics in spite of difficulties associated with contact angle measurements that are well recognized in the literature. Considering that the velocity of the *contact line* is the pertinent quantity for spreading, it is therefore reasonable to regard the change in the contact area as the *flux* of the process. It is only recently that a rational link has been made between the contact angle and the contact area using spherical cap approximation. We have introduced a new measuring parameter for wettability based on the liquid/solid contact area. The term "contact ratio" has been coined to denote the new parameter. The contact ratio is defined as the ratio of the spreading contact area between liquid and the solid surface to the surface area of the spherical drop before spreading. Measurements of low-rate dynamic contact radius and low-rate dynamic contact angles for various liquid/solid systems were carried out using the ADSA-P technique. The liquid drop volume and solid/liquid contact radius were also measured simultaneously. Subsequently, the contact ratio is determined. The theoretical relation between the contact ratio and the contact angle is based on spherical cap approximation. The results show that even with a high value of contact angle, there is a good agreement between the theoretical relation and the experimental values. Since the contact angle is well recognized as a wettability parameter because of its unique value, hence the contact ratio may also be considered as a wettability

parameter for its unique value of a specific system. Therefore, contact ratio can be presented as a new concept in measuring wettability alternative to contact angle. Moreover, contact ratio may provide a more precise measure of wettability than contact angle.

The spreading kinetics (in term of dynamic contact ratio) of different viscosity (100 cP, 500 cP, 1000 cP, 10 000 cP) silicon oils (PDMS) on three different solid surfaces, namely soda-lime glass, poly(methyl methacrylate) (PMMA), and polystyrene (PS) have been studied. A fixed liquid volume of 1.5 μL was used. The kinetics measurements of silicon oils with various viscosities were compared with theoretical models presented by Diez et al. (1994) and Chebbi (2000). The results show that Chebbi's model fits the experimental data better than that of the Diez et al. model. The results show, for the spreading kinetics of silicon oils with various viscosities on the same type of solid surface, that the lower the liquid viscosity, the faster the spreading. Overall, the results suggested that as the silicon oil viscosity increases, the viscous force becomes more effective where the liquid-solid intermolecular fore seems do not have effect on the kinetics of spreading. As silicon oil viscosity decreases, other spreading forces, especially the liquid-solid intermolecular forces, might play a significant role in the spreading kinetics.

Acknowledgments

First of all, I thank Almighty Allah for His Blessing and for providing me the capability to successfully complete this work.

I would like to thank my advisor, Dr. Abdullatif Mohammed Alteraifi Alshamsi. His sincere guidance, encouragement, fruitful discussion, critical reviewing of manuscript, unlimited assistance, and providing me the required facilities during the various phases of this work greatly aided its completion.

I wish also to express my sincere gratitude to Prof. Rashid Chebbi. The model part would not have been completed without his contribution. I would like to thank him also for his advices.

I wish also to thank Dr. Daniel Kwok. He gave me the opportunity to carry out a part of the experimental work in his Lab. (Nanoscale Technology and Engineering Laboratory) at University of Alberta in Canada.

Great thanks go to the staff of central laboratories unit at UAE University for their help. Especially the great help of Mr. Essam Attia in the SEM lab. My thank also to Mr. Ali Mohamed Dowaidar, who helped me in preparation of chemical solutions.

Special appreciation is expressed to my colleagues and friends in UAE University, especially my office buddy Aladdin Abu Assi, who supported, helped and encouraged me during my study.

No words can ever express my great gratitude and special thanks to my great family especially my parents for their unfailing support and help throughout my study.

Table of Contents

Page

List of Tables

List of Figures

Chapter 1

Introduction & Literature Review

1.1 Introduction

Wetting is the term used to describe all phenomena which involve contacts between phases, of which at least two are fluid. Figure 1.1 shows wetting system that consists of a liquid phase spread over a solid phase and surrounded by a third fluid phase: liquid, gas or vapor.

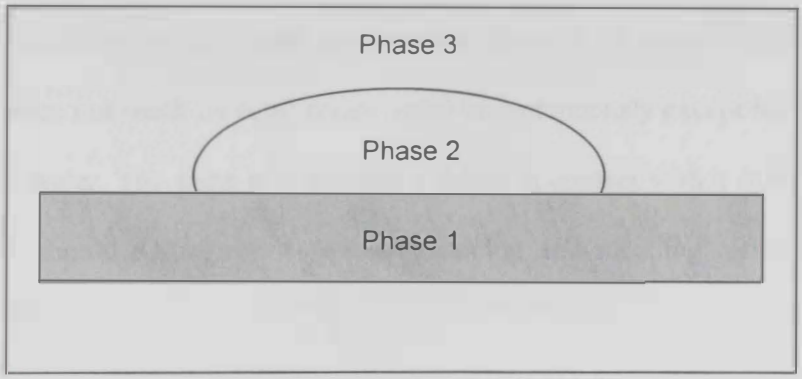

Fig1.1 Schematic of wetting system.

These phases should be reach to equilibrium state that is controlled by their own energies. Hence, when a drop of (pure) liquid rests on the flat surface of a (pure) solid ,with an influence of gravity, the shape is not a simple spherical lens but is determined by a balance between the liquid-vapor γ_{lv}, solid-vapor γ_{sv}, and solid-liquid γ_{sl} interfacial energy densities (interfacial tensions). The relation between the three interfacial energies is defined by Young's equation:

$$\gamma_{lv} \cos\theta_Y = \gamma_{sv} - \gamma_{sl} \qquad (1.1)$$

Young's equation was introduced in 1805 (Young, 1805). It relates the three interfacial energies with an angle called contact angle, θ_y , which is described in detail in the next section.

1.2 Basic definitions and relations of wetting phenomena

1.2.1 Contact angle

Contact angle (θ) is an important parameter in surface science; for the solid-liquid-vapour system (Figure 1.2) it is defined geometrically as the angle formed between the solid/liquid interfacial line and the tangent line to the liquid/vapour interface, at the droplet edge where the liquid comes in contact with the solid surface. Experimentally, when a liquid comes in contact with a solid and another phase, it is usually observed that the contact angle does not reach its equilibrium value instantaneously except for low viscosity liquids such as water. The same is true when a liquid in contact with a solid is displaced. Therefore, one should distinguish between advancing and receding contact angles (see Section 1.2.8.1V).

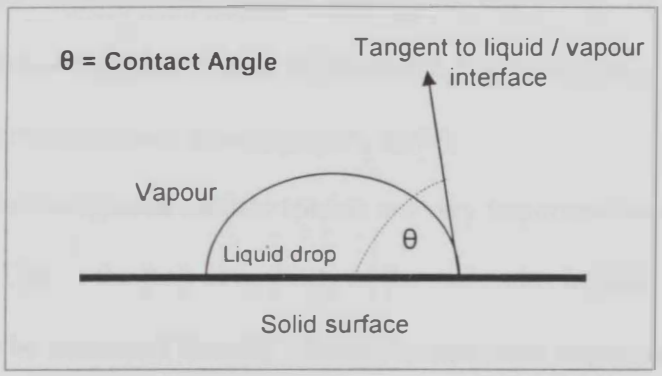

Fig.1.2 Schematic of sessile-drop contact angle

Contact angle is in general used as a measure of wettabilty i.e. the ability of a liquid to spread over the solid surface. Contact angle plays an important role in many important fields including composites and polymers (Adamson, 1997), adhesives (Ashleya et al., 2003), biological processes (Neinhuis and Barthlott, 1997), biomedical applications (Kasemo, 2002; Ashleya et al., 2003), coatings (Adamson, 1997), oil recovery (Adamson,

1997; Drummond and Israelachvili, 2002), and different environmental and engineering applications (Sasa, 2003). A more specific application for the measured contact angle is to calculate the interfacial tensions (interface energies) of the solid-phase interfaces of the wetting systems (Kwok, 1998).

1.2.2 Surface free energy and surface tension, γ

Surface tension is a property of liquid-gas interface. The surface tension acts along the surface and tends to minimize its area. Its unit is force per length. When an area, A, of a new surface is created, work, W, must be done. Surface free energy is then defined as the ratio W/A; its dimension is then energy per area. The dimensions of surface tension and surface energy are therefore identical. In this study, the symbol γ represents both the surface tension and the surface free energy, and the two terms are treated as equivalent.

Analogous to the surface tension and surface free energy of liquid-gas or solid-gas surfaces, the terms interfacial tension or interfacial free energy may be used in the case of interfaces between condensed phases (Myers, 1999).

Interfacial energies or surface tension are very important parameters in many fields of technology. Due to the lack of mobility of the molecules in solid surfaces, solid surface tensions cannot be measured directly. Several independent approaches have been used to estimate the solid surface energy, including:-

1. Contact angle measurements (Fowkes, 1964; Zisman, 1964; van Oss et al., 1988).
2. Direct force measurements (Derjaguin et al., 1980; Pashley et al., 1988; Fogden and White, 1990).
3. Film flotation (Fuerstenau et al., 1990)
4. Sedimentation of particles (Vargha-Butler et al., 1987)
5. Solidification front interaction with particles (Chen et al., 1977)

6. Gradient theory (Guermeur et al., 1985).
7. Lifshitz theory of van der Waals forces (Israelachvili, 1972; van Giessen et al., 1997).
8. Theory of molecular interactions (Sullivan, 1981; Matyushov and Schmid, 1996).

Among these approaches, researchers consider the contact angle measurement approach to be experimentally the simplest and the most straightforward.

1.2.3 Zisman plots and critical surface energy

This approach was developed by Zisman at the Naval Research Laboratory (Zisman, 1964). The plot is made by plotting the cosine of the contact angle ($\cos\theta$) versus the surface free energy of various wetting liquids on a given solid. The resulting plot is a straight line. Thus, there exists some unique value for each solid where the cosine of the contact angle is unity ($\theta = 0$). This value is termed the critical surface free energy of the solid. The term "critical" is used because any liquid on the Zisman plot whose surface tension is greater than the "critical surface tension" makes a finite contact angle with the substrate, i.e. a liquid with surface free energy below the critical value will wet and spread over the solid surface, whereas a liquid with surface energy above the critical value might wet but will not spread.

In Figure 1.3 (Sasa, 2003), the Zisman plot is divided into three regions: a "Non-wetting" region, where the angle between liquid and solid is equal or greater than 90°, a "Wetting" region, where the angle between the liquid and the solid is greater than 0° and less than 90°, and a "Complete spreading" region where the contact angle is equal to 0°. The line separating the "Wetting" region and the "Complete spreading" region is called the "critical surface energy" of solid. Figure 1.4 (Shaw, 1992) shows a Zisman plot for a

variety of liquids wetting Teflon. Zisman critical surface energy for Teflon solid equals 20 mN/m.

Critical surface energy values are useful empirical values that characterize relative degrees of surface energy of solid substrates (Shaw, 1992). Using the concept of critical surface energy, it is possible to characterize a wide variety of polymers and correlate the critical surface energy with polymer structure. Fluorinated materials have low values of critical surface energy. Hydrogenated materials, such as polyethylene and polypropylene, have slightly higher values. For other sub-stituents (Cl, O, N), the critical surface free energy is a little higher (Shaw, 1992). From the critical surface energy data just given, fluorinated and hydrogenated materials will be among the least wettable.

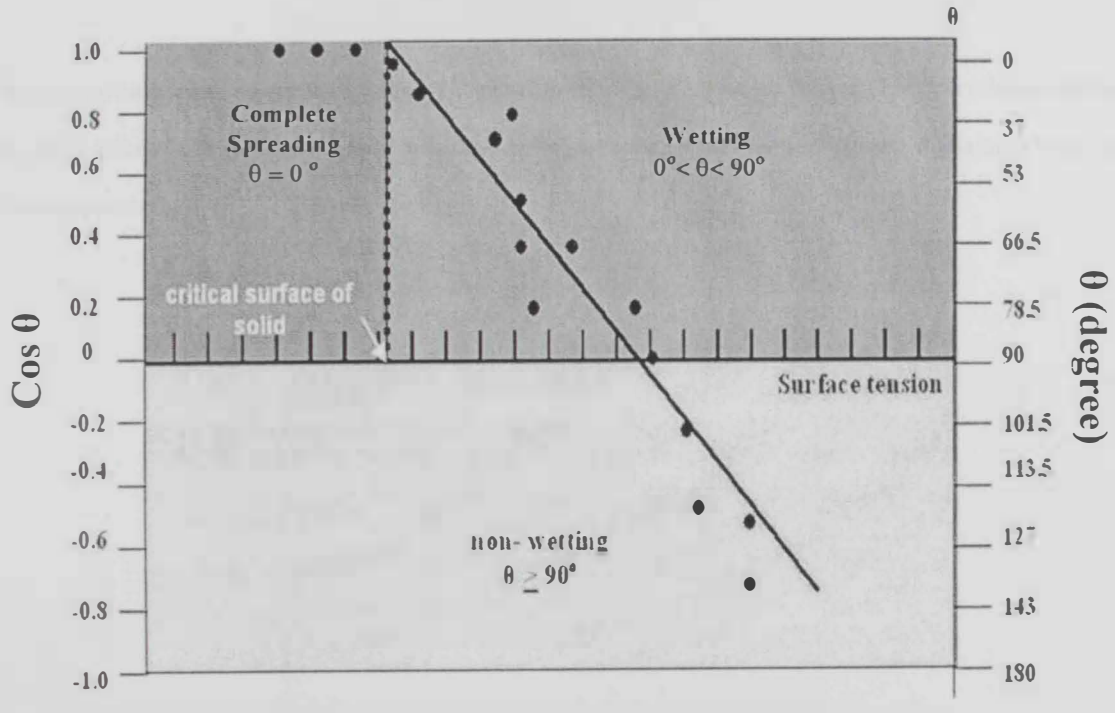

Fig 1.3 Illustrative sketch showing Zisman plots regions (Sasa, 2003)

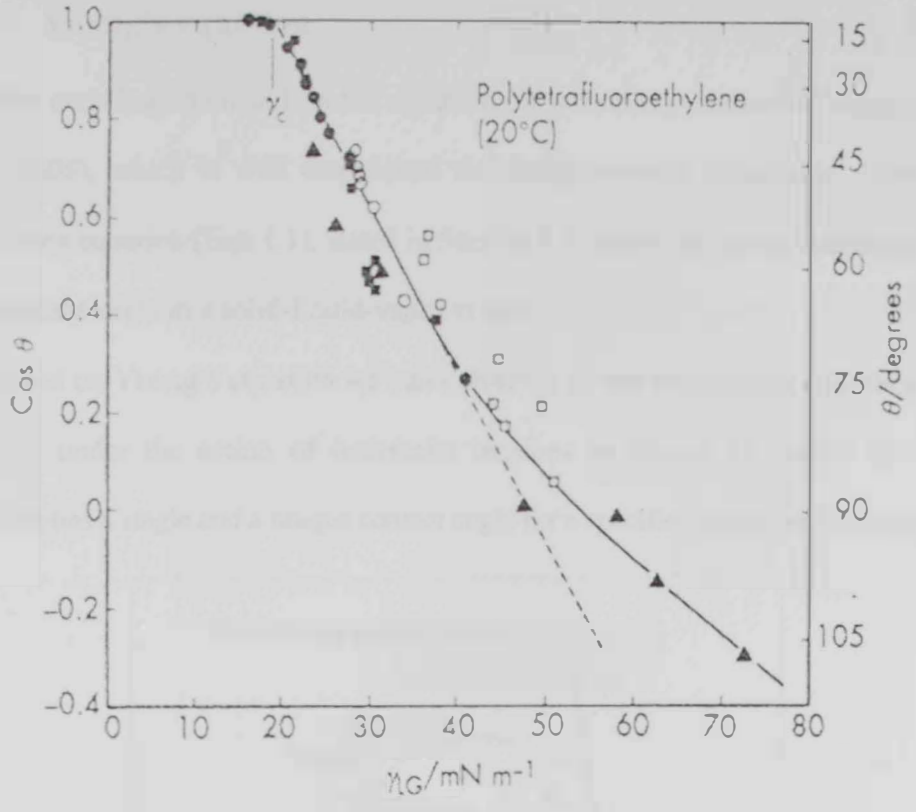

Fig 1.4 Zisnam plots of contact angle of various homologous series on Teflon (Polytetrafluoroethlene) at 20°C (Shaw, 1992) •, n-alkanes; ○, other hydrocarbons; ■, esters and ethers; □, halocarbons and halohydrocarbons; ▲, different liquids

1.2.4 Young's equation

The most important and central equation for wettability studies is Young's equation (Young, 1805), which is well established thermodynamically (Matijevic, 1969; Myers, 1999). Young equation (Eqn 1.1), stated in Section 1.1, relates the three interfacial tensions and the contact angle in a solid-liquid-vapor system.

Based on Young's equation we can define θ_Y by the mechanical equilibrium of the liquid drop under the action of interfacial tensions as shown in Figure 1.5. Young's equation implies a single and a unique contact angle for a specific vapour-liquid-solid system.

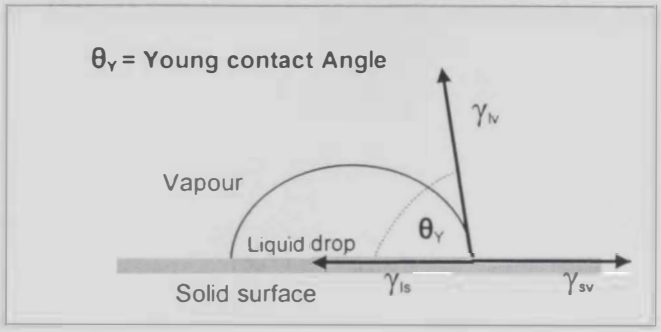

Fig 1.5 Schematic of the mechanical definition of Young's equation. Horizontal balance of forces: Young's equation $\gamma_{SV} = \gamma_{SL} + \gamma_{LV} \cos\theta$

Wetting can be defined by the contact angle value; $\theta = 0$ for complete wetting, $0<\theta<90$ for partially wetting and $90 \leq \theta < 180$ for non wetting (Figure 1.6).

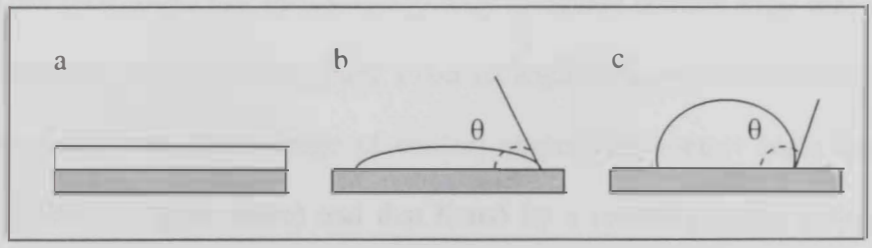

Fig 1.6 Schematic of a) complete wetting, $\theta = 0$ b) partially wetting, $0<\theta<90$ and c) non wetting, $90 \leq \theta < 180$

Young's equation (Eqn 1.1) contains only two measurable parameters, the liquid-vapour interfacial tension γ_{lv} and the contact angle θ_Y. In order to determine γ_{sv}, γ_{sl}, an additional relations should be involved (Neumann et al.,1974)

Because γ_{sv}, γ_{sl} and γ_{lv} are considered as thermodynamic properties of the solid-liquid-vapour systems, Equation 1.1 implies that there is only one unique value for the contact angle for the specific solid-liquid-vapour system. However, experimentally it is difficult to have one unique value for the contact angle of a specific solid-liquid-vapour system because, based on Young's equation derivation, certain restrictions were imposed on the solid surface. The solid surface should be characterized as (Budziak, 1992; Kwok, 1998; Lam, 2001)

1. Smooth
2. Homogenous
3. Rigid
4. Non-deformable, and
5. Inert with respect to the liquid used

In practice, no solid exhibits all these attributes and all solid surfaces usually have defects like roughness and heterogeneity. Therefore, the measured contact angle for a specific system can attain different values based on how the experiment is performed. In general, it has been found that the experimentally measured contact angle may or may not be equal to the true contact angle (Young's contact angle) (Neumann, 1974; Kwok, 1998).

The real system has a range of contact angles; the contact angle found by the advancing liquid θ_a (upper value) and that found by a receding liquid θ_r (lower value), which are not identical. Nearly all solid surfaces such behavior, which is called hysteresis (H):

$$H = \theta_a - \theta_r \tag{1.2}$$

Based on the previous discussion, one might say that not all experimental measured contact angles are equal to θ_Y (Kwok, 1998) and that the contact angle phenomena are complicated (Neumann, 1974; Marmur, 1996; Kwok, 1998). The contact angle phenomenon arises from various complexities in the experimental measurements. Several models have been employed to gain a deeper understanding of the thermodynamic status of contact angles (see Section 1.4).

1.2.5 Droplet Laplace pressure

The Capillary phenomena were studied in the early part of the 19th century (Yang et al., 2002). Capillary phenomena can be defined quantitatively in terms of surface tension. Surface tension makes the surface of a liquid, act as an elastic cover, which minimizes the surface area of liquid so as to minimize the energy of the fluidic system minimal.

It is commonly theorized that capillary forces balanced by viscous resistance are the sole forces acting in the spreading process. The existing continuum-based kinetics models relate the rate of spreading to surface tension and viscosity; both are properties of the liquid. Nevertheless, a liquid droplet in equilibrium on a solid substrate is a system governed by the three energies defined by the Young's equation. As the contact line moves towards equilibrium, viscous dissipation processes control its rate. The pressure across the liquid-vapour interphase is considered as the driving force. The droplet is a curved surface reservoir, whose pressure is determined by the surface tension γ and the radius of curvature, as shown in Figure 1.7 in accordance with Laplace-Young equation, i.e.

$$\Delta p = \frac{2\gamma}{\rho} \tag{1.3}$$

where Δp is the pressure across the surface, γ is the surface tension of the liquid; ρ is the

radius of curvature. The radius of curvature seen in Figure 1.7 is related to the contact radius R_c thus:

$$\rho = \frac{R_C}{\sin\theta} \tag{1.4}$$

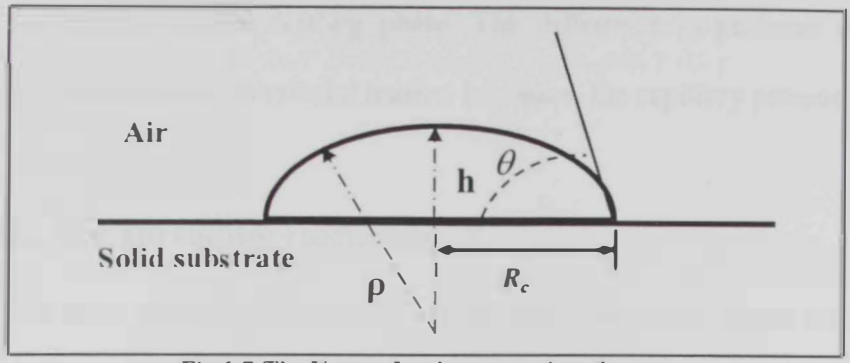

Fig 1.7 The Young-Laplace equation element

It should be mentioned that Equation 1.4 valid only for spherical cap shape of liquid drop. Thus the direct relation between pressure at the surface and contact radius R_c, which can be measured experimentally, can be given as:

$$\Delta p = \frac{2\gamma\sin\theta}{R_C} \tag{1.5}$$

According to Alteraifi and Moet (2004), it is imperative to note that as the contact area increases, the radius of curvature increases giving rise to a corresponding lessening of the Laplace pressure, which amounts to a continual decrease in the driving force. Consequently, the spreading must cease to grow when the driving component can no longer overcome its resistance. The latter is obviously dictated by the specific nature of the liquid/solid pair.

Laplace's equation describes the pressure inside a drop because its surface is curved. We can describe capillary pressure, where there is no gravity effect as the

difference between the pressure for the non-wetting phase and the pressure for the wetting phase.

$$P_C = P_{NW}\ P_W = \frac{2\gamma\cos\theta}{\rho} \qquad (1.6)$$

Where P_C is the capillary pressure, P_{NW} is the pressure of the non-wetting phase, P_W is the pressure of the wetting phase. The difference in pressure is related to the interfacial tension and as interfacial tension increases, the capillary pressure increases.

1.2.6 The spreading coefficient, *S*

It is some times useful to define a term other than contact angle to indicate from the thermodynamic point of view whether a given liquid-solid system will be a wetting system ($\theta = 0$) or not ($\theta > 0$). Such a term is the spreading coefficient, *S*.

Spreading coefficient, *S*, is defined as the free energy change per unit area of the spreading of a liquid film on the solid, or as a free energy difference between a bare solid, directly in contact with the vapour and a solid covered by a flat, thick liquid layer. The free energy of the spreading process should be negative in order for it to happen spontaneously. The relationship for the spreading coefficient can be written, in terms of surface free energies, and is defined for a solid-liquid-vapour system (Myers, 1999) as:

$$S_{L/S} = \gamma_{SV} - (\gamma_{LV} + \gamma_{SL}) = \gamma_{SV} - \gamma_{LV} - \gamma_{SL} \qquad (1.7)$$

where the subscript $S_{L/S}$ refers to the spreading coefficient for the system, and γ_{sv}, γ_{lv}, γ_{sl} refer to the solid-vapour, liquid-vapour; solid-liquid interfacial energy respectively. For complete spreading ($\theta = 0$), *S* should equal zero, otherwise ($S<0$) incomplete spreading will occur ($\theta > 0$).

1.2.7 Line tension

Line tension can be defined as the force acting in the one-dimensional three-phase contact line, or as the free energy per unit length of the contact line of the three phases (Boruvka and Neumann, 1977; Budziak, 1992), or, as "a certain linear tension" at the three-phase line (Amirfazlia and Neumann, 2004). Line tension considerations are very important in measuring accurate contact angles. As shown below, the effect of line tension is to increase the contact angle for drops below a certain drop diameter. For that reason, to measure contact angles that are free of line tension effects, either the line tension magnitude has to be known a priori, or the experimental conditions must be chosen so that the line tension has no effect. Line tension effect on contact angle is described by the so called Modified Young Equation (Boruvka and Neumann, 1977; Budziak, 1992; Amirfazli, 2001)

$$\gamma_{LV}\cos\theta = \gamma_{SV} - \gamma_{SL} - \sigma K_{gs} \tag{1.8}$$

where σ is the line tension and K_{gs} is the geodesic curvature of the three-phase line (local curvature of the three-phase contact line in the plane of the solid phase). For a axisymmetric sessile drop, the curvature of the three-phase line in the Modified Young Equation will be:

$$K_{gs} = \frac{1}{R} \tag{1.9}$$

where R is the base radius of the three-phase contact radius. Thus Equation 1.8 can be reduced to:

$$\gamma_{LV}\cos\theta = \gamma_{SV} - \gamma_{SL} - \frac{\sigma}{R} \tag{1.10}$$

When $R \to \infty$, Equation 1.10 will be replaced by the classical Young's equation (Eqn.1.1):

$$\gamma_{lv}\cos\theta_Y = \gamma_{sv} - \gamma_{sl} \tag{1.11}$$

Combining Equations 1.11 and 1.10 yields:

$$\cos\theta = \cos\theta_Y - \frac{\sigma}{\gamma_{LV} R} \qquad (1.12)$$

Equation 1.12 indicates that the measured contact angle will vary with the size of the drop, or more accurately, with the radius of the three-phase contact area (R). The significance of Equation 1.12 is that the line tension can be determined from an experimental study of the drop size dependence of contact angles. Based on Equation 1.12, only the contact angles of large drops drops should be measured.

1.2.8 Parameters that affect spreading

The liquid spreading phenomenon is affected by many parameters, such as temperature, evaporation rate, roughness and heterogeneity of the surface, and chemical effects.

I. The effect of temperature

Influence of the temperature on the contact angle of partially wetting drops was studied by de Ruijter et al (1998). they reported that the contact angle decreases as temperature increases, as shown in Figure 1.8 (Ruijter et al. 1998) for squalane on PTE. According to Young's equation (Eqn 1.1), the contact angle value depends mainly on the surface energy of the solid and the surface tension of the liquid. The surface tension of the liquid decreases with increasing temperature (de Ruijter et al., 1998). For example, the surface tension of squalane decreases significantly with temperature as shown in the Figure 1.9 (de Ruijter et al., 1998).

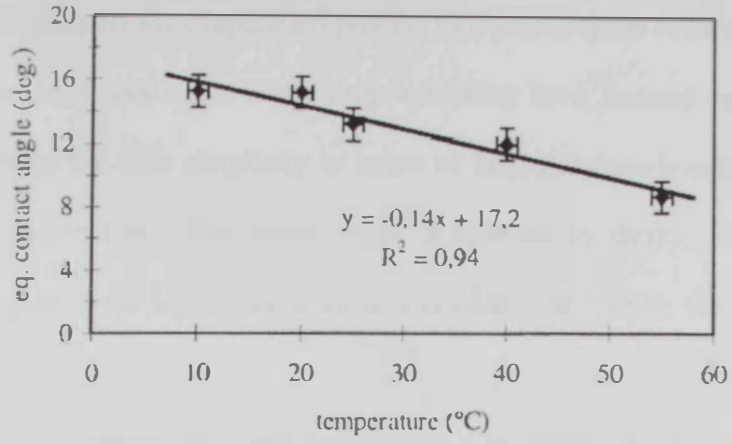

Fig 1.8 Variation of the equilibrium contact angle with temperature of squalane-PTE (de Ruijter et al, 1998)

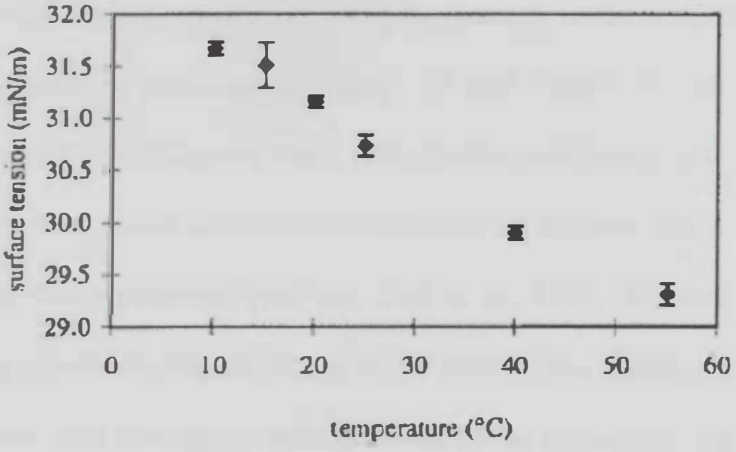

Fig 1.9 shows the change of surface tension of squalane with increases temperature (de Ruijter et al, 1998)

For a solid, surface energy is a function of temperature (Zhao et al., 2004, Hall et al., 1987). In general the effect of temperature increase can be an increase or decrease in the surface free energy of the solid which is calculated by Owens–Wendt geometric mean approach (Zhao et al., 2004).

II. Effect of evaporation rate of liquid

One would expect the evaporation process of liquid droplets to have been described many years ago. Most studies of liquid drop spreading have focused on the nonvolatile liquid sessile drops for their simplicity in terms of both the experimental measurements and the theoretical analysis. The contact angle is affected by thermal radiation incident upon a droplet that cause liquid evaporation (Chandra et al., 1996; van den Doel et al, 1999).

While, the occurrence of liquid evaporation is inevitable for atmospheric humidity less than 100%, the effects of evaporation on spreading and the contact angle become very important for a more complete understanding of these processes (Zhang and Chao, 2001; Chao and Zhang, 2001). If the contact angle hysteresis is large, contact angle decreases continuously during droplet evaporation, while the diameter of the wetted region under the droplet remains constant, as shown in Figure 1.10 and Figure 1.11 which illustrate the behavior of a water droplet (Chandra et al., 1996; Crafton and Black, 2004).

On the contrary, some underlying principles of the dynamic process of evaporation have just recently been published (van den Doel et al., 1999). It seems that during the evaporation of a liquid droplet, the liquid at the edge of the droplet is "pinned" to the underlying surface. This pinning prevents the droplet from shrinking. This implies that the footprint of the droplet remains constant. The evaporated liquid at the edge is replenished by liquid from the bulk of the droplet. This means that there is a flow of liquid moving towards the edge of the droplet. If the liquid droplet contains particles, as in a droplet of coffee, these particles will be transported outwards by the flow. Finally, when all the liquid has evaporated, the (coffee) particles will form a ring of stain (van den Doel et al., 1999).

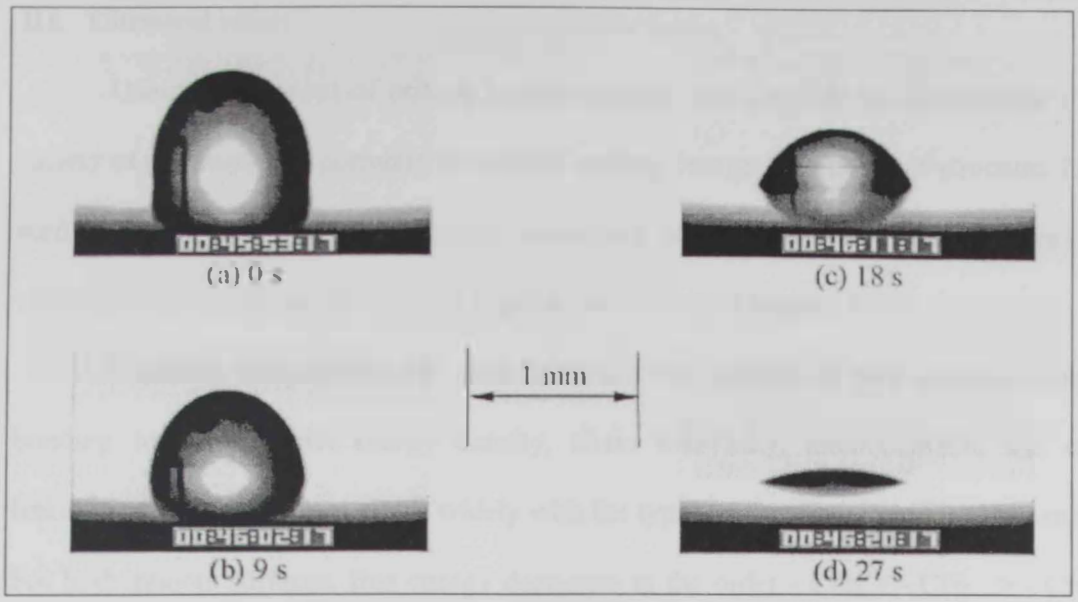

Fig. 1.10 Sequence of water droplets on an aluminum surface at 60° C (Crafton and Black, 2004)

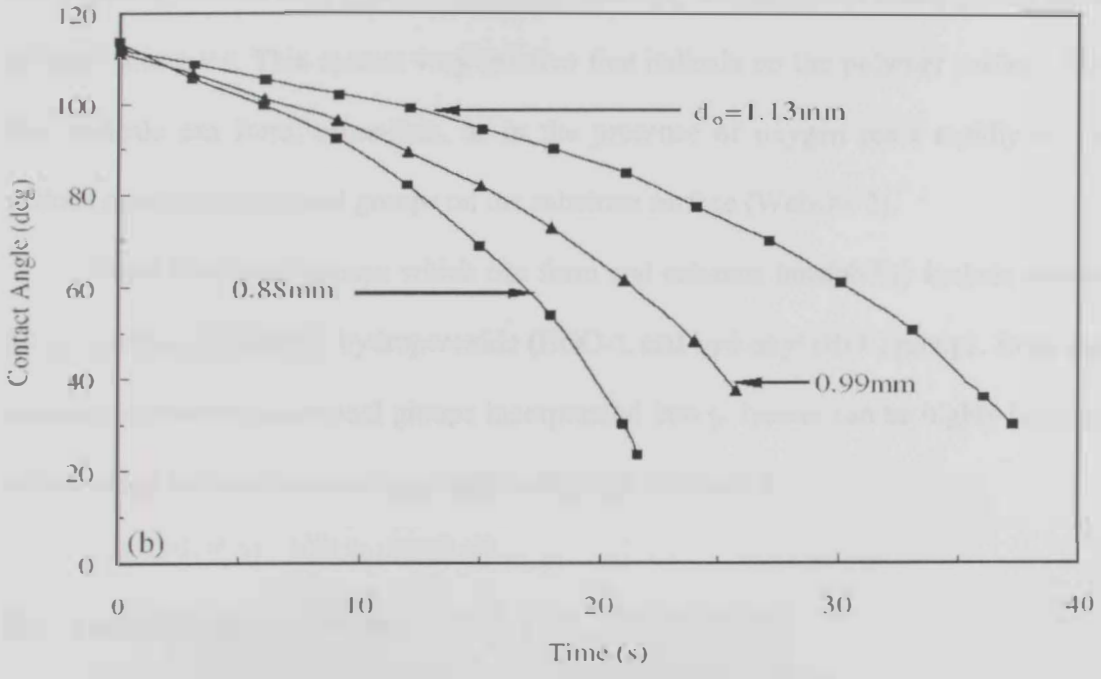

Fig. 1.11 Normalized height for water droplets at 60° C on (a) an aluminum surface and (b) a copper surface (Crafton and Black, 2004)

III. Chemical effect

Using the concept of critical surface energy, it is possible to characterize a wide variety of polymers and correlate the critical surface energy with polymer structure. Lower surface energy polymers have weakly interacting atoms in the backbone, whereas high values arise from strong interactions in polar materials (Schlangen, 1996).

Chemical composition and molecular structure depend on side groups, secondary bonding forces, cohesive-energy density, chain branching, entanglements and cross-linking.Surface free energy varies widely with the types of functional groups at the surface. For hydrophobic surfaces, free energy decreases in the order - CH_2 > - CH_3 > - CF_2 > - CF_2H > - CF_3 (Balkenende, 1998).

Also, free electrons, ions, metastables, radicals and UV generated in plasma regions can impact a surface with energies sufficient to break the molecular bonds on the surface of most substrates. This creates very reactive free radicals on the polymer surface. These free radicals can form, cross-link, or in the presence of oxygen react rapidly to form various chemical functional groups on the substrate surface (Website 2).

Polar functional groups which can form and enhance bondability include carbonyl (C=O), carboxyl (HOOC), hydroperoxide (HOO-), and hydroxyl (HO-) groups. Even small amounts of reactive functional groups incorporated into polymers can be highly beneficial to improving surface characteristics and wettability (Website 2).

IV. Contact angle hysteresis

Young's equation assumes that the solid surface is smooth, homogeneous, rigid, and it should also be chemically and physically inert with respect to the liquids to be employed. Ideally, according to Young's equation, a unique contact angle is expected for a given system. In a real system, however, two reproducible contact angles can be measured

experimentally on a solid surface. One of these contact angles is called the advancing contact angle, θ_a and it is produced by the advancing liquid over the solid surface. The other is called the receding contact angle, θ_r, and is produced by liquid receding over the solid surface. The difference between the advancing and receding contact angles has been defined as the contact angle hysteresis.

$$H = \theta_a - \theta_r \tag{1.13}$$

In practice, all real solid surfaces exhibit contact angle hysteresis. Because of the existence of contact angle hysteresis, contact angle interpretation in terms of Young's equation is arguable. Wenzel (1936) was the first to recognize that Young's equation might not be a universal equilibrium condition because the physical interaction between the liquids and the solid surfaces.

Although contact angle hysteresis has been recognized for at least 100 years, the underlying causes and its origins are not completely understood. Several studies have attributed contact angle hysteresis to surface roughness (Oliver and Mason, 1980), heterogeneity (Marmur, 1994; Decker and Garoff, 1996), and deformation of the solid surface (Neumann, 1974; Li, 1991). The latter cause of hysteresis can be eliminated by appropriately selecting liquid-solid combinations such that the liquid does not deform the solid, either mechanically or chemically (Budziak, 1992).

A. The effect of surface roughness

The earliest and still most useful correlation that correlates the observed contact angle of a liquid over solid to the roughness of the solid is Wenzel's (1936) relationship which offers a thermodynamics relationship.

$$\sigma_{12}\cos\theta = R_w(\sigma_{s2} - \sigma_{s1}) \tag{1.14}$$

where R_w is defined as the surface roughness factor, the ratio of the true and the apparent surface areas of the solid (Figure 1.12). If the apparent contact angle is θ', R_w can be defined by (Lee and Patankar, 2004):

$$R_w = \frac{\cos\theta}{\cos\theta'} \tag{1.15}$$

Equation 1.15 may be taken as a fundamental definition of the effect of surface roughness on wetting and spreading phenomena. Based on Equation 1.15, if the "intrensic" contact angle of a liquid is less than 90 on a smooth solid surface, the apparent contact angle will be smaller on a rough one. For a intrensic contact angle larger than 90° on smooth solid surface, on rough one the apparent contact angle will be larger i.e. for $\theta < 90°$, $\theta' < 0$; for $\theta > 90°$, $\theta' > \theta$. The previous conclusion has a great impact on practice; the preceding relationships indicate that if a liquid partially wets a surface, better wetting may result if the surface is roughened. On the other hand, if surface wetting is not preferred and a contact angle is larger than 90°, the situation can be improved by roughening the solid surface.

$R_w = 1$ means a smooth surface which is essentially nonexistent. Highly polished surfaces usually have $R_w \geq 1.5$ (Myers, 1999). Even the geometry of the roughness has no meaning from a thermodynamic standpoint. However, the type of surface topography may carry certain practical consequences. If the surface has pores, capillaries, crevices, or other types of structure, the apparent contact angle value is affected by the thermodynamics and kinetics associated with the type of topography structure (Myers, 1999; Zografi and Johnson, 1984).

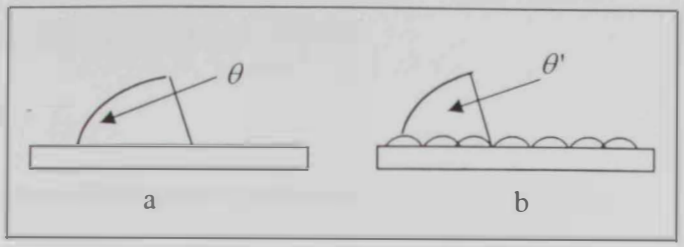

Fig 1.12: The apparent contact angle of a liquid on a surface may differ from that expected, the true (a) contact angle, (b) due to solid surface roughness

B. The effect of surface heterogeneity

In practice, it is difficult to find homogenous solid surfaces. Whether metals, polymers or minerals, surfaces are usually non homogenous. They are usually composed of two or more different materials that differ from each other in their interfacial properties (energy), thus showing heterogeneous characteristic. A chemically heterogeneous surface contains domains of different surface free energy. Heterogeneous domains are usually very small relative to the size of the liquid drop used in the measurement of the contact angle, so it will not be easy to distinguish between the influence of the different domains on the contact angle (Turunen, 2004).

Cassie and Baxter (1944) analyzed the smooth composite solid surfaces with varying degree of heterogenety. For the two components (*a* and *b*), Cassie (1948) derived an equation to describe the contact angle changes:

$$\cos\theta' = f_a \cos\theta_a + f_b \cos\theta_b \qquad (1.16)$$

where f_a is the fraction area of material '*a*' that has intrinsic contact angle θ_a, f_b is the fraction area of material '*b*' that has intrinsic contact angle θ_b, and where $f_b=1-f_a$.

Theoretically, if the contact angles of a test liquid on one of the homogenous surfaces are known, then the composition of a composite surface can be determined from a

contact angle measurement. Equation 1.16 can be reduced to the Cassie-Baxter equation for a porous surface (Cassie and Baxter, 1944):

$$\cos\theta' = f_1 \cos\theta_1 + f_2 \tag{1.17}$$

where f_2 is the fraction of open area (porosity).

1.3 Techniques for measuring contact angle

This section outlines a number of techniques that have been used for the measurement of contact angle. The choice of method for measuring the contact angle depends on several factors: 1) the geometry of the system, for example, the simplest configuration where the contact angle can be readily measured is the flat plate. Other configurations, like the inner surface of a capillary tube, porous substrates, biological surfaces, fibres, and powders have geometries for which contact angles are not easily measured; 2) the particular configuration of the sample; 3) the required accuracy; 4) cost and 5) time constraints. A survey of techniques for measuring contact angles is found in the reference (Neumann and Good, 1972).

1.3.1 Direct measurement of contact angle from profiles

The easiest and the most obvious and commonly used method of measuring contact angles involves direct measurement of the profile of a liquid drop (Figure 1.6) on a plane solid surface. In this technique a tangent is aligned with the liquid at the point of contact where the liquid meets with the solid. This can be done on a projected image, or photographs can be taken and then the angle can be directly measured with a protractor or using a telescope equipped with a goniometer eyepiece. This technique does not require a knowledge of the density and surface tension of the liquid, it employs relatively simple instruments. The solid surface does not have a large area and the required amount of the liquid is small. The measurement with a goniometer is performed in a short time frame, a single measurement usually taking less than 2 minutes. However, the results are subjective and operator dependent. It is commonly claimed that the accuracy of this method at best is $\pm 2°$ (Budziak, 1992). However, it is generally the most convenient method if high

accuracy is not required or when quick preliminary measurements are taken prior to actual measurements with a more accurate technique (Neumann and Good, 1972; Budziak, 1992).

1.3.2 Axisymmetric Drop Shape Analysis (ADSA)

This is an indirect method to find the contact angle of the liquid based on the shape of a sessile drop. By using this contact angle technique, besides contact angle, liquid surface tension, surface area of the liquid drop, volume of the liquid drop, and the contact radius of the liquid drop on the solid surface can also be measured.

The shape of the drop is governed by the known Laplace equation of capillarity, which describes the equilibrium condition for two homogeneous fluids separated by an interface. The Laplace equation represents the mechanical equilibrium condition between two opposing forces, gravity force and surface tension force, imposed on two fluid phases separated by a curved phase. The force of gravity tries to pull down the drop, and the surface tension force tends to make the drop spherical:

$$\gamma_{lv}\left[\frac{1}{R_1}+\frac{1}{R_2}\right]+\Delta\rho\, g\, z=\Delta P \qquad (1.18)$$

where $R_1$and R_2 are the principal radii of curvature, $\Delta\rho$ is the density difference across the liquid-vapour interface, g is the acceleration of gravity, z is the ordinate of a point of the liquid at interface at which the principal radii of curvature are R_1 and R_2, and ΔP is the pressure difference or the capillary pressure. The interfacial tension can be determined by numerical integration of Equation 1.18. This technique was developed at the University of Toronto by Rotenberg (1983).

This technique fits the Laplace equation of capillarity to an arbitrary number of coordinate points from the profile of a drop (Spelt ,1985; Cheng, 1990; Amirfazli, 2001) The required inputs are: a) the profiles of the sessile drop, b) the local gravity constant and

c) the densities of the two fluids. The advantages of this technique are: a) it is applicable to all axisymmetric liquid-fluid interfaces , b) it is independent of the skill and experience of the operator and c) it is automated using computer based imaging technology or digital image analysis to acquire the profile coordinate points of drops (Cheng, 1990)..

1. Axisymmetric Drop Shape Analysis-Profile (ADSA-P)

The ADSA-P technique involves constructing a function that expresses the deviation of the observed profile, of the liquid drop on the solid surface, from a theoretical curve that satisfies the Laplace equation of capillarity, Equation 1.18. If the force of the gravity is the only external force affecting the liquid drop, then ΔP can be expressed as:

$$\Delta P = \Delta P_o + \Delta\rho\, g\, z \tag{1.19}$$

As shown in Figure 1.13, if the origin of the coordinate system is placed at the apex point of the drop and the x-axis is the tangent axis to the origin and normal to the axis of symmetry, Equation 1.19 can be expressed as:

$$\gamma\,[\frac{1}{R_1} + \frac{\sin\phi}{x}] = 2\frac{\gamma}{R_o} + (\Delta\rho)\, g\, z \tag{1.20}$$

As shown in Figure 1.13, R_1 turns in the plane of the paper, $R_2 = x/\sin\phi$ rotates in the plane normal to the plane of the paper and a bout the axis of symmetry and R_o is the radius of curvature at the origin, ϕ is the turning angle measured to interface at (x,z) and the horizontal plane through the same point (x,z) and represents the contact angle at the point where the liquid touches the solid surface. The interface can be described by the meridian section because the drop is axisymmetric (Kwok, 1998). If the interface is expressed as:

$$u = u(x,z) \tag{1.21}$$

The meridian curve can be expressed by:

$$x = x(s) \qquad z = z(s) \tag{1.22}$$

where s is the arc length parameter measured from the origin.Equation 1.20 (Laplace equation) can be parameterized and the results are as follow

$$\frac{dx}{ds} = \cos\phi \tag{1.23}$$

$$\frac{dz}{ds} = \sin\phi \tag{1.24}$$

$$\frac{d\phi}{ds} = \frac{2}{R_o} + \frac{(\Delta\rho)g}{\gamma} z - \frac{\sin\phi}{x} \tag{1.25}$$

$$x(0) = z(0) = \phi(0) = 0 \tag{1.26}$$

By integrating Equations 1.23-1.26 simultaneously, the theoretical profile of the drop is matched with the experimental drop profile, where the previous is calculated with the surface tension as one of the variable parameters.

A set of arbitrary but accurate coordinate points from drop profile is one of the required inputs, and this procedure has been automated by Cheng et al (1983) by development an automated system to acquire coordinates of any number of the points a long the meridian profile of the drop using digital image analysis. To locate the meridian profile for an experimental drop the digital image processing module of ADSA-P uses SOBEL 3x3 pixel.

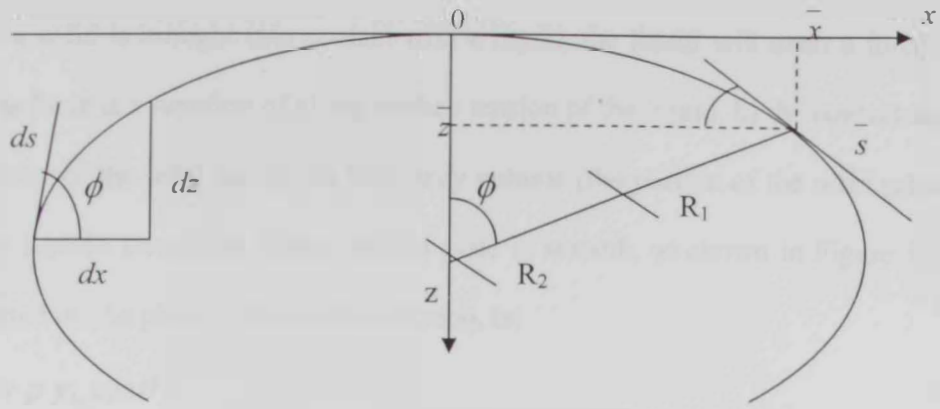

Fig 1.13 Coordinate system definition. R_1, R_2 are the two principle radii of curvature of the drop

II. Axisymmetric Drop Shape Analysis-Contact Diameter (ADSA-CD)

For low contact angles (below 30), the accuracy of the ADSA-P technique, significantly decreases since the profile of the drop become gradually flatter. Hence, the accuracy in acquiring coordinate points along the drop profile becomes low.

Axisymmetric Drop Shape Analysis-Contact Diameter (ADSA-CD) was developed by Skinner et al. (1989) to allow measuring low contact angles. Instead of viewing the drop from the side, in this technique the drop is viewed from the top, and hence the flatness of the drop does not reduce the precision of the contact angle measurement. In addition, because the whole contact line can be viewed when the drop is imaged from the top , the ADSA-Cd technique lends itself readily to averaging procedures and it can therefore be used to determine the average contact angle (Amirfazli, 2001).

1.3.3 Wilhelmy-Gravitational method (vertical rod method)

Contact angle can be measured directly on a vertical rod or plate partially immersed in a liquid. The advancing and receding angles are obtained simply by immersing and

withdrawing the plate or the rod.

If a solid is brought into contact with a liquid, the liquid will exert a force on the solid. This force is a function of a) the surface tension of the liquid, b) the contact angle, c) the perimeter of the solid and d) the buoyancy volume (the portion of the solid submerged below the liquid's interface). If the vertical plate is smooth, as shown in Figure 1.14, the force exerted on the plate by the surface tension, is:

$$F = mg + p\,\gamma_{lv}\cos\theta \tag{1.27}$$

Where F is the downward force exerted by the liquid on the plate, p is the solid perimeter, γ_{lv} is the liquid-vapour surface tension, m is the plate mass, θ is the contact angle, and the mg term is the weight of the plate in air before the plate is brought into contact with the liquid. For non zero immersion depth Equation 1.27 has to be corrected for the buoyancy force as follows:

$$F = mg + p\,\gamma_{lv}\cos\theta - V\,\Delta\rho\,g \tag{1.28}$$

Where V is the displaced volume of the liquid and $\Delta\rho$ is the density of the displaced fluid. To evaluate the contact angle, the surface tension, γ_{lv}, must be known; To measure γ_{lv} a plate material is used where the contact angle is zero, so that cos(θ) is equal to one. In the case where the immersion depth is zero, Equation 1.27 further reduces to:

$$F = p\,\gamma_{lv} \tag{1.29}$$

In Equation 1.29 the liquid-vapour surface tension is proportional directly to the downward force exerted by the liquid on the plate. As it is a measurable quantity, the weight of the plate has been dropped from Equation 1.29. The γ_{Lv} of the liquid should be known before measuring θ. This can be done as follows;

a) The surface tension is measured with a completely wetted plate (θ = 0),

b) Knowing γ_{Lv}, the contact angle of the solid of interest is measured.

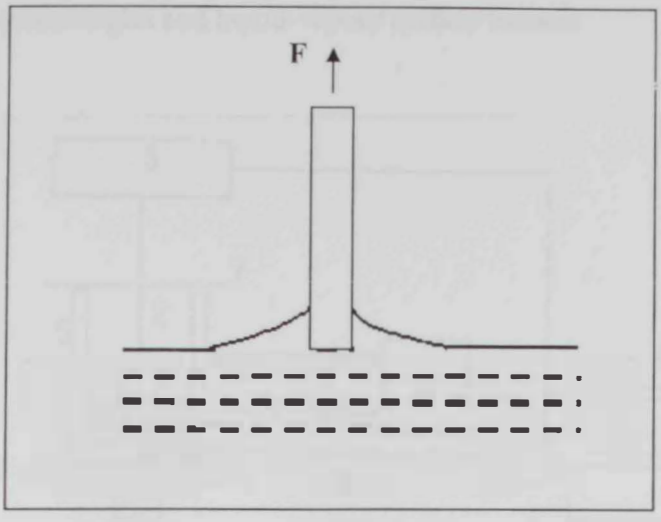

Fig. 1.14 Vertical plate in contact with a liquid

The basic setup of the automated Wilhelmy Plate Technique is shown in Figure 1.15 (Budziak, 1992). The components are as follows: The plate (1) is suspended by a thin rod (2) from an electro balance (3). The electro balance is interfaced with a computer (4) which records the downward force. The liquid to be measured (6) is contained in a double walled beaker (5), covered with a lid (7) and connected to a temperature bath (8). The temperature of the bath is measured with a thermocouple (9), also interfaced with the computer. The table (10) carrying the double-walled beaker may be moved up and down by means of a screw mechanism (11) driven by the electric motor (12). The direction and speed of the motor is also controlled by the computer.

The Gravitational Wilhelmy technique drawbacks which limit the applicability of this method, are (Neumann and Good, 1972; Budziak, 1992): only if the perimeter of the plate is known and constant, the high sensitivity of the electro balance can be exploited. The plate morphology and composition must be the same at all four vertical surfaces. Moreover, adsorption of the vapour of the liquid on the plate above the three-phase contact line and at various parts of the gravimetric system adds to the weight readings. On the

other hand, the Gravitational Wihelmy plat method has a high sensitivity for the measurement of contact angles and liquid-vapour surface tension.

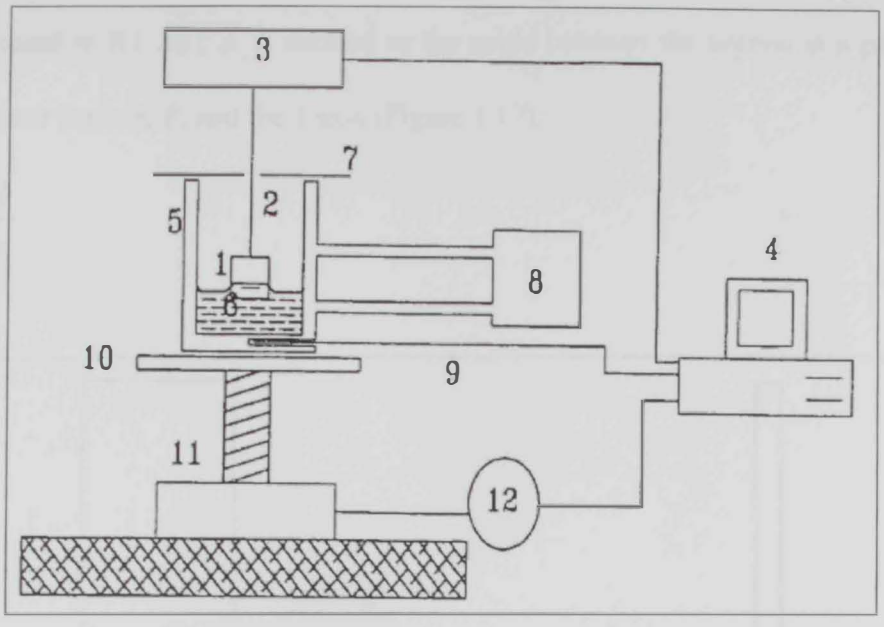

Fig. 1.15 Schematic for the Wilhelmy-Gravitational technique (Budziak, 1992)

1.3.4 Capillary method

The liquid rise in a capillary is one of the most familiar manifestations of liquid surface tension. The capillary height, h is related to the liquid vapour surface tension. From h, the contact angle can be obtained by integration of the Laplace equation of capillarity. Pioneer work in measuring contact angles by using this method is attributed to Neumann (1962).

When a vertical flat plate is put it into contact with a pool of liquid, the liquid will rise on the plate above the undisturbed surface (Figure 1.16). For a liquid in contact with an infinitely wide vertical plate, the Laplace equation can be simplified by noting that one of the radii of curvature is infinite (Budziak, 1992), hence:

$$\gamma_{lv} [\frac{1}{R_1}] = \Delta\rho\ g\ z = \Delta P \tag{1.30}$$

For the geometry of the liquid surface, the element *ds* along the surface of the liquid is equal to R1 $d\phi$; ϕ is defined as the angle between the normal at a point on the liquid-vapour surface, P, and the z axis (Figure 1.17):

$$\frac{1}{R_1} = \frac{d\phi}{ds} \tag{1.31}$$

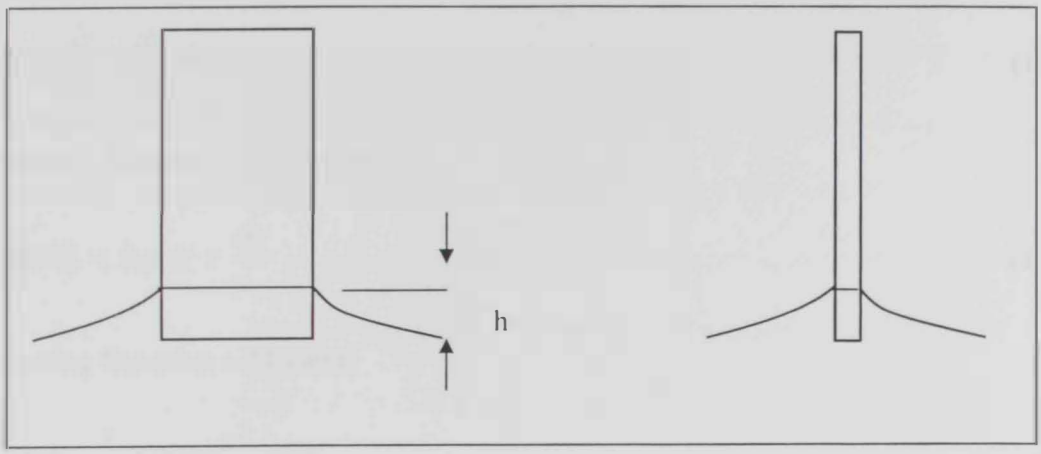

Fig 1.16 Capillary rise on a vertical plate

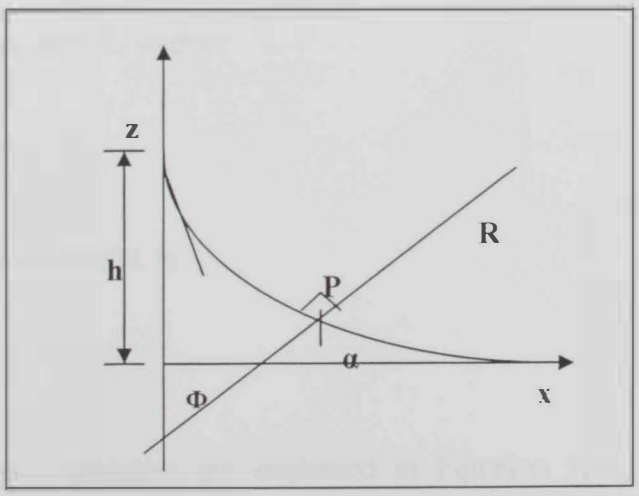

Fig 1.17 Capillary rise at a vertical plate

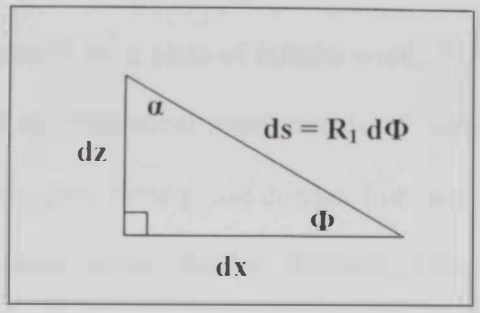

Fig 1.18 Element *ds* on the liquid interface

From Figure 1.18,

$$\sin\phi = \frac{dz}{ds} = \frac{dz}{R_1}\,d\phi \tag{1.32}$$

Equation 1.30 can now be written:

$$\sin\phi\; d\phi = \Delta\rho\; g\; z\; \frac{dz}{\gamma_{lv}} \tag{1.33}$$

Integrating Equation 1.33 yields

$$-\cos\phi = \frac{1}{2}\,\Delta\rho\; g\; \frac{z^2}{\gamma_{lv}} + K \tag{1.34}$$

When P is on the z axis, z = h and $\phi = 90° - \theta$. Since z = 0 at $\phi = 0$, it follows that the constant of integration K = -1, so that:

$$1 - \cos\phi = \frac{1}{2}\,\Delta\rho\; g\; \frac{z^2}{\gamma_{lv}} \tag{1.35}$$

In terms of the meniscus height, h:

$$\sin\theta = 1 - \frac{\Delta\rho\; g\; h^2}{2\,\gamma_{lv}} \tag{1.36}$$

A total of five variables are contained in Equation 1.36, where the density difference, the gravity constant and the liquid surface tension can be independently measured. Thus, the task of measuring a contact angle is reduced to measuring a length, the

capillary rise h.

The above integration is for a plate of infinite width. For practical purposes, plates that are 2 cm wide satisfy the theoretical requirements of "infinite" width (Neumann and Good, 1972). For such plates, the three-phase contact line is straight in the middle of the plate for all liquids of moderate surface tension, including water. Near the two ends of the plate, the capillary height is lower than it is in the middle.

Besides the fact that the measurement of an angle has been reduced to the measurement of a length, which can be performed with much higher precision and accuracy, there are other advantages of the capillary rise technique. Three of these advantages have been discussed in the introduction: the capability of measuring advancing and receding contact angles; the ability to directly observe the three-phase contact line; and the ability to combine this technique with the Wilhelmy balance to simultaneously measure the surface tension and the contact angle. Furthermore, the perimeter of the plate is not required as an input nor is it to be kept constant as in the Wilhelmy technique (Budziak, 1992).

Another advantage of the capillary rise technique involves line tension. Since, in the capillary rise method the three-phase contact line is straight, the line tension does not influence the contact angle (Budziak, 1992; Myers, 1999). The disadvantages of the capillary rise method are that a large volume of liquid and a large surface of uniform morphology and composition are required; also the equipment needed is relatively expensive.

In a summery the advantages and the disadvantages of the previous techniques are presented in Table 1.1.

Table 1.1:The advantages and the disadvantages of contact angle measurement techniques

Technique	Advantages	Disadvantages
1. Direct Measurement of Contact Angle from Profiles	1. The easiest and most obvious, and the commonly used method. 2.This technique does not require a knowledge of the density and surface tension of the liquid. 3.The solid surface does not have a large area and the required amount of the liquid is small. 4.The measurement is performed in a short time frame (less than 2 minutes for a single measurement).	1. The results are subjective and operator dependent. 2. Low accuracy (At best ± 2°).

Table 1.1 (Continued): The advantages and the disadvantages of contact angle measurement techniques

2. Axisymmetric Drop Shape Analysis (ADSA)	1. Can also measure liquid surface tension, THE surface area of the liquid drop on the solid surface, the volume of the liquid drop, and the contact radius of the liquid drop on the solid surface. 2.It is applicable to all axisymmetric liquid-fluid interfaces. 3.It is independent of the skill and experience of the operator. 4.It is automated using computer based imaging technology or digital image analysis to acquire the profile coordinate points of drops. 5.Accuracy 0.3°.	1.Indirect method to measure the contact angle. 2.Complicated setup. 3.The equipment needed is relatively expensive.

Table 1.1 (Continued): The advantages and the disadvantages of contact angle measurement techniques

3. Wilhelmy-Gravitational method (vertical rod method)	1. Simple setup and procedures. 2. Liquid surface tension can also be measured. 3. High sensitivity for the measurement of contact angles and liquid-vapour surface tension.	1. The high sensitivity of the electro balance can be exploited only if the perimeter of the plate is known and constant. 2.The plate morphology and composition must be the same at all four vertical surfaces. 3.Adsorption of the vapour of the liquid on the plate above the three-phase contact line and at various parts of the gravimetric system adds to the weight readings.

Table 1.1 (Continued): The advantages and the disadvantages of contact angle measurement techniques

4. Capillary methods	1. The measurement of an angle has been reduced to the measurement of a length, which can be performed with much higher precision and accuracy. 2. The ability to directly observe the three-phase contact line. 4.The line tension does not influence the contact angle.	1. A large volume of liquid and a large surface of uniform morphology and composition are required. 2. The equipment needed is relatively expensive.

1.4 Dynamics of spreading

1.4.1 Incomplete spreading

All liquids placed in contact with a solid surface exhibit spontaneous spreading rate at the start of the process, then pass through a transition zone. After transition, the droplets either continue to spread at a slower rate (i.e. complete spreading) to reach very small contact angle ($\theta \approx 0$) or cease to spread (i.e. incomplete spreading or partial spreading) i.e $\theta > 0$ (Fig 1.6).

Several studies of the partial wetting have been carried out (Brochard-Wyart and de Gennes, 1992; Van Remoortere and Joos, 1993; de Coninck et al., 2001). Many wetting systems that exhibit partial wetting have a non zero spreading coefficient $S < 0$ (sec 1.2.6). Among these partial wetting systems is glycerol liquid on soda-lime glass solid surfaces. Figure 1.19 (Alterifai and Sasa, 2003) shows the spreading kinetics of glycerol on glass presented as contact area versus spreading time for 1.5μL drop volume; contact area and contact angle parameters are shown in Table 1.2 (Alterifai and Sasa, 2003).

Table 1.2 contact areas (cm2), contact angles and *n* values for spreading of glycerin on glass, PMMA and PS (Alterifai and Sasa, 2003)

Solid	Glass	PMMA	PS
Contact Area (cm^2)	0.086	0.042	0.032
Contact Angle, Eq. (4)	26.5	70.6	104.5

1.4.2 Complete spreading

In complete spreading systems, the liquid completely spreads over the solid surface resulting in zero contact angle ($\theta = 0$), these systems have a spreading coefficient value of zero, $S = 0$.

A reviews of the literature on spreading dynamics by Marmur (1983), de Gennes (1985) and several other contributors to a more recent book edited by Berg (1993) attest to continued interest in the subject. Silicon oil is considered to exhibit complete spreading.

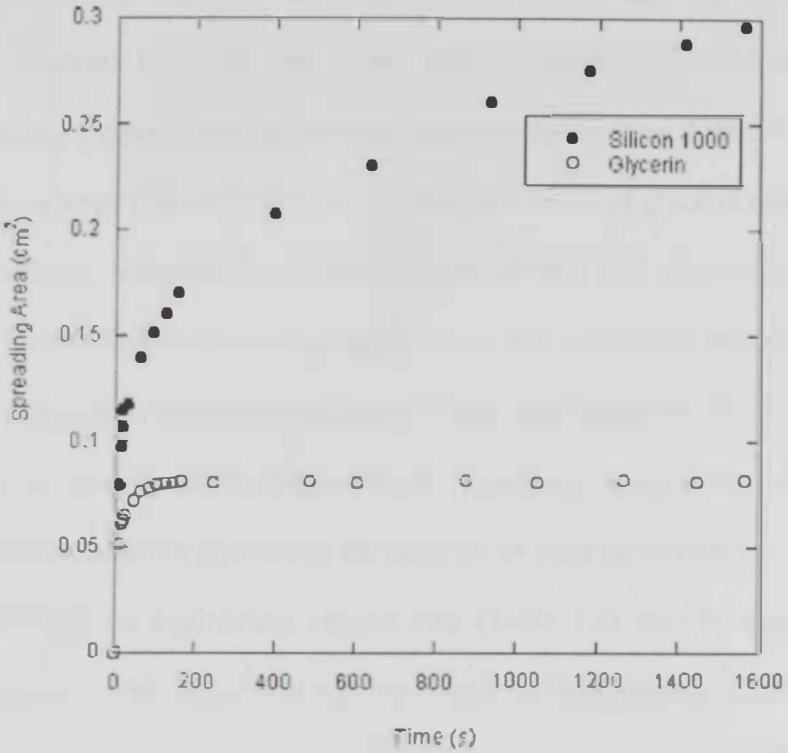

Fig 1.19 Spreading kinetics of PDMS 1000 and glycerol on soda-lime glass (Alteraifi and Sasa 2003)

1.4.3 The role of the solid on spreading kinetics

Alteraifi and Sasa (2003) provided experimental evidence that the solid substrate plays a significant role in the spreading kinetics of liquids and in determining equilibrium (static) contact angle. The latter was found explainable on basis of the axiom "like wets like". Contributions of the solid substrate to spreading kinetics are attributed to specific solid-liquid interactions of dissipative nature, which

manifest themselves only at the interface. The term "interfacial viscosity" has been coined to account for this phenomenon (Alteraifi and Sasa, 2003). For the case of a low surface energy liquid, hexadecane has been selected for its relatively low surface energy liquid (32 dyne/cm) and for its non-polar character (Alteraifi and Sasa, 2003). In addition, hexadecane is known to exhibit incomplete spreading on soda-lime glass (Alteraifi et al., 2003). Glycerol has been selected for its relatively high surface energy (67.6 dyn/cm) (Alteraifi and Sasa, 2003). Figures 1.20, 1.21 show the spreading kinetics of glycerol and hexadecane respectively, on three different solids in terms of surface energy (Table 1.3) and the spreading kinetics of glycerol on the same three solids surfaces. Noting that a constant volume droplet (1.5 μl) was used in all experiments, the equilibrial contact area may be taken as a measure of wettability.

Right away the contributions of each of the solid substrates to the wetting process is obvious, and the axiom "like wets like" appears to apply in the both cases; spreading of hexadecane and glycerin on the same set of solid substrates.

As expected, the equilibrium contact area (Table 1.4) may be qualitatively ranked in accordance with the critical wetting energy of each respective solid. Glass caused hexadecane to assume the least equilibrium spreading (smallest contact area). At the other end, PS with the lowest surface energy produces the most wetting (smallest contact angle) by hexadecane. In the case of glycerol the largest equilibrial spreading (largest contact area) was noted to occur on glass, the least on PS and on PMMA it was intermediate.

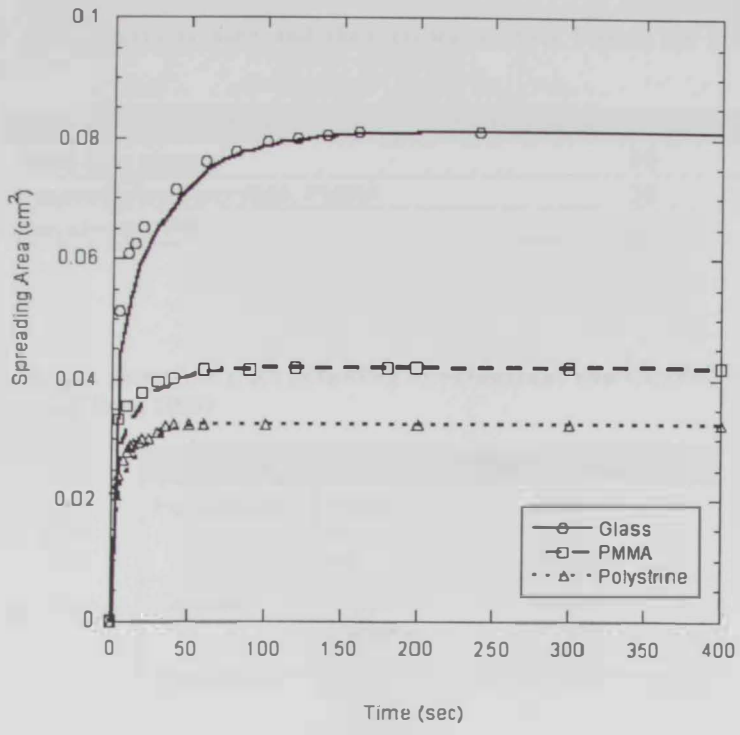

Fig 1.20 Spreading kinetics of glycerol on glass, PMMA, and PS (Alteraifi and Sasa, 2003)

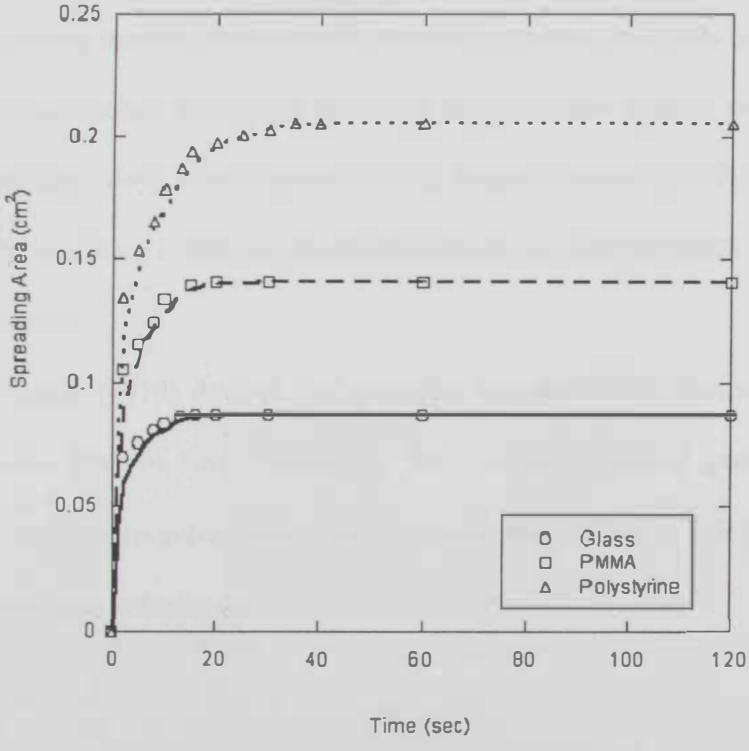

Fig 1.21 Spreading kinetics of hexadecane on glass, PMMA, and PS (Alteraifi and Sasa, 2003)

Table 1.3 List of surfaces used and their critical surface tension for glass, PMMA, and PS (Myers, 1999)

Solids	Critical Wetting Energy (mN/m)
Soda-lime glass	70
Polymethylmethacrylate, PMMA	39
Polystyrene, PS	33

Table 1.4 Contact areas (cm^2), for spreading of hexadecane and Glycerol on glass, PMMA and PS (Alteraifi and Sasa, 2003)

Liquid	Solid	Contact Area (cm^2)
Hexadecane	Glass	0.081
	PMMA	0.141
	PS	0.205
Glycerin	Glass	0.086
	PMMA	0.042
	PS	0.032

1.4.4 Models of spreading dynamic

Several theories deal with the spreading kinetics of liquids on a solid substrate, most of which relate the rate of spreading to the surface tension, and the viscosity of the liquid only. de Genne's model (1985), Tanner's model (1979) and that proposed by Seaver and Berg (1993) expressed the rate of spreading in terms of surface tension and viscosity.

Tanner (1979) derived the spreading equation from Navier-Stokes equations for viscous flow in two dimensions. The author expressed pressure gradient by surface tension curvature; hence, he introduced the surface profile κ which relates to the droplet edge velocity as:

$$U = \frac{dR}{dt} = -\frac{\gamma \kappa}{3 \mu} \tag{1.37}$$

where U is the film advancing velocity with constant profile shape, κ is a profile constant; μ and γ are the liquid viscosity and surface tension, respectively. Here,

again, the "surface profile" κ is a non-dimensional parameter that has to be determined empirically. Furthermore, Tanner suggested the following relationships:

$$\tau = \frac{1}{10}\kappa^{10} \qquad \text{For } \kappa < 0.9 \tag{1.38}$$

and

$$1 - k \cong \exp(-6\tau) \quad \text{For } 0.9 < \kappa < 1.0 \tag{1.39}$$

where $k = \frac{R}{R_f}$ and $\tau = \frac{\kappa \gamma t}{\mu R_f}$, R_f is the equilibrium contact radius.

Subsequently, Seaver and Berg (1994) assumed that the fluid dynamics of the spreading of a spherical cap droplet may be approximated by a cylindrical disk. Then, they examined the disk spreading in quasi-steady laminar Couette flow driven by "effective radial surface tension gradient" at the upper surface. Accordingly, the rate equation has been derived for complete spreading as:

$$\frac{dR}{dt} = \frac{4\gamma V_d^3}{\pi^3 \mu R^9} \tag{1.40}$$

For incomplete spreading, the authors derived the rate equation as:

$$\frac{dR}{dt} = \frac{4\gamma V_d^3}{\pi^3 \mu R^9} - \frac{\gamma \beta V_d}{2\pi \mu R^3} \tag{1.41}$$

where R is the radius of the spreading droplet, V_d is the cylindrical disk volume ($V_d = \pi h d R^2$), $\beta = 1 - \cos\theta_\infty$, θ_∞ is equilibrium contact angle and μ is liquid viscosity.

Apparently due to the difficulty of applying these models, Lelah and Marmur (1981) suggested that the kinetics of spreading could be described by a simple power law as follows:

$$A(t) = c_1 t^n \tag{1.42}$$

where A is the contact area, measured at time t, and c_1 and n are empirical coefficients. Subsequently, the author applied this equation to the spreading data reported by several investigators for a relatively large number of fluids. It was noted that the value of n in most of the cases falls within 0.20 to 0.29.

Further analysis of data where the droplet volume (V) was independently varied revealed that c_1 was found to be proportional to V^m. The power m was found to range from 0.60 to 0.72. This observation prompted Marmur (1983) to suggest that c_1 scales with $V^{2/3}$. Thus, the rate of spreading normalized with respect to $V^{2/3}$ was expressed as:

$$\frac{A}{V^{2/3}} = c_2 t^n \tag{1.43}$$

An early attempt to derive the rate of spreading was advanced by Ogarev and coworkers, in the mid seventies (Ogarev, 1974). The Ogarev model approximated the shape of the spreading droplet as a cone, whose geometric parameters were used to derive the spreading equation through a force balance implementation. For a given moment, the authors balanced the forces due to change in the free surface energy of the (droplet-on-solid substrate) system and the viscous resistance. They derived the following equation for spreading kinetics:

$$R(t) = \left(\frac{24 V f}{\pi \mu} \right)^{1/4} t^{1/4} \tag{1.44}$$

where R is the radius of the contact area, V is the droplet volume, and μ is the viscosity. The function f relates to the surface energy of the spreading liquid as defined by Young's equation (1.1) as:

$$f = \gamma(\cos\theta_\infty - \cos\theta(t)) \tag{1.45}$$

for incomplete spreading, and

$$f = \gamma_{sv} - \gamma_{sl} - \gamma \cos\theta(t) \qquad (1.46)$$

for complete spreading

Recognizing earlier inference by Hoffman (1975) and others that the spreading process is generally driven by surface forces and is retarded to viscous forces, de Gennes (1985) introduced what may be considered as a theoretical rational for the empirical power law of Marmur (1983). The argument suggested by de Gennes is based on the earlier finding of Hoffman (1975) that the "apparent" contact angle can be correlated as a function of the capillary number ω plus a shift factor when interfacial and viscous forces are the dominant forces controlling the system. The capillary number ω defined as

$$\omega = \frac{U\,\mu}{3\,\sigma} \qquad (1.47)$$

where U is the velocity of the contact line. In this regard, it is worth noting that a related expression was suggested earlier by Schonhorn et al (1966) to correlate the kinetics of spreading on surfaces using polymer melts (de Gennes, 1985). The argument further assumes that Hoffman's data, in the low velocity limit, may be presented as

$$\omega = \text{constant} * \theta^{m} \qquad (1.48)$$

It is further suggested that for relatively small droplets, where gravitational effects are negligible, the macroscopic shape of the spreading droplet may be approximated by spherical cap geometry (de Gennes, 1985). This approximation has been used to relate the contact angle to the radius and the volume of the spreading droplet, i.e. the droplet height $h = \frac{1}{2} R\,\theta$, and it is volume $V = \frac{1}{2}\pi h R^{2}$. Accordingly de Gennes (1985) derived "the spreading law" as

$$R^{3m+1} = \frac{\gamma}{\mu} t V^{m} \qquad (1.49)$$

Furthermore, the author ascertained that m=3 is "indeed expected theoretically for all cases of dry spreading" which dose not satisfy all liquids (Alterifi et al., 2002).

Lopez et al. (1975) reported that at the final stage of spreading, intermolecular forces replace gravity as the chief factor causing spreading, and after an initial stage of spreading in which inertial effects are important, there is a stage where the balance between the gravitational and viscous effects controls the spreading rate.

Fay (1969) studied spreading of oil on calm water. He showed that inertia and viscous forces act as resisting forces, while gravity and line forces (the force which act at the edge of the oil film on water, pulling it outward) promote spreading. In their model Gue and Li (1998) used an overall energy balance (OEB) method and lubrication theory approximation. By comparing the numerical predictions with experimental spreading data of silicon oil drops on horizontal smooth solid surfaces (soda-lime glass) measured by Chen and Wada (1992), they found that over the entire observed spreading period they agreed well within the measurement error. They also concluded that the viscous force and the interfacial tension forces control the spreading process.

The existence of a precursor film that can be defined as a thin film of liquid preceding the advance of a thicker film during spreading over solid surface has been proved experimentally (Dussan, 1979) and theoretically (de Gennes, 1985; Hervert and de Gennes, 1984). Tanner et al. (1979) showed experimentally that the free surface of the liquid drop has an inflexion point that was also shown theoretically by Diez et al. (1993) and Chebbi and Selim (1997). The curvature of the drop surface profile is constant in the major part of the drop where the viscous forces are

negligible. Viscous forces are effective and the curvature of the drop profile changes significantly in the neighborhood of the inflexion point. On the other hand van der Waals forces become important and cannot be ignored in the near vicinity of the contact line (Chebbi, 2000).

Chebbi (2000) presented a model that concerned the complete wetting and accounts for capillary, viscous, and van der Waals effects, with two spreading geometries, namely: Axisymmetric and cylindrical (like oil on water) . The model is not based on any fitting parameter, and it is obtained by matching the outer solution that proposed by Chebbi and Selim (1997) and the inner solution proposed by Starov et al. (1994). The outer solution is valid in the major part of the liquid drop, and this solution takes into consideration the capillary opposed by the resisting viscous forces. The inner solution is valid for small thicknesses, which accounts in addition for van der Waals forces (Chebbi, 2000). A complete solution is obtained by matching the inner and the outer solutions at the inflexion point that is presented on the free surface of the liquid drop (Tanner, 1979; Diez et al., 1994).

Chebbi model studied the effect of changing both the dimensionless thickness and the slope on the behavior of the inner . This study of the inner region allows, after matching with the outer solution, determination of the spreading kinetics without the necessity of restoring to the approximation made in Chebbi and Selim (1997) and Starov et al.(1994) models. A numerical study of the inner solution in this model is shown to yield the deviations from the asymptotic approximation used in Chebbi and Selim (1997) and Starov et al.(1994) models for the inner solution at the inflexion point Chebbi (2000). By equating the thicknesses, and the slopes given by the inner and outer solutions at the inflexion point, Chebbi's model can determine the complete drop profile.

Chebbi model's results show drastic changes of the slope in the near vicinity of the contact line, and minimum slope variations at the inflexion point (Chebbi, 2000). This model is based on Navier-Stockes equations for one dimensional slow viscous flow and concerns the case of small slopes, which allows the use of the lubrication approximation which is valid for low contact angle (small slope of liquid drop curvature) (Lopez et al., 1976). In addition, inertia and gravity effects are neglected.

The spreading law $\bar{x}(t)$ (Fig 1.22) is given by Chebbi (2000) as:

$$\bar{x} = \bar{x}_0 (1 + \alpha T)^{1/(7+3\varsigma)} \tag{1.50}$$

where T is a dimensional time,

$$T = \frac{t}{\bar{t}} \quad ; \quad \bar{t} = \frac{3 \mu \bar{x}_o^4}{\gamma \bar{h}_0^3} \tag{1.51}$$

subscript 0 denotes initial values and α is defined as:

$$\alpha = \omega(7+3\varsigma)\left(\frac{I_0}{I}\right)^3 \tag{1.52}$$

where I is defined as:

$$I = 2\pi^{\varsigma} \int_0^1 \eta^{\varsigma} \varphi \, d\eta \tag{1.53}$$

where $\eta = \frac{x}{\bar{x}}$ and φ related to ω and η as:

$$\omega\eta = \varphi^2 \frac{d}{d\eta}\left(\frac{d^2\varphi}{d\eta^2} + \frac{\varsigma}{\eta}\frac{d\varphi}{d\eta}\right) \tag{1.54}$$

where ω is determined by matching between the outer solution and inner solution (Chebbi, 2000).

Diez et al. (1993) model concerns the complete spreading of liquid over a smooth rigid horizontal surface with the Laplace pressure as the dominant force. Mass

and energy conservation are invoked as the conditions to determine the flow. In the development of this model the particular attention is paid to the behavior of the liquid as the height become very small and the introduction of the global energy balance as a constrain to determine the solution and the gravity effect is neglected.

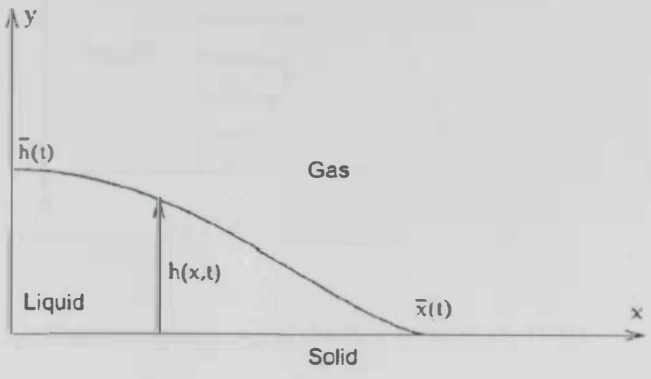

Fig 1.22 Schematic figure of the right side of a symmetric drop spreading over a smooth solid surface (Chebbi, 2000)

Diez et al. (1993) model is based on the Navier-Stockes equations for the one dimensional slow viscous flow and the lubrication approximation for this flow.

Both $h_o(t)$ and $x_f(t)$ (Fig 1.23) must be power laws on time, of the form

$$h_o(t) = \lambda_o\, k\, t^{\beta} \quad , \quad x_f = \xi_f\, b\, t^{\varsigma} \tag{1.55}$$

where $h_o(t)$ is the thickness at the center (x = 0), and x_f is the front position of the droplet.

The nondimensional exponents β, ς, and the dimensional constants k, b can be obtained simply from the law of mass and energy conservation, while the calculation of the nondimensional constants λ_o, ξ_f requires the complete solution of a set of equations (Diez et al., 1993).

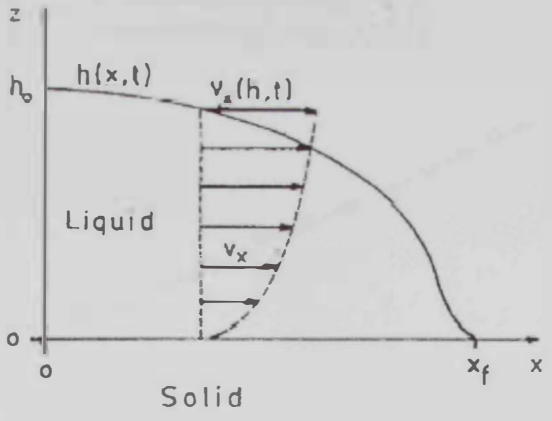

Fig 1.23 Schematic diagram of the flow (Diez et al., 1993)

Chebbi (2000) compared the two previous models with the experimental data of Diez et al. (1993). The corresponding results are shown in Figure 1.24. For comparison with the data of Diez et al., Hamaker's constant is estimated to be nearly equal to the one reported in Starov (1994), since experiments were made for the same liquid-solid system, silicone oil (PDMS)-Glass. It can be seen from Figure 1.24 that there is a better agreement between Chebbi model and the experimental data than is the case with Diez model.

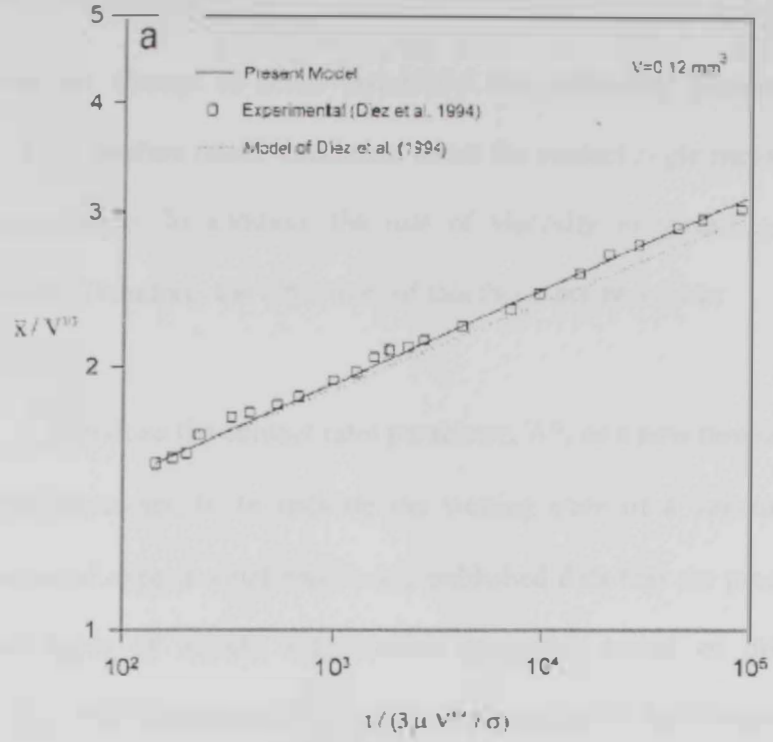

Fig. 1.24 Comparison between Diez et al model and Chebbi model with Diez et al.'s data for Silicon oil (V =0.12 mm3) on Glass (Chebbi, 2000)

1.5 Thesis Objectives

In this thesis, we attempt to better understand the underlying phenomenon of wettability. The literature raised concerned about the contact angle measurements and its interpretation. In addition, the role of viscosity in spreading kinetics remains unclear. Therefore, the objectives of this thesis are two folds:

1) Introduce the contact ratio parameter, A*, as a new measure instead of contact angle parameter, θ, to indicate the wetting state of a vapour-liquid-solid system. The set of experimental results and published data that are presented below use different types of liquids with various properties tested on different solid substrates. The results presented discuss the applicability of the contact ratio as an alternative measure of wettability to contact angle.

2) The effect of viscosity on the spreading kinetics is investigated by studying the spreading kinetics of liquids with various viscosities. The results are presented using silicone oils (PDMS) liquid with various viscosities (50 cP, 100 cP, 500 cP, 1,000 cP, 10,000 cP) tested on glass, PMMA, and PS solid surfaces. In this study the gravity and inertia forces are neglected in comparison with other forces. Also, the results present a comparison between the experimental data and the published theoretical models.

Chapter 2

Materials & Methods

2.1 Liquids

2.1.1 Silicon oils (PDMS)

Silicon oils or Polydimethylsiloxanes (PDMS) with different viscosities (100 cP, 500 cP, 1,000 cP, 10,000 cP) were used in the study of dynamic contact area (contact area as a function of spreading time) measurement. Silicon oil was selected because it satisfies the following requirements:

a) Complete spreading on the used solid surfaces (Sec 2.5).

b) Has a wide range of viscosity with the same surface tension (21.5 dyn/cm).

c) Non-hazardous.

d) Non reactive with the solid surface.

Table 2.1 lists the properties of the silicon oils that were used to measure the dynamic contact area.

Table 2.1: Silicon oil (PDMS) properties

Materials	Supplier	μ (cP)	σ (dyne/cm)
Silicon oil	Aldrich	50	21.5 ± 0.03
Silicon oil	Aldrich	100	21.5± 0.03
Silicon oil	Aldrich	500	21.5± 0.03
Silicon oil	Aldrich	1000	21.5± 0.03
Silicon oil	Aldrich	10 000	21.5± 0.03

The name silicone was given by Kipping in 1901 (Elschenbroich and Salzer, 1992) to describe new compounds of the generic formula R_2SiO. These were rapidly identified as being polymeric and actually corresponding to polydialkylsiloxanes. The

name was adopted by the industry and usually refers to polymers with the formulation in Figure 2.1, where R = Me (methyl group).

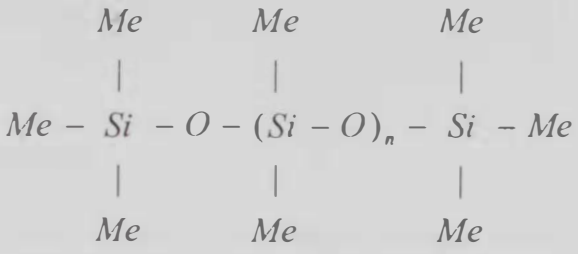

Fig 2.1 Chemical formula of silicone oil (where n=0, 1...)

Silicon oil has many synonyms, such as: alpha-Methyl-omega-methoxypolydimethylsiloxane; carboxypropyldimethyl; Dimethylpolysiloxane hydrolyzate; Polydimethyl silicone oil; Polydimethylsiloxane, Polyoxy (dimethylsilylene), Silicon and Siloxane.

The accompanying number of the Silicone (50, 100, 500, 1000, 10 000) is the viscosity value in centipois, which is correlated reciprocally to the silicon's density, which depends on the molecular weight only. Molecular weight is dependent on the n value in Figure 2.1 (Valignat et al., 1999)

Silicon oils are described as hydrophobic liquids and they have the property of completely wetting the most solid surfaces, since they have a low surface tension equal to 21.5 dyn/cm. With the methyl groups pointing to the outside, that gives very hydrophobic films and good spreading area on most surfaces.

The reason behind the extraordinary properties of silicon materials may be traced back to the idiosyncrasies of the Si-O-Si (Siloxane) bond. The high flexibility

of $(-Me_2SiO-)_n$ chains suggests low barriers of conformational changes (Elschenbroich and Salzer, 1992).

Silicon oil has many advantages, such as high thermal stability and small temperature coefficients for viscosity. These advantages are a result of its structure (Elschenbroich and Salzer, 1992).

2.1.2 Other liquids

Eight liquids were chosen in the study of low-rate dynamic contact angle and contact ratio. Selection of these liquids was based on the following criteria: 1) liquids should include a wide range of intermolecular forces; 2) be non-toxic; and 3) surface tension should be higher than the anticipated solid surface tension (Neumann et al., 1974). The physical properties and surface tensions of these liquids are listed in Table 2.2. They are, in order of increasing surface, diethylene glycol, 3-pyridylcarbinol, ethylene glycol, diiodomethane, 2,2-thiodiethanol, formamide, glycerol and water.

Table 2.2 Supplier, purity, and surface tension of the liquid used (all data provided by the suppler)

Liquid	Supplier	%Purity	Density (g/cm^3)	$\gamma_{lv}(mJ/m^2)$
diethylene glycol	Aldrich	99	1.118	44.68 ± 0.03
3-pyridylcarbinol	Aldrich	98	1.124	47.81 ± 0.03
ethylene glycol	Aldrich	99+	1.113	48.66 ± 0.06
diiodomethane	Aldrich	99	3.325	49.98 ± 0.02
formamide	Aldrich	99.5+	1.134	59.08 ± 0.04
glycerol	Baker analyzed	99.8	1.258	63.13 ± 0.10
Water	Lab. prepared	double distilled	0.977	72.70 ± 0.09

2.2 Solids

2.2.1 Soda-lime glass

Soda-lime glass (SiO_2) slides were used in the study of dynamic contact area. Soda-lime glass slides measuring 26 x 26 mm were obtained from Menzel-Glaser Company Geschnitten, Germany.

Soda lime glass, commonly known as window glass, is the most commonly used substrate. Microscope slides are commonly made from this glass, either using a float glass process or a draw glass process. In the case of a float glass process, the glass is cooled over a bath of molten tin, enriching its "float" side with tin oxide. Both the float and draw glass forming processes result in a flat glass sheets that are smooth on a molecular scale, requiring no further polishing. Soda-lime glass contains about 13% sodium oxide. This component is highly soluble in water, reacting to form sodium hydroxide, and this gives glass its hydrophilic property. This reaction occurs in ambient air. The humidity in the air will generate a coating of sodium hydroxide, coating the surface of the glass. This layer may interfere with adhesion to the glass surface and it is best removed by rinsing in water. Another effect of the formation of sodium hydroxide is its reaction with carbon dioxide in air, leading to the formation of a white sodium carbonate powder on the glass surface, also referred to as "blooming" (Website 3).

Cleaning process

Cleaning glass is a very strict process, because glass can be polluted very easily, and catches grime or chemicals from the air (Berg, 1993). The method of the cleaning is tested by using SEM technique. The procedure for the efficient cleaning of glass is as follows:

1. Immersion in high concentration chromic acid solution ($K_2Cr_2O_7 + H_2SO_4$) for 4-6 hour's.
2. Rinse with distilled water
3. Rinse with acetone.
4. Allow to dry by placing glass slide in a vacuum-oven for ½ hr at 90°C to allow evaporation of acetone.
5. Cooling the slides in a vacuum.
6. The slides are carefully transferred to the dissector, where they are stored for a short time period until the time of use.

Slides are used only for a single measurement. The cleanness of glass is tested using SEM as shown in Figures 2.2 and 2.3.

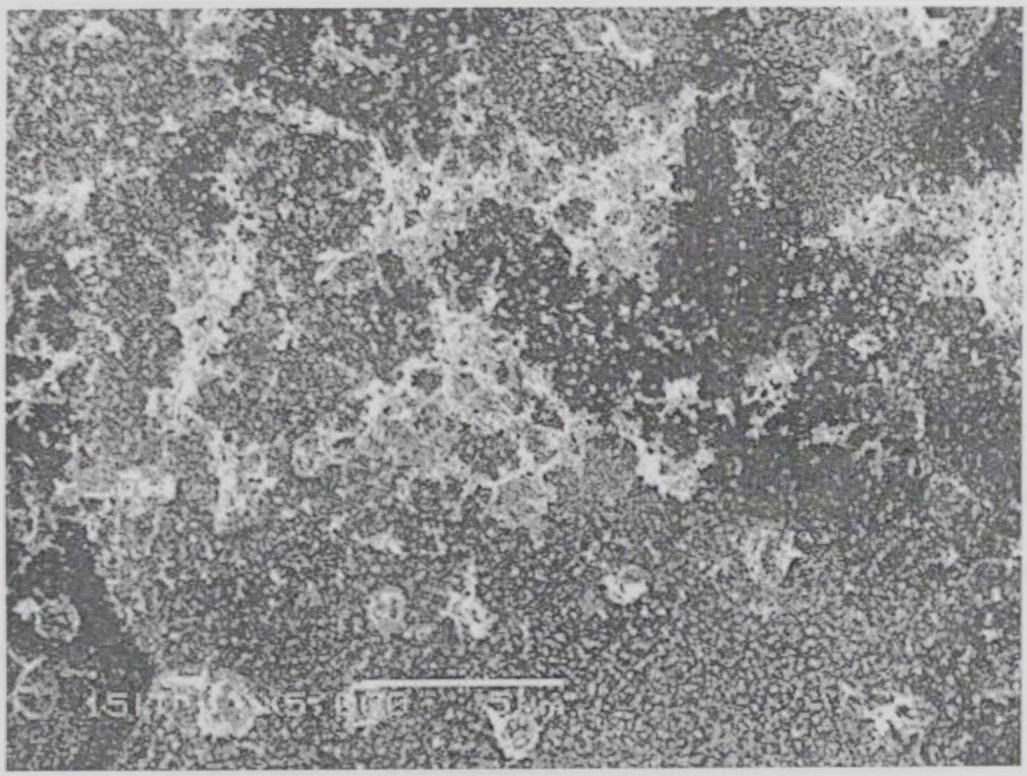

Fig 2.2 Unclean glass surface (before cleaning) showing grime and impurities

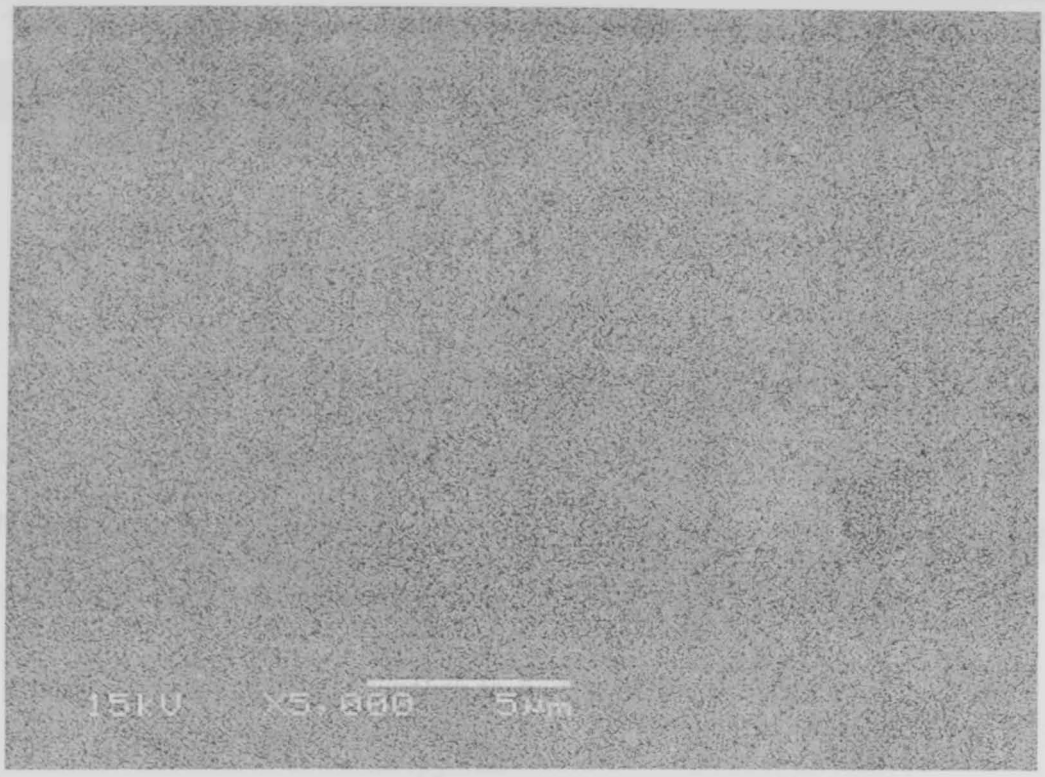

Fig 2.3 SEM image of clean glass showing no particles on the surface

2.2.2 Poly(Methyl methacrylate) (PMMA)

In this work two types of PMMA were used based on source. In contact area measurements the ready made PMMA slides were used. For contact angle and contact ratio measurement glass slides that coated by PMMA layer were used.

Poly(methyl methacrylate) or PMMA is commercially available under trade names such as Perspex or Plexiglass. For the dynamic contact area study, PMMA slides with 26 x 26 mm were used. The physical and chemical properties of PMMA are shown in Table 2.3.

Table 2.3 Physical properties of PMMA (Website 1)

Materials	State	Characterization
PMMA	Solid	Formula: $C_5H_8O_2$ Density: 1.188 (which is less than half that of glass (approximately 2.6 g/cm3) Molecular Weight: 100.117 white (as beads), highly transparent, crystal like solid similar to glass at room temperature, and light weight.

PMMA is a polymer material. Basically, it is a long chain polymer made from Methyl methacrylate (MMA) $C_5H_8O_2$. The chemical composition is shown in Figure 2.4. PMMA is solid at room temperature.

Cleaning process

Commercial PMMA slides are used. Slides are usually covered by an adhesive sheet of paper to protect them from scratch (Fig 2.5)

The PMMA cleaning method quality is examined by using SEM (Fig 2.6). Effective cleaning is achieved as follows:

1. Immerse the PMMA slides in Ethanol for 2 hours.
2. Rub the surface with a soft sponge to get rid of any gum layer (or the sides should be rubbed gently with a soft sponge in order to get rid of adhesive layer).
3. Rinse the PMMA slides with water and immerse the slides in deionized H_2O for at least five minutes.
4. Finally allow slides to dry in atmospheric air just before the start of the experiment.

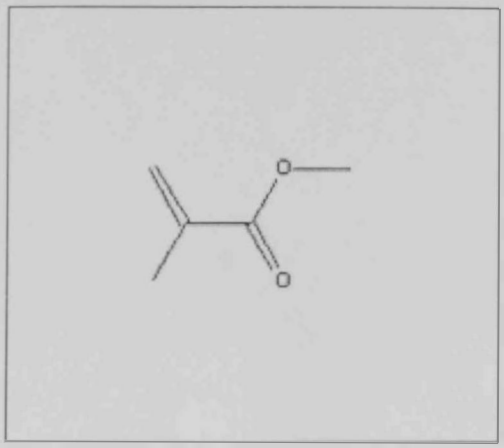

Fig 2.4 Chemical composition of Methyl-meth-acrylate

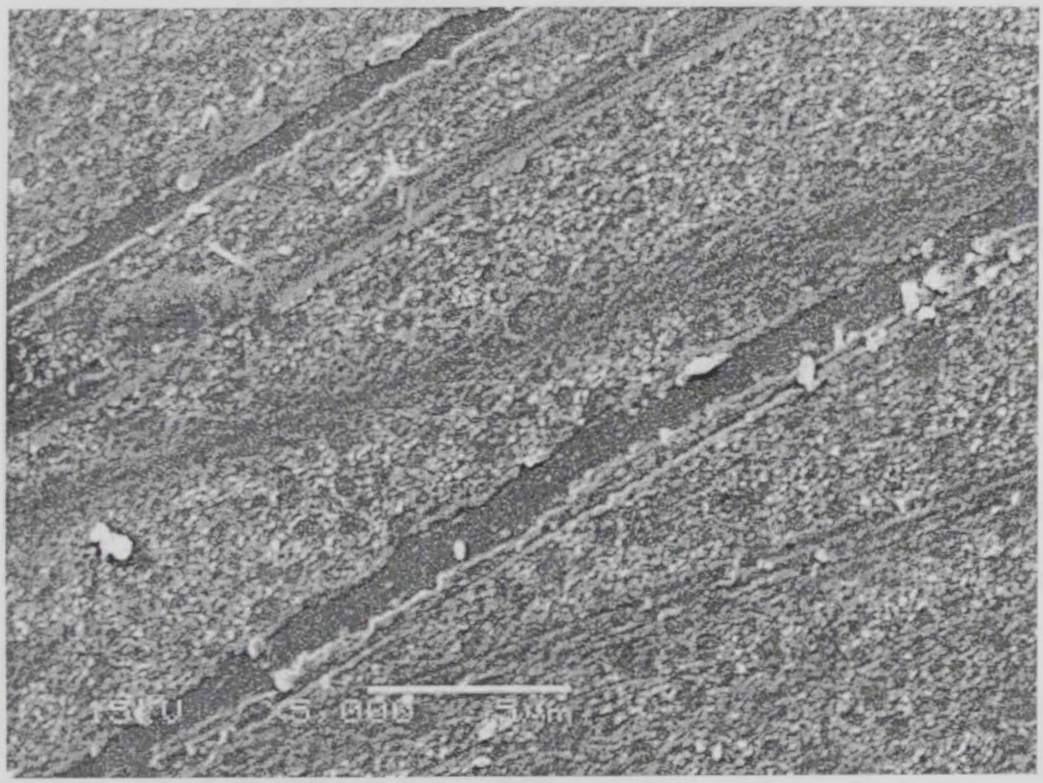

Fig 2.5 Unclean PMMA surface with adhesive layer

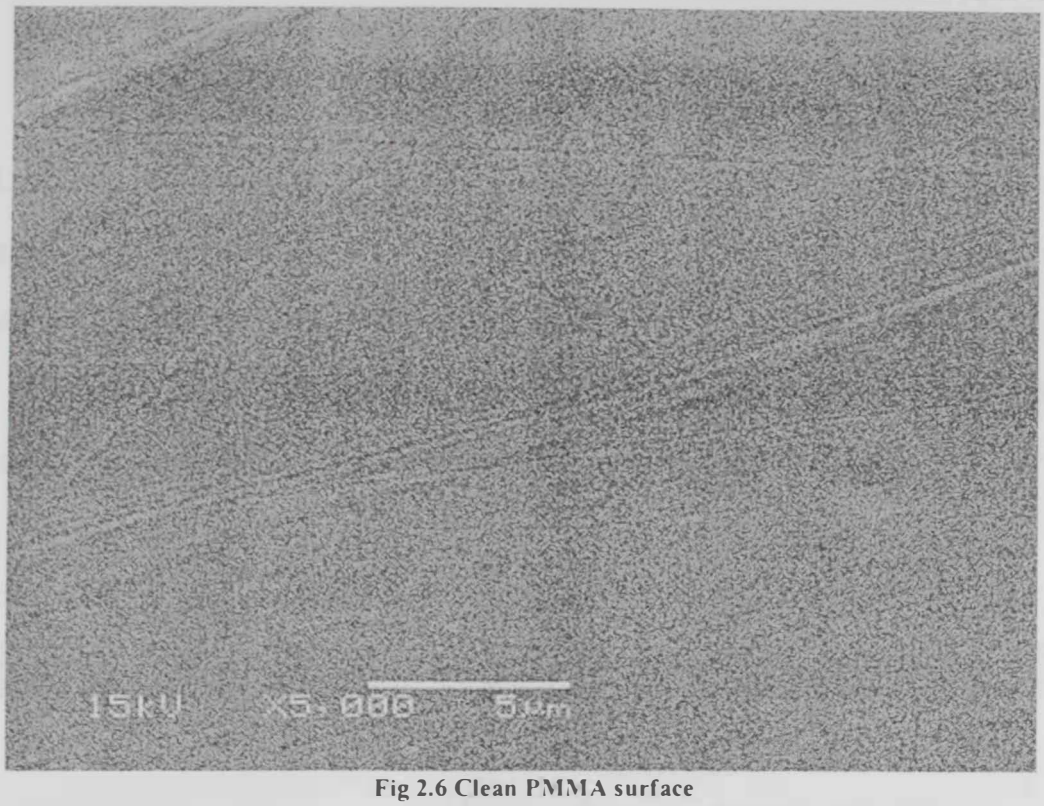

Fig 2.6 Clean PMMA surface

For the low-rate dynamic contact angle and contact ratio study, PMMA beads (cat# 04553, MW 5 75,000) were obtained from Polysciences Company, Warrington, PA, USA. A 0.5 % PMMA/toluene solution was prepared using toluene (Sigma-Aldrich, 99.8% HPLC grade) as the solvent. Glass slides were selected as the substrate for low-rate dynamic contact angle and contact ratio measurements. They were obtained as square slides (26 x 26 mm). Each slide was then soaked in chromic acid for at least 24h., rinsed with distilled water, and dried inside an oven at 90° C before coating with polymer.

The PMMA-coated surfaces were prepared by a solvent casting technique: a few drops of the 0.5% PMMA/toluene solution were deposited on a dried glass slide; the solution spread and a thin layer of the PMMA formed on the slide surface after the toluene evaporated. This preparation produced good quality coated surfaces.

2.2.3 Polystyrene (PS).

For the dynamic contact area study, sheets of Polystyrene, obtained from Central Laboratories Unit (CLU), United Arab Emirates UAE, were used. The physical and chemical properties of PS are shown in Table 2.4 and the chemical composition is shown in Figure 2.7.

Polystyrene is an amorphous, thermoplastic polymer and white powder. A free radical growth polymer, styrene is easily polymerized by benzoyl peroxide.

Table 2.4 Physical properties of PS (Website,1)

Material	State	Properties
PS	Solid	Formula: C_8H_8 Density: 1.05 Molecular Weight: 104.1512 Melting Point: 240 °C Refractive Index :1.59 White powder.

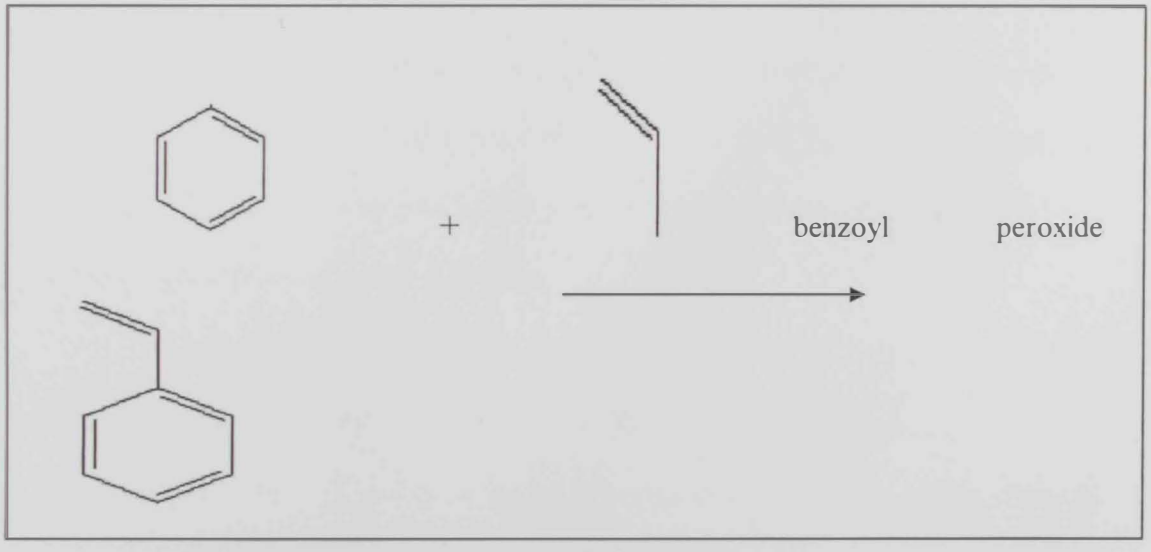

Fig 2.7 Constituting polystyrene

Cleaning process

A clean sheet of Polystyrene is used in this study, obtained from Bibby sterilin Led Company, UK. Sheets were examined under the SEM to make sure that the surfaces were smooth and free from any residues (Fig 2.8)

For the low-rate dynamic contact angle and contact ratio study, PS beads (cat# 00574, MW 125,000-250,000) were obtained from Polysciences Company, Warrington, PA, USA. A 0.5 % PS/toluene solution was prepared using toluene (Sigma-Aldrich, 99.8% HPLC grade) as the solvent. Glass slides were selected as the substrate for low-rate dynamic contact angle and contact ratio measurements. They were obtained as square slides (26 x 26 mm). Each slide was then soaked in chromic acid for at least 24h., rinsed with distilled water, and dried inside sn oven at 90° C before coating with polymer.

The PS-coated surfaces were prepared by a solvent casting technique: a few drops of the 0.5% PS/toluene solution were deposited on a dried glass slide; the solution spread and a thin layer of the PS formed on the slide surface after the toluene evaporated. This preparation produced good quality coated surfaces.

Fig 2.8 PS with clean surface

2.3 Experimental procedures

2.3.1 Dynamic contact area measurement procedures

The experimental setup is shown in Figure 2.9. To conduct the experiment, the liquid was charged into a 5-μl syringe obtained from SGE International Company, Australia. The syringe was attached to a metal stand and mounted vertically by a micromanipulator on top of the substrate.

The micromanipulator is used to adjust the position of the needle tip of the syringe carefully above the clean glass slide. The tip of the syringe was positioned a few millimeters from the surface of the glass to eliminate any impact effect when the droplet was released. The droplet volume was selected to be 1.5 μl so that the effect of gravity is negligible (Bond number (B_o) = 0.23 << 1).

The syringe is cleaned by immersing in acetone and allowing to dry in an oven. Before conducting the experiment the syringe is flushed with the liquid of interest once or twice. At least seven measurements were taken with each liquid over the same solid.

The solid substrate was placed on an optical stand within the focus of a half-inch CCD digital video camera (JVC TK-c1380, Japan) with 10x eyepiece magnification, placed underneath the glass slide. The camera was connected to a video recorder, which was in turn connected to an image analysis system (analySIS soft Imaging System, GmbH ltd, Germany). The light was source was ring light fiber optics (model LG-R66. OLYMPUS – JAPAN). Using fiber optic light reduces the heat produced by normal light. Heat may affect the surface tension of the liquid and also produce a blurred image. All experiments were carried at ambient conditions, i.e., 25±1°C and 47%±3%RH.

Typical images frames acquired by the image analysis system are displayed in Figure 2.10 below. The images were grabbed by the image analyzer from which the contact area was digitized and measured as a function of time

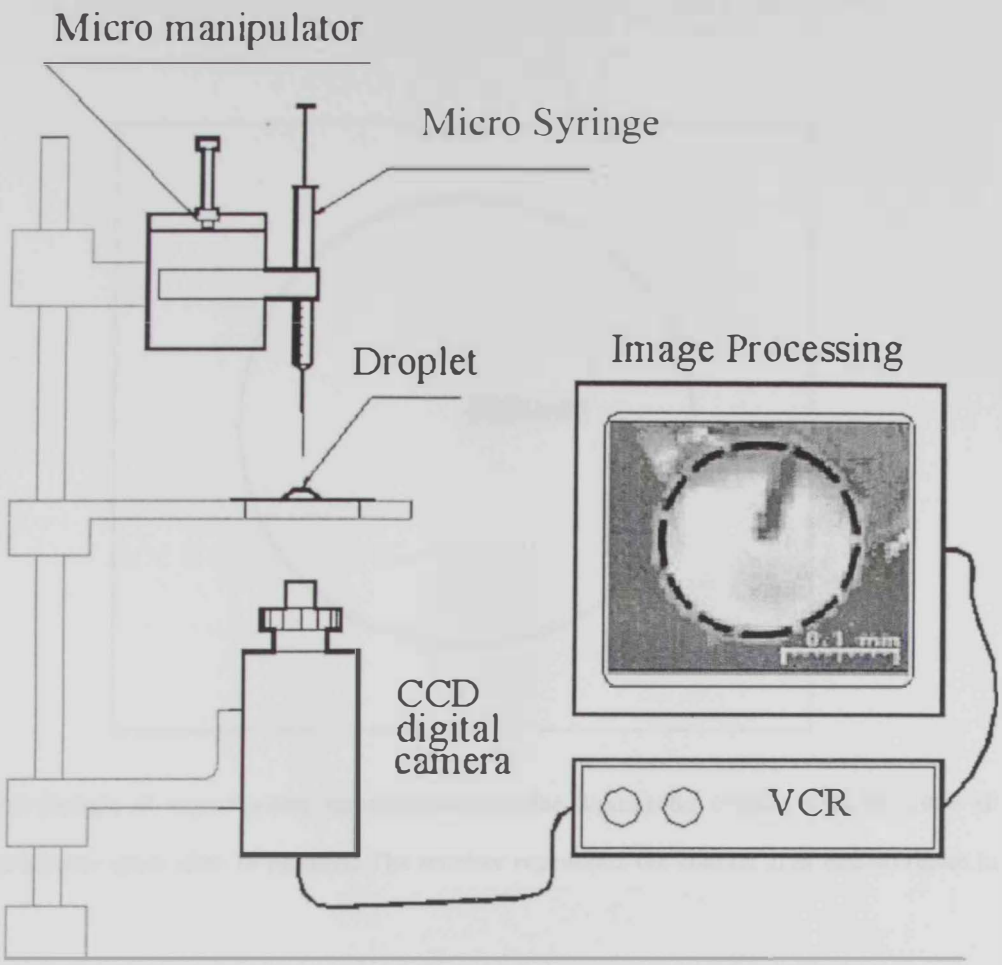

Fig 2.9:Shows the experimental setup for contact area measurement

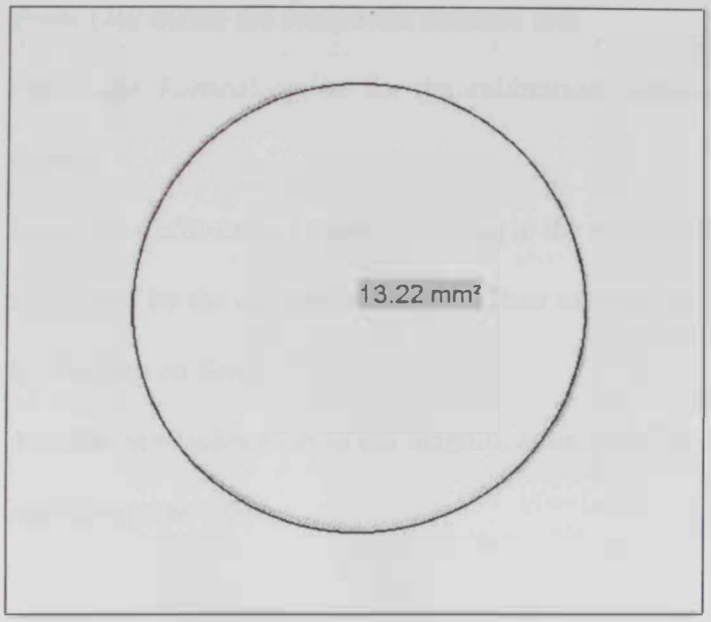

Fig. 2.10 Sample of experimental measurements of the liquid/solid contact area for 1000 cP Silicone oil over glass after 18 minutes. The number represents the contact area measurement in mm

Software and Calibration (dynamic contact area)

The magnification is calibrated using a calibration sample image analysis software (analySIS 3.0 Soft Imaging System GmbH Germany March 1999)

Calibration methods:

1. The standard calibration sample (Micrometer) is placed on the 10X objective (Fig 2.11). We used 10X due to search of the wide spreading area.
2. Acquire the focused and enhanced image from the microscope
3. Snapshot the image
4. From the image menu select *Set Input*

5. Click on the XY Calibration tab and Insert the required *Magnification*
6. From *Unit* define the calibration distance unit.
7. Select the *Vertical* option for the calibration distance to be defined
8. Insert the *Calibration Length* according to the selected distance as defined by the calibration sample. Then save the calibration by clicking on *Save*
9. Add the new calibration to the magnification table by clicking *Add* then press *OK*

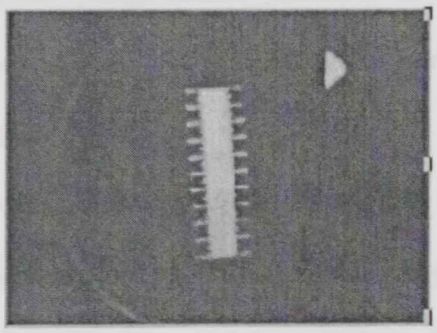

Fig 2.11 Shows the magnification of 10x

2.3.2 Low-rate dynamic contact angle and contact ratio measurement procedures

The experimental set-up schematic for low-rate dynamic contact angle and contact ratio measurements is shown in Figure 2.12. Sessile drop contact angle measurements using ADSA-P were performed dynamically, by using a motor driven syringe to pump the liquid steadily into the sessile drop from below the surface (Kwok et al., 1998). The dynamic receding contact angle measurements can be performed by pulling the syringe plunger of a motorized syringe mechanism, leading to a decrease in drop volume. A schematic of this mechanism is shown in Figure 2.12. Normally, 5 up to 7 dynamic contact angle measurements were performed on a new solid surface each time. In this thesis, all contact angles were measured at 23.0° C.

As mentioned before, the liquid is supplied into the sessile drop from below the solid surface using a motorized syringe device (Kwok et al., 1998). A hole of about 1 mm a diameter was made in order to make such an experimental procedure possible. The method of pumping liquid from below the surface was pioneered by Oliver et al. (1983). This approach has potential for avoiding drop vibrations and for measuring true advancing contact angles without disturbing the drop profile. To avoid leakage of liquid from the gap between the a stainless steel needle and the surface hole, Teflon tape was wrapped around the end of the needle before insertion into the hole.

In the dynamic experiments, by using a Hamilton syringe with a stainless steel needle, an initial liquid drop of about 0.3 cm radius was carefully deposited to cover the hole on the surface. This was to ensure that the drop will increase axisymmetrically in the centre of the image field when liquid is supplied from the bottom of the surface and will not hinge on the edge of the hole (Amirfazli, 2001;

Kwok, 1998). By adjusting the voltage from a voltage controller, the motor in the motorized syringe mechanism was set to a specific speed leading to push the syringe plunger and then increasing in drop volume and the three-phase contact radius. A series of pictures of the growing volume drop were then recorded by the computer. For each low-rate dynamic contact angle experiment at least 20 images were normally taken.

ADSA-P determines the advancing dynamic contact angle and the three-phase contact radius for each image as a function of the three-phase contact radius (i.e. location on the surface) can be obtained. Besides that, the change in the contact angle, drop volume, drop surface area, and the three-phase contact radius can also be studied as a function of time.

The contact ratio of the liquid drop on the solid surface can be obtained as a function of time from Equation 3.1, where the radius of the liquid drop before contact with the solid surface can be found from the volume of the liquid drop, and the three phase contact radius is one of the ADSA-P outputs.

It should be noted that there is another advantage to measuring contact angles as a function of the three phase contact, which that the quality of the surface is observed indirectly in the measured contact angles. When the measured contact angles are irregular and inconsistent as a function of surface location, the solid surface is not very smooth. When the measured contact angles are essentially constant as a function of surface location, the solid surface can be considered smooth enough. The mean contact angle for a specific rate of advance can be obtained by averaging the contact angles. The mean contact ratio for a specific rate of advance can also be obtained by averaging the contact ratios.

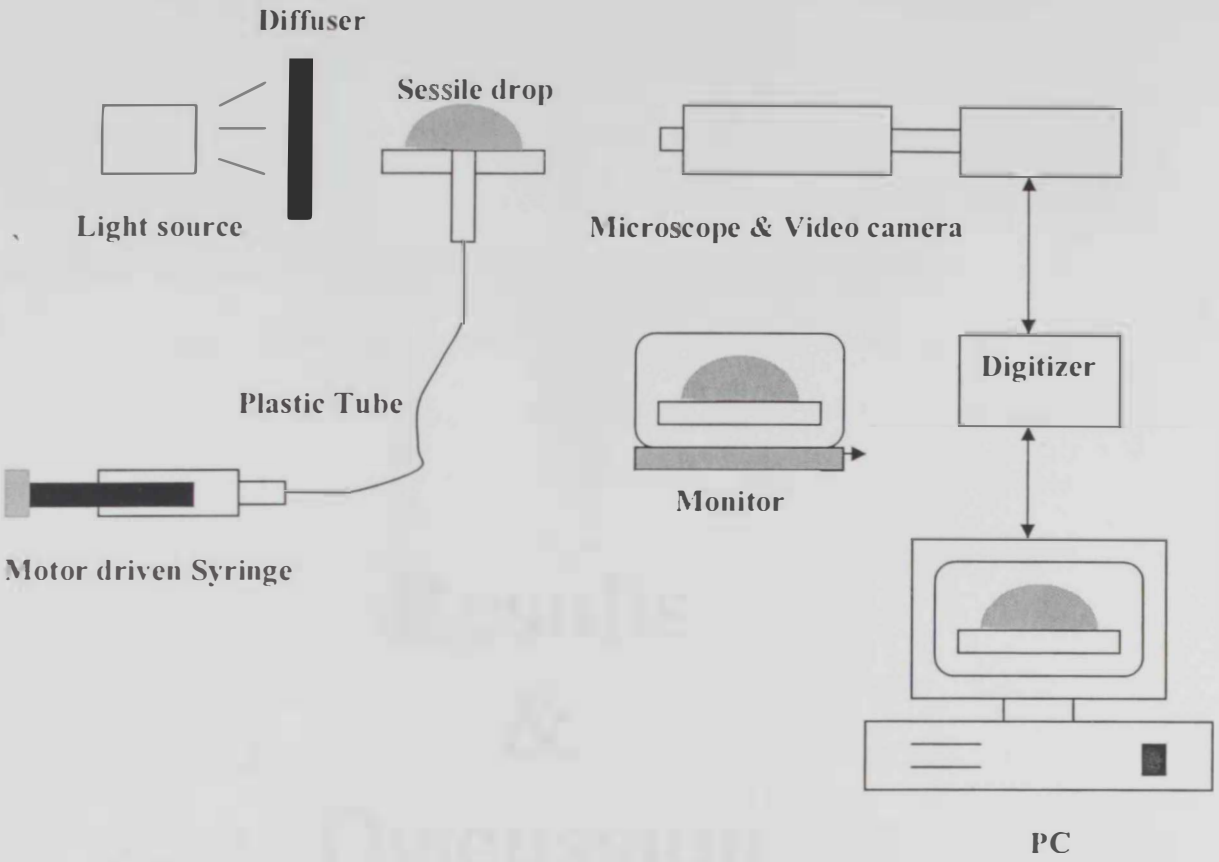

Fig 2.12 The experimental set-up schematic for low-rate dynamic contact angle and contact ratio measurements

Chapter 3

Results & Discussion

3.1 Contact ratio verses contact angle

Ever since the pioneering observation of Hardy (1919), it is noted that ceaseless efforts have been advanced to formulate the rate of spontaneous spreading. In view of Young's equation, in which the contact angle θ and liquid surface tension γ_{lv} are the only measurable parameters, the contact angle has been widely conceived as a thermodynamic quantity. Accordingly, θ remained to be the main focus of most theoretical and experimental investigations. The rate of change in the contact angle has been commonly used as the relevant parameter of spreading dynamics in spite of difficulties associated with contact angle measurements that are well recognized in the literature (Marmur, 1983; Berg, 1993; de Ruijter et al., 1998). Although measuring contact angle seems easy to conduct, contact angle phenomena are complicated (Amirfazil, 2001; Kwok, 1998; Neuman, 1974).

Several restrictions were imposed on solid surfaces in deriving Young's equation: the solid should be smooth, homogenous, rigid and inert with respect to the liquid used (Lam, 2001). Practically all solid surfaces have some degree of heterogeneity and roughness and, hence, for the same system the contact angle can have different values depending on the experiment conditions (Budziak, 1992; Amirfazil, 2001; Kwok, 1998).

The thermodynamic equilibrium angles on rough as well as heterogeneous surfaces are called Wenzel angle (Wenzel, 1936; Myers, 1999; Oliver and Mason, 1980) and Cassie angel (Wenzel, 1936; Myers, 1999; Miracle-Solé, 2002), respectively, and they are not equal to Young's equation contact angle (θ_Y) (Amirfazil, 2001; Kwok, 1998; Neuman, 1974; Budziak, 1992). Up to now, there are no general criteria to show how smooth a solid surface should be for the measurement

of contact angle that is not affected by the roughness of the solid surface (Kwok, 1998).

Line tension (a free energy of the three phase contact line, or as a force operating in the three phase line (Oktatan, 2002)) is another important factor that has a great effect on the contact angle measurements and has its own complexities (Amirfazil, 2001; Budziak, 1992; Amirfazli and Neumann, 2004).

3.1.1 Contact ratio

In this part of the thesis, a new precise measurement for wettability defined as the *contact ratio* (A^*) is introduced. Figure 3.1 shows a schematic of liquid drop on a solid surface, where R_c is the radius of the drop-solid substrate contact area, ρ is the radius of curvature, and h is the height of the drop with respect to the surface.

Contact ratio is a ratio of contact area of the liquid drop with solid surface to the surface area of the liquid sphere before spreading (Fig. 3.1):

$$A^* = \frac{A_c}{A_s} \tag{3.1}$$

where A_c is a contact area of the liquid drop on the solid surface:

$$A_c = \pi R_c^{\,2} \tag{3.2}$$

where R_c is the radius of the contact area of the liquid drop on the solid.

A_s represents the surface area of the drop before spreading:

$$A_s = 4\pi R_0^2 \tag{3.3}$$

where R_0 is the radius of the drop sphere before spreading.

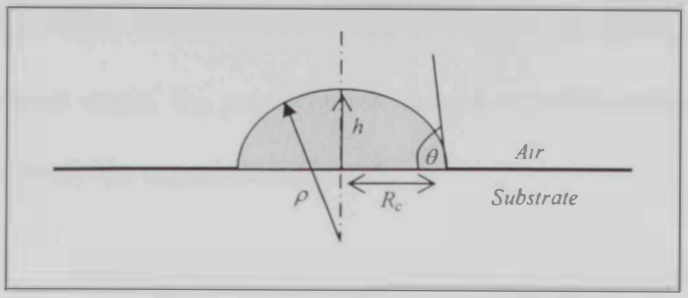

Fig. 3.1: Schematic representation of the spreading drop, R_c is the radius of the drop-substrate contact area, ρ is the radius of curvature, and h is the height of the drop with respect to the surface

The relation between contact angle and contact ratio can be derived from the definition of the contact ratio and the spherical cap approximation relation (Eqn. 3.4) that relates the volume of the spherical droplet and the radius of the contact area of the drop to the contact angle, as follows:

$$\theta = \frac{4V}{\pi R_c^{\ 3}} \tag{3.4}$$

where V is the drop volume given as:

$$V = \frac{4}{3}\pi R_0^3 \tag{3.5}$$

One should mention that the spherical cap approximation (Eqn. 3.4) can only be applied for low contact angle value, where $\theta < 90^{\circ}$. Substituting Equations 3.2 and 3.5 in equation 3.4 and use the definition of contact ratio (Eqn. 3.1) and surface area (Eqn 3.3) reduces A^* to be a function of θ only:

$$A^* = \left(\frac{2}{3}\theta\right)^{-2/3} \tag{3.6}$$

3.1.2 Experimental validation of Young's relation

In order to verify that the measured contact angles are the true contact angles i.e Young's contact angle, θ_Y, one requires careful experimentation and a certain methodology to verify the experimental results.

I. Methodology to verify the experimental results

The methodology is based on the finding of Li et al. (1992, 1993) that, $\gamma_{lv}\cos\theta$ depends only on γ_{lv} (the liquid) and γ_{sv} (the solid). Figure 3.2 (Kwok, 1998) shows experimental contact angle values in a plot of $\gamma_{lv}\cos\theta$ vs. γ_{lv} for different liquids. It can be seen that, for a given solid surface, $\gamma_{lv}\cos\theta$ changes smoothly and systematically with γ_{lv} (the solid surface tension, γ_{sv} , of a given solid surface is expected to be constant, i.e. independent of the choice of the testing liquid used). Figure 3.2 also implies that $\gamma_{lv}\cos\theta$ depends only on γ_{lv} at constant γ_{sv} . Replacing the hydrophobic FC-721 solid surface with the hydrophilic PET surface shifts the curve in a regular manner. Therefore, one has to conclude that the values of $\gamma_{lv}\cos\theta$ depend only on γ_{lv} (the liquid) and γ_{sv} (the solid), independent of any specific intermolecular forces of the liquids and solids (Kwok, 1998; Li and Neumann, 1992; Li et al., 1993), i.e.:

$$\gamma_{lv}\cos\theta = f(\gamma_{lv},\gamma_{sv}) \qquad (3.7)$$

where f is an unknown function. Because of Young's equation, the experimental contact angle patterns (Fig.3.2) imply, in light of Equation 3.7, that the solid-liquid interfacial tension γ_{sl} depends only on the liquid-vapor γ_{lv} surface tensions and solid-vapor γ_{sv} surface energy. Combining Young's equation (Eqn.1.1) with Eqn.3.7 yields:

$$\gamma_{sv} - \gamma_{sl} = f(\gamma_{lv}, \gamma_{sv}) \tag{3.8}$$

and consequently

$$\gamma_{sl} = \gamma_{sv} - f(\gamma_{lv}, \gamma_{sv}) = F(\gamma_{lv}, \gamma_{sv}) \tag{3.9}$$

where F is as yet another unknown function.

Thus, one can simply change the contact angle by changing either γ_{lv} or γ_{sv}. While the specific intermolecular forces determine the primary surface tensions of liquids and solids, they do not have any additional and independent effects on the contact angles, in the context of Young's equation.

Figure 3.3 shows experimental contact angle results of water and glycerol on PMMA and PS solid surfaces, and published contact angle values of different liquids on PMMA and PS solid surfaces, in a plot of $\gamma_{lv}\cos\theta$ vs. γ_{lv} . It can be seen that, for a given solid surface (PMMA or PS), $\gamma_{lv}\cos\theta$ changes smoothly and systematically with γ_{lv}. Since the solid surface energy, γ_{sv}, of a given solid surface is expected to be constant, i.e. independent of the choice of the testing liquid used, replacing the solid surface from the PMMA to PS shifts the curve in a very regular manner. Figure 3.3 implies that $\gamma_{lv}\cos\theta$ depends only on γ_{lv} at constant γ_{sv} and the specific intermolecular forces of the liquids and the solids do not have additional and independent effects on the contact angles. Thus, the contact angle value can be changed, and based on Young's equation, so can the solid-liquid interfacial tension, by simply changing either the liquid or the solid. In conclusion, the measured contact angles, based on the mentioned metrology, are the true contact angles and there was no additional and independent effect of intermolecular forces on the measured contact angles.

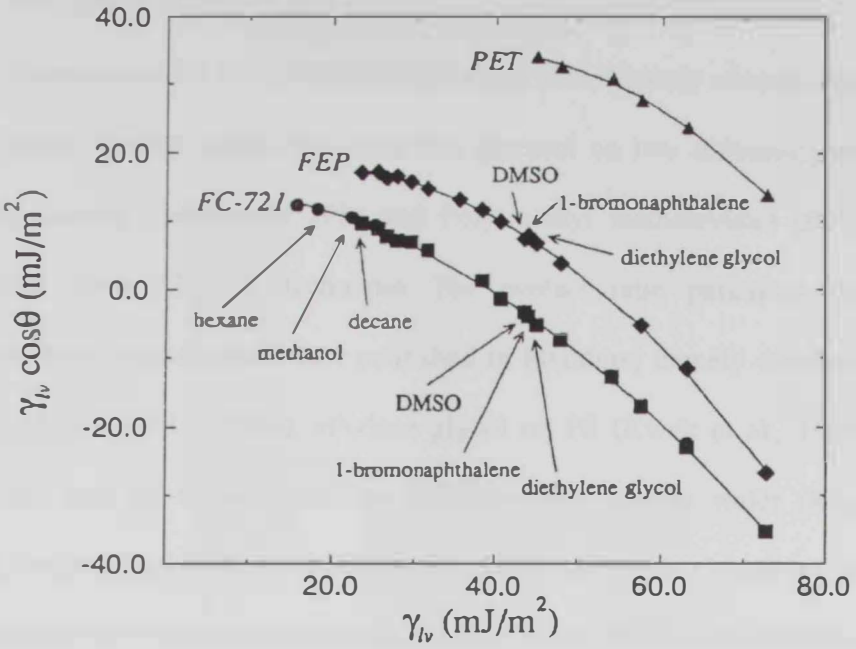

Fig. 3.2 γ_{lv}cosθ vs γ_{lv} for three well prepared inert solid surfaces: FC-721-coated mica, heated pressed Teflon FEP (fluorinated ethylene propylene), and poly(ethylene terephthalate) PET. The smoothness of the curve suggests that γ_{lv}cosθ depends only on γ_{lv} and γ_{sv} (Kwok, 1998)

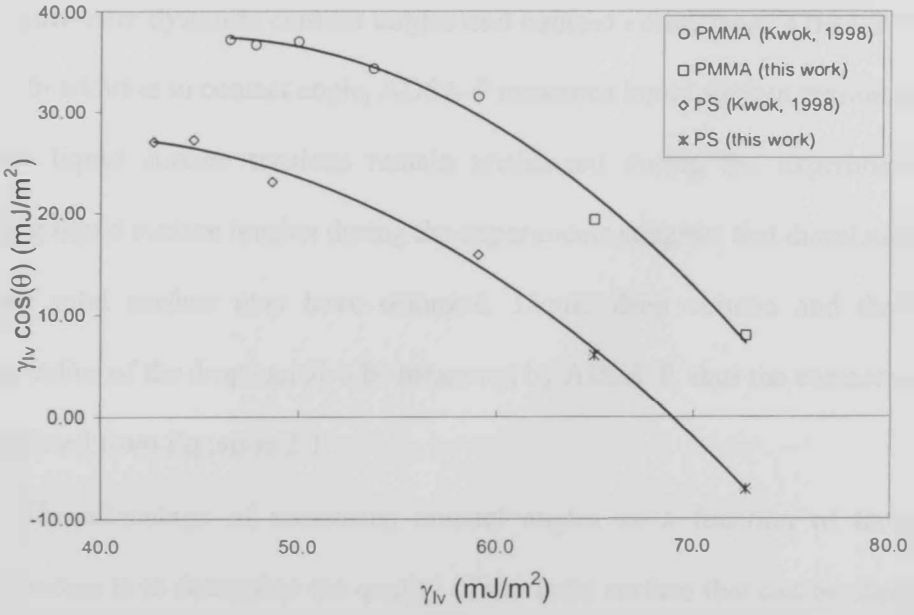

Fig 3.3 γ_{lv} cosθ vs. γ_{lv} for Poly(methyl methacrylate) (PMMA) and Polystyrene (PS). The smoothness of the two curves suggests that γ_{lv} cosθ depends only on γ_{lv} and γ_{sv}

3.1.3 Experimental results

Experimentally, the measurements of low rate dynamic contact ratios and low rate dynamic contact angles for water and glycerol on two different polymer solid surfaces, namely Polystyrene (PS) and Poly(methyl methacrylate) (PMMA) were conducted using ADSA-P technique. The contact ratio parameter was further validated using experimental data published in literature, namely diiodomethane on PMMA (Kwok et al.; 1998c), ethylene glycol on PS (Kwok et al., 1998d), water, formamide and 2,2-thiodiethanol on FC-725-coated silicon wafer (Kwok et al., 1998b), 3-pyridylcarbinol on P(MMA/EMA, 30/70) (Kwok et al., 1999a), triacetin on Poly(propene-alt-N-(n-hexyl)maleimide) (Kwok et al., 1998a) and diethylene glycol, glycerol and formamide on P[S-(H/CM)] (Kwok et al., 1999b). The data were examined for low rate dynamic contact angles. Using contact radius and volume of the liquid, contact ratios were calculated.

I. Low–rate dynamic contact angles and contact ratios from ADSA-P

In addition to contact angle, ADSA-P measures liquid surface tension to insure that the liquid surface tensions remain unchanged during the experiments. The changing liquid surface tension during the experiments suggests that dissolution of the polymer solid surface may have occurred. Liquid drop volume and three-phase contact radius of the drop can also be measured by ADSA-P, thus the contact ratio can be calculated from Equation 3.1.

The advantage of measuring contact angles as a function of three-phase contact radius is to determine the quality of the solid surface that can be observed in the measured contact angles. Irregular and inconsistent values for the measured

contact angles will be seen as a function of the contact three-phase radius when the solid surface is not smooth (Kwok, 1998 ; Kwok and Neumann, 1999).

For specific experiments the mean contact angle can be obtained by averaging the contact angles when the contact angles are basically constant as a function of the three-phase contact radius and large volume of the liquids. The line tension has no effect on the measured contact angle of a large volume liquid drop (Duncan et al., 1995; Amirfazli et al., 1998).

Water on PS

Figure 3.4 shows a typical example of a low-rate dynamic contact angle experiment result namely, water on a PS solid surface. As mention in Chapter 2 (Materials and Methods), a small volume of the liquid drop is deposited from above, covering the solid surface hole completely. This procedure is to avoid hinging the drop at the edge of the hole, but this lead to the production of a contact angle smaller than the advancing contact angle. Figure 3.4 shows that linearly increasing the drop volume (Fig. 3.4.d) from approximately 0.05 cm^3 to approximately 0.07 cm^3, by the motorized-syringe mechanism, increases the contact angle, θ, (Fig3.4.b) from approximately 91.30° to 96.37° at essentially constant three-phase contact radius R (0.36 cm) as shown in Figure 3.4.c. This indicates that the measured contact angle is somewhere between advancing and receding. The initial drop front takes time, depends on the tested solid-liquid-vapour system, to start advancing. As the drop volume increases beyond a critical volume of 0.07 cm^3 causes the three-phase contact line to advance, with the contact angle θ essentially constant as contact radius R increases. Increasing the drop volume in this manner ensures the measured θ to be an advancing contact angle.

For this specific experiment (water over PS), averaging the measured contact angles after *R* reaches 0.36 cm (Fig. 3.4.c) is convenient since the contact angles are essentially constant. The drop is guaranteed to be in the advancing mode and line tension effects are negligible (Duncan et al., 1995; Amirfazli et al., 1998). Averaging the measured contact angles after *R* reaches 0.36 cm yields a mean contact angle of $95.56^{\circ}\pm0.80^{\circ}$ for water over PS. The surface tension-time plot for this experiment indicates that the surface tension of the water used keeps constant with time (72.83 mJ/m^2). This proves that no dissolution of the polymer occurs which causes γ_{lv} to change from that of the pure liquid (Kwok, 1998).

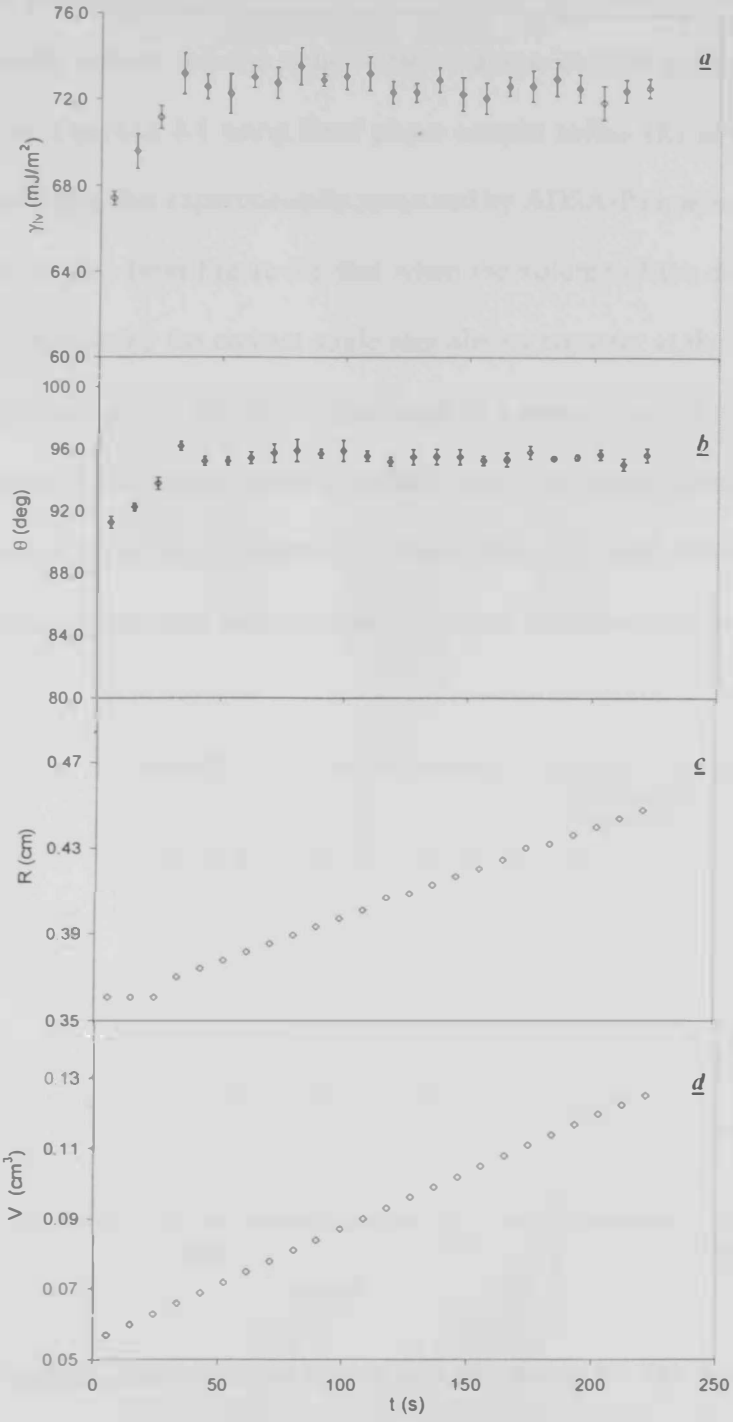

Fig 3.4 Time verses (a) Surface tension (b) Low-rate dynamic contact angle (c) Contact radius (d) Volume for low-rate dynamic contact angles experiment of water on a polystyrene

Figure 3.5 plots the volumes of the water liquid over PS solid surface against the contact angle values and the contact ratio values. contact ratios (A*) can be calculated from Equation 3.1 using three phase contact radius (R) and the volumes (V) of the liquid drop that experimentally measured by ADSA-P equipment.

It can be seen from Figure 3.5 that when the volume of the drop reach 0.07 cm^3 and keeps increasing the contact angle stay almost constant at the average value of 95.56°. Thus one can say that the contact angle is a property of the system because the system has only one unique value of contact angle (advanced contact angle). For the same range of liquid drop volumes i.e. larger than 0.07 cm^3, where the contact angle is constant, contact ratio remains almost constant at the average value of 0.52.

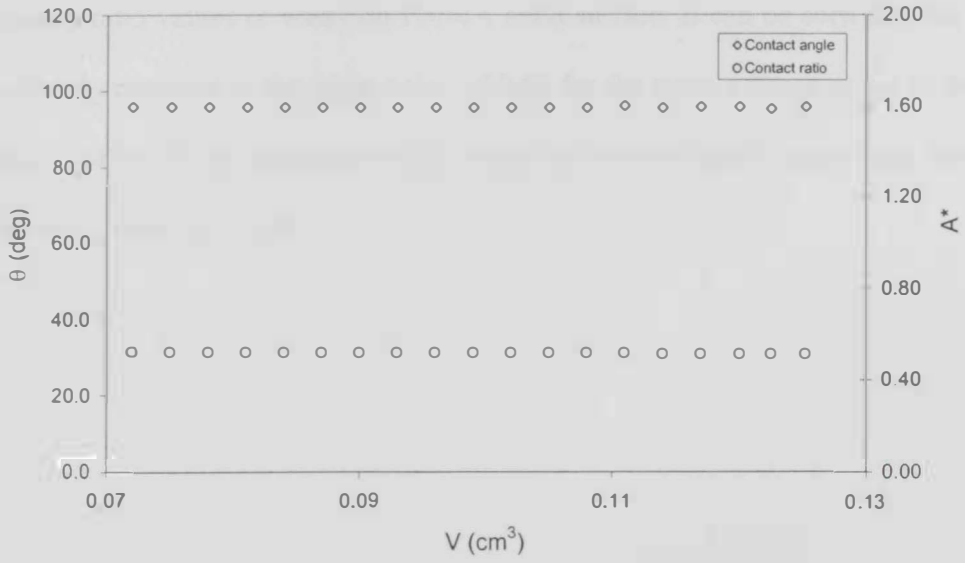

Fig 3.5 Volume against contact angle and contact ratio of water on PS. This figure shows that there is only one unique value of the contact ratio

Water on PMMA

The contact angle measurement experiment results of water on PMMA are shown in Figure 3.6. It shows that Linearly increasing the drop volume V (Fig. 3.6.d) from approximately 0.01 cm^3 to approximately 0.06 cm^3 by the motorized-syringe mechanism, increases the contact radius R from approximately 0.21 cm^3 to 0.40 cm^3 (Fig 3.6.c) at an essentially constant contact angle (mean contact angle: $83.68^{\circ}\pm0.70^{\circ}$) that is shown in Figure 3.6.b. The surface tension-time plot for this experiment indicates that the surface tension of the water used keeps constant with time (71.34 mJ/m^2). This proves that no dissolution of the polymer occurs that causes γ_{lv} to change from that of the pure liquid (Kwok, 1998).

Figure 3.7 plots the volumes of water against the contact angle values and the contact ratio values of water on PMMA solid surface. It can be seen that the contact ratio stay constant at the mean value of 0.60 for the same volume range of the water drop (0.01-0.06 cm^3 approximately), where the contact angle values keep constant at the mean value of 83.68°.

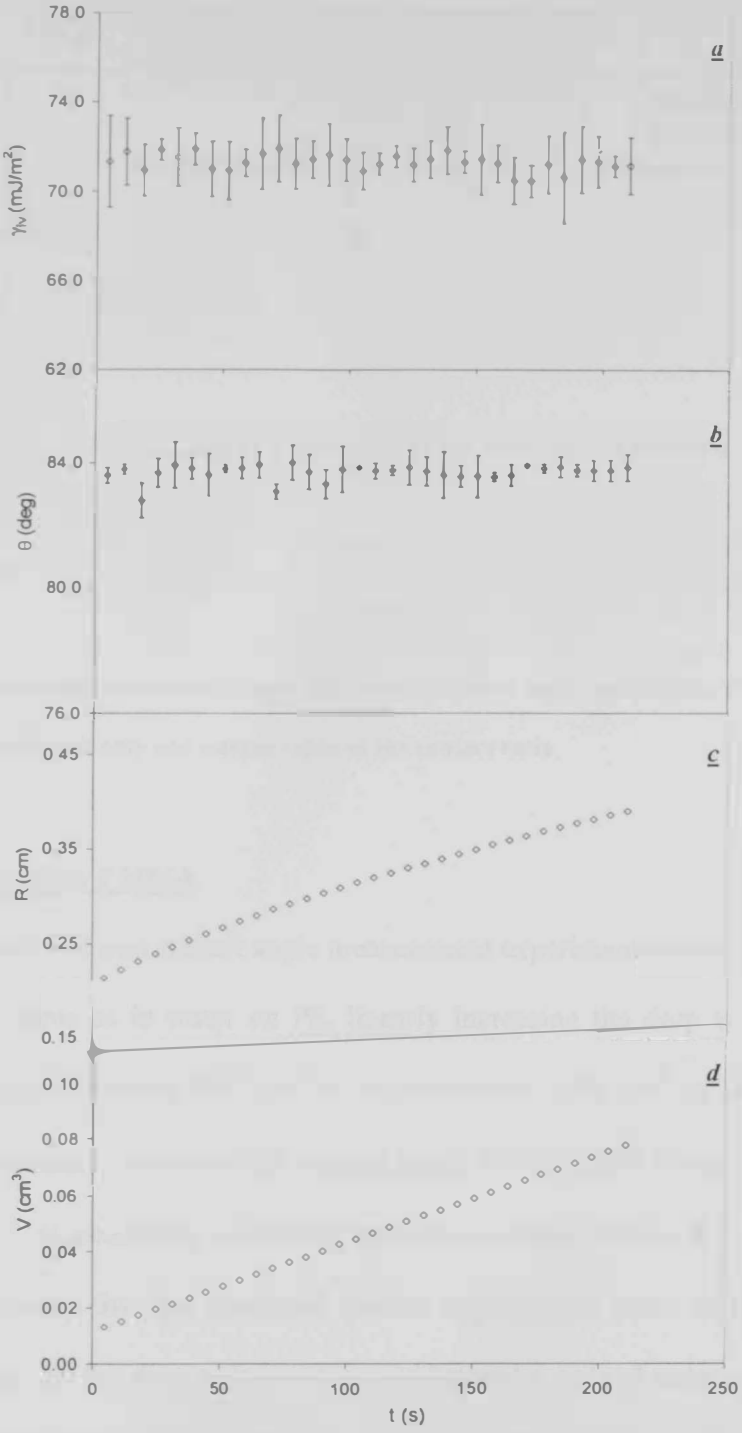

Fig 3.6 Time verses (a) Surface tension (b) Low-rate dynamic contact angle (c) Contact radius (d) Volume for low-rate dynamic contact angles experiment of water on PMMA

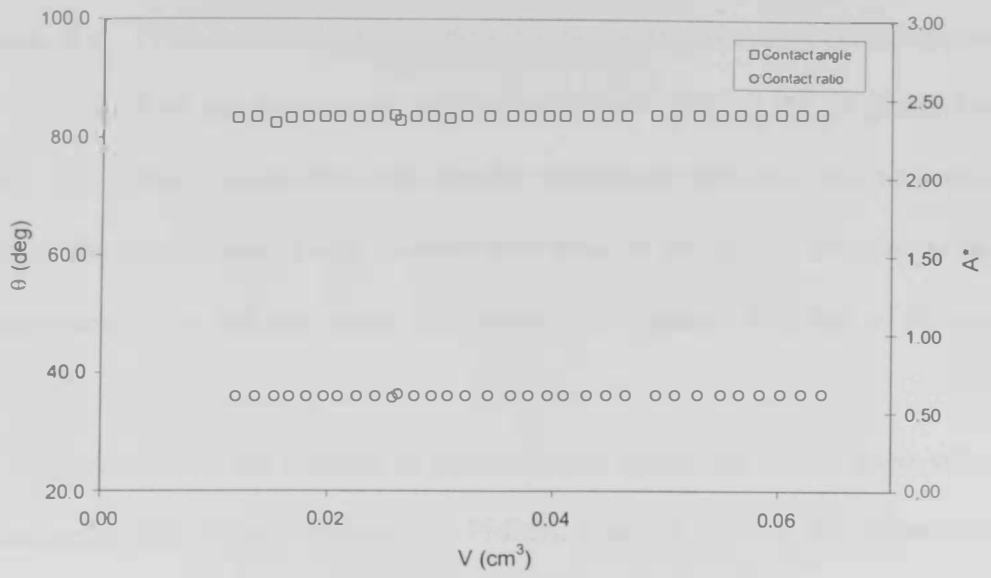

Fig 3.7 Volume against contact angle and contact ratio of water on PMMA. This figure shows that there is only one unique value of the contact ratio

Glycerol on PMMA

Figure 3.8 shows contact angle measurement experiment results of glycerol on PMMA. The same as in water on PS, linearly increasing the drop volume V (Fig. 3.8.d) from approximately 0.07 cm^3 to approximately 0.08 cm^3 by the motorized-syringe mechanism, increases the contact angle θ (Fig 3.8.b) from approximately 71.28° to 73.5° at essentially a constant three-phase contact radius R = 0.44 cm (Fig 3.8.c). This means that the measured contact angle is not equal to the advancing contact angles. As the drop volume increases beyond a critical volume of 0.08 cm^3 causes the three-phase contact line to advance with contact angle θ essentially constant as contact radius R increases. Increasing the drop volume in this manner ensures the measured θ to be an advancing contact angle. For this specific experiment (glycerol on PMMA), averaging the measured contact angles after *R* reaches 0.45 cm (Fig.3.8.c) is convenient since the contact angles are essentially constant, the drop is

guaranteed to be in the advancing mode and that line tension effects are negligible (Duncan et al., 1995; Amirfazli et al., 1998). Averaging the measured contact angles, after R reaches 0.45 cm, yields a mean contact angle of $72.66^{\circ}\pm0.60^{\circ}$ for glycerol on PMMA. The surface tension-time plot for this experiment indicates that the surface tension of the glycerol used keeps constant with time (64.68 mJ/m^2). This proves that no dissolution of the polymer occurs that causes γ_{lv} to change from that of the pure liquid.

Figure 3.9 plots the volumes of glycerol liquid against the contact angle values and the contact ratio values of glycerol on PMMA. It can be seen that the contact ratio values remain constant at the mean value of 0.71 for the same range of volume of glycerol drop (0.08-0.12 cm^3 approximately), where the contact angle values remain constant at the mean value of 72.66°.

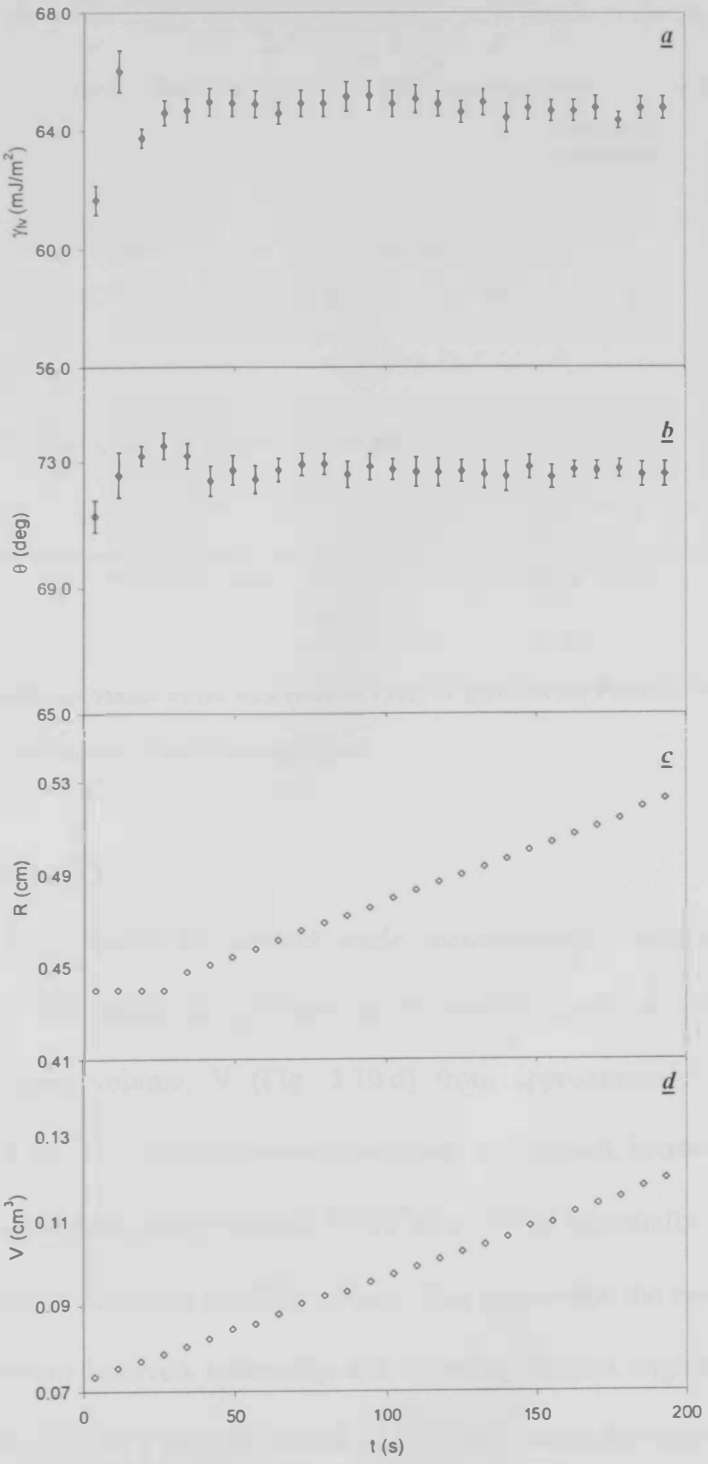

Fig 3.8 Time verses (a) Surface tension (b) Low-rate dynamic contact angle (c) Contact radius (d) Volume for low-rate dynamic contact angles experiment of glycerol on PMMA

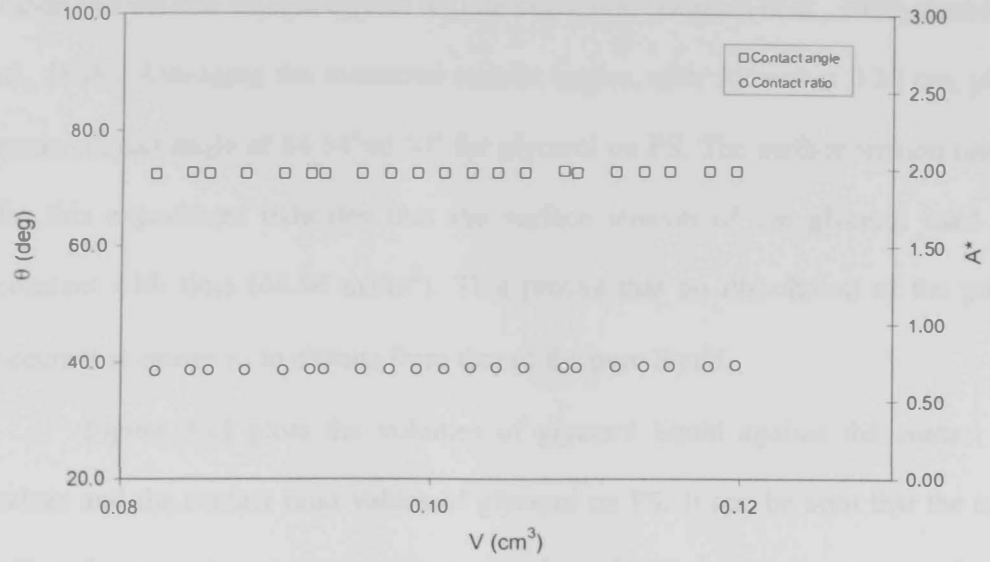

Fig 3.9 Volume against contact angle and contact ratio of glycerol on PMMA. This figure shows that there is only one unique value of contact ratio

Glycerol on PS

Figure 3.10 shows the contact angle measurement experiment results of glycerol on PS. The same as in Water on PS and Glycerol on PMMA, linearly increasing the drop volume, V (Fig. 3.10.d) from approximately 0.045 cm^3 to approximately 0.052 cm^3, by the motorized-syringe mechanism, increases the contact angle θ (Fig 3.10.b) from approximately 83.34° to 84.57° at essentially constant three-phase contact radius R = 0.34 cm (Fig 3.10.c). This means that the measured contact angle is somewhere between advancing and receding contact angles. As the drop volume increases beyond a critical volume of 0.05 cm^3 causes the three-phase contact line to advance with the contact angle θ essentially constant as contact radius R increases. Increasing the drop volume in this manner ensures the measured θ to be an advancing contact angle. For this specific experiment (glycerol on PS), averaging the measured contact angles after *R* reaches 0.36 cm (Fig 3.10.c) is convenient, since the

contact angles are essentially constant. The drop is guaranteed to be in the advancing mode and the line tension effects will be negligible (Duncan et al., 1995; Amirfazli et al., 1998). Averaging the measured contact angles, after R reaches 0.36 cm, yields a mean contact angle of $84.54^{o}\pm0.50^{o}$ for glycerol on PS. The surface tension-time plot for this experiment indicates that the surface tension of the glycerol used keeps constant with time (64.54 mJ/m^2). This proves that no dissolution of the polymer occurs that causes γ_{lv} to change from that of the pure liquid.

Figure 3.11 plots the volumes of glycerol liquid against the contact angle values and the contact ratio values of glycerol on PS. It can be seen that the contact ratio values remain constant at the mean value of 0.62 for the same range of volume of the glycerol drop (0.05-0.09 cm^3 approximately), where the contact angle values stay constant at the mean value of 84.54^{o}.

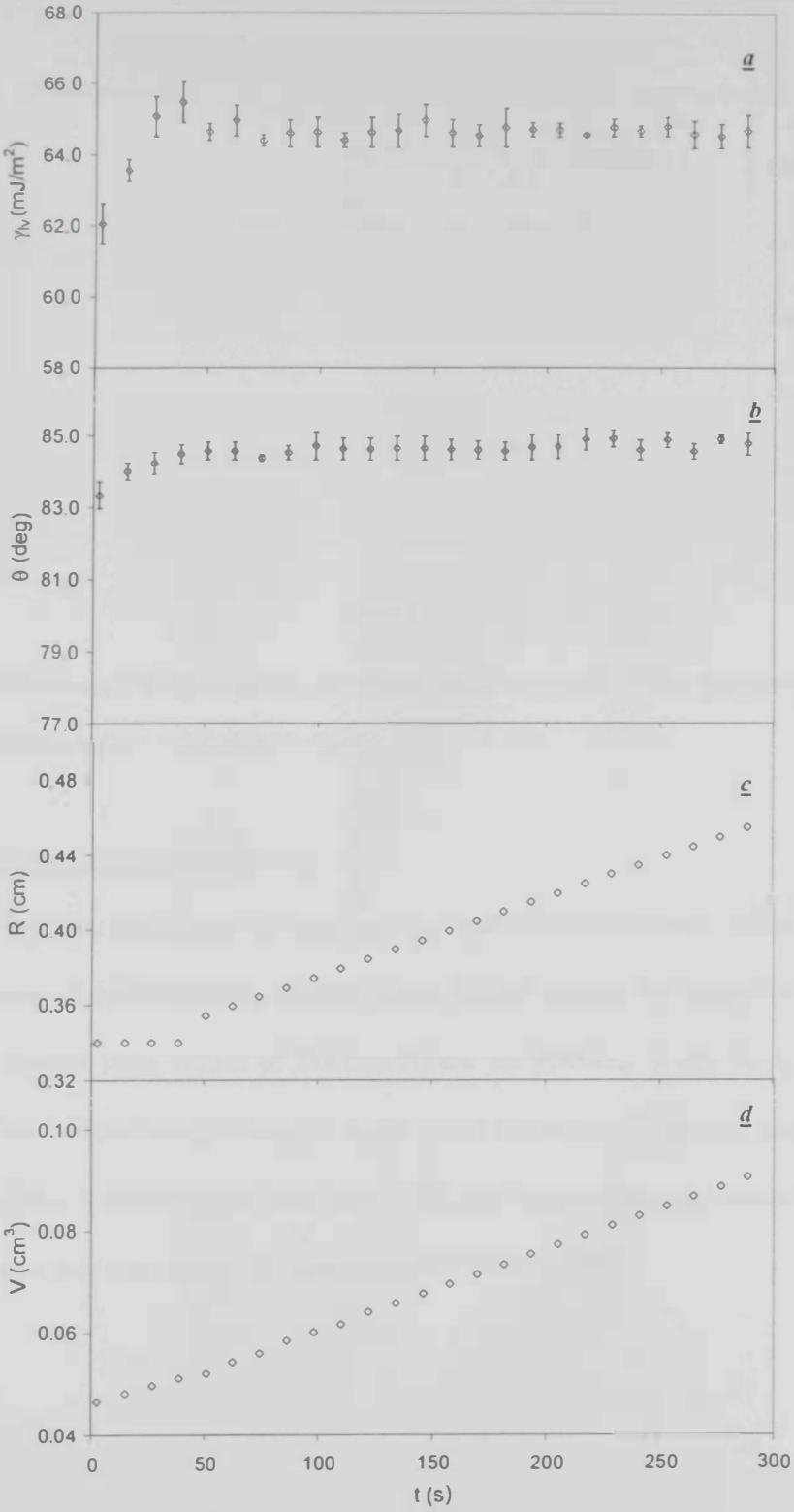

Fig 3.10 Time verses (a) Surface tension (b) Low-rate dynamic contact angle (c) Contact radius (d) Volume for low-rate dynamic contact angles experiment of glycerol on PS

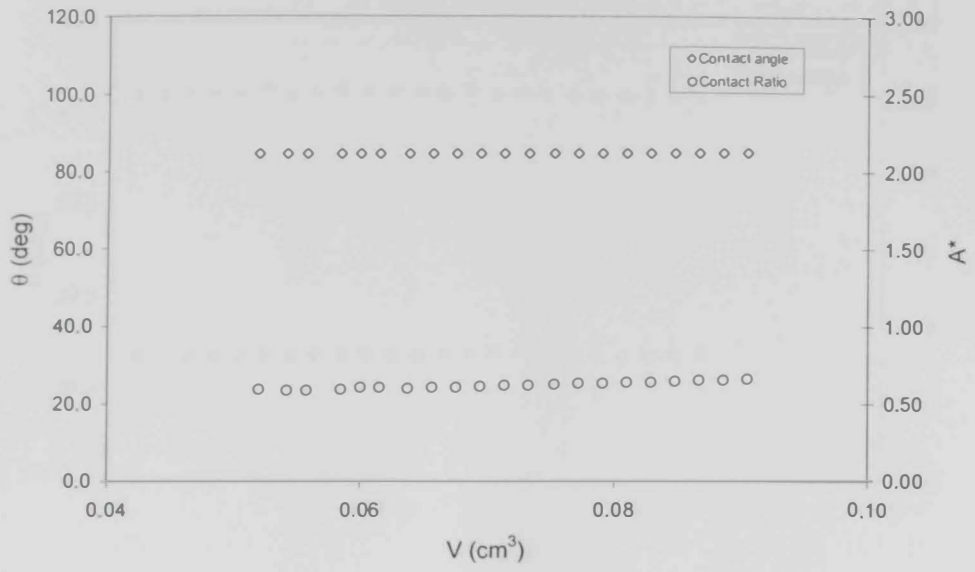

Fig 3.11 Volume against contact angle and contact ratio of glycerol on PS. This figure shows that there is only one unique value of contact ratio

Other liquid/solid systems

The same results can be seen in other solid-liquid systems. Figure 3.12 plots the volumes of diiodomethane (Kwok et al.; 1998c) against the contact angle values and the contact ratio values of diiodomethane on PMMA. It can be seen that the contact ratio values remain constant at the mean value of 0.81 for the same range of volume of the diiodomethane drop (0.02-0.05 cm^3 approximately), where the contact angle values stay constant at the mean value of $41.18^{o}\pm0.06^{o}$.

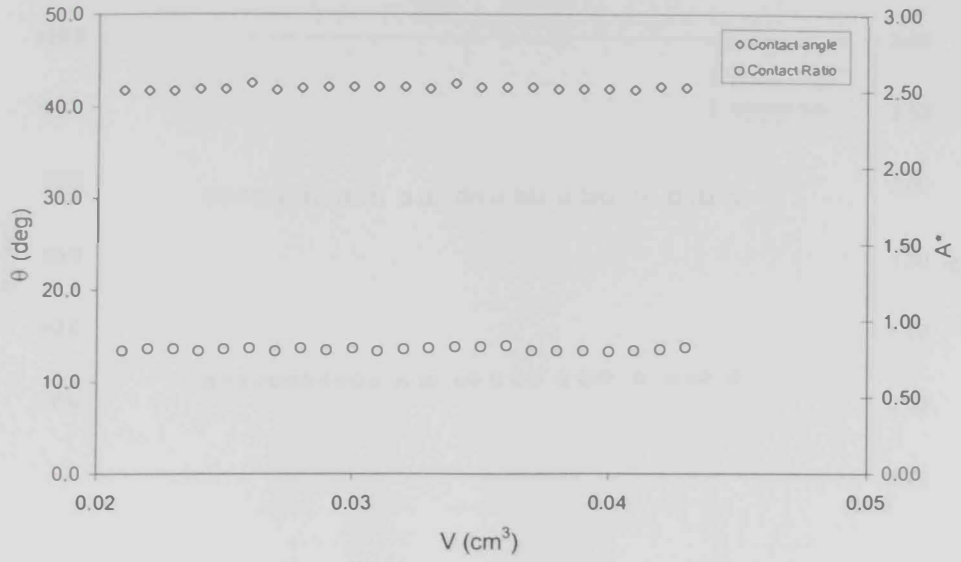

Fig 3.12 Volume against contact angle and contact ratio of diiodomethane on PMMA. This figure shows that there is only one unique value of contact ratio

Figure 3.13 plots the volumes of formamide (Kwok et al.; 1998d) against the contact angle values and the contact ratio values of formamide on PS. It can be seen that the contact ratio values remain constant at the mean value of 0.65 for the same range of formamide drop volume (0.06-0.14 cm^3 approximately), where the contact angle values stay constant at the mean value of $75.95^{\circ}\pm0.13^{\circ}$.

Fig 3.13 Volume against contact angle and contact ratio of formamide on PS. This figure shows that there is only one unique value for contact ratio

Figure 3.14 plots the volumes of ethylene glycol (Kwok et al.; 1998d) against the contact angle values and the contact ratio values of ethylene glycol on PS. It can be seen that the contact ratio values remain constant at the mean value of 0.84 for the same rang of ethylene glycol drop volume (0.04-0.10 cm^3 approximately), where the contact angle values stay constant at the mean value of $61.65^o \pm 0.06^o$.

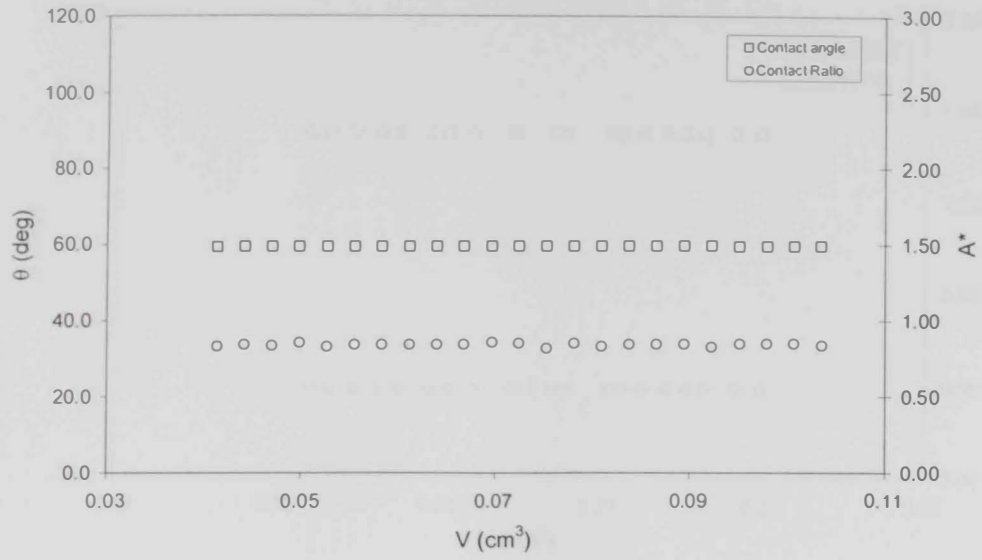

Fig 3.14 Volume against contact angle and contact ratio of ethylene glycol on PS. This figure shows that there is only one unique value of contact ratio

Figure 3.15 plots the volumes of water (Kwok et al., 1998b) against the contact angle values and the contact ratio values of water on FC-725-coated silicon wafer. It can be seen that the contact ratio values remain constant at the mean value of 0.38 for the same range of volume of the waterdrop (0.19-0.22 cm^3 approximately), where the contact angle values stay constant at the mean value of $119.21^{\circ}\pm0.08^{\circ}$.

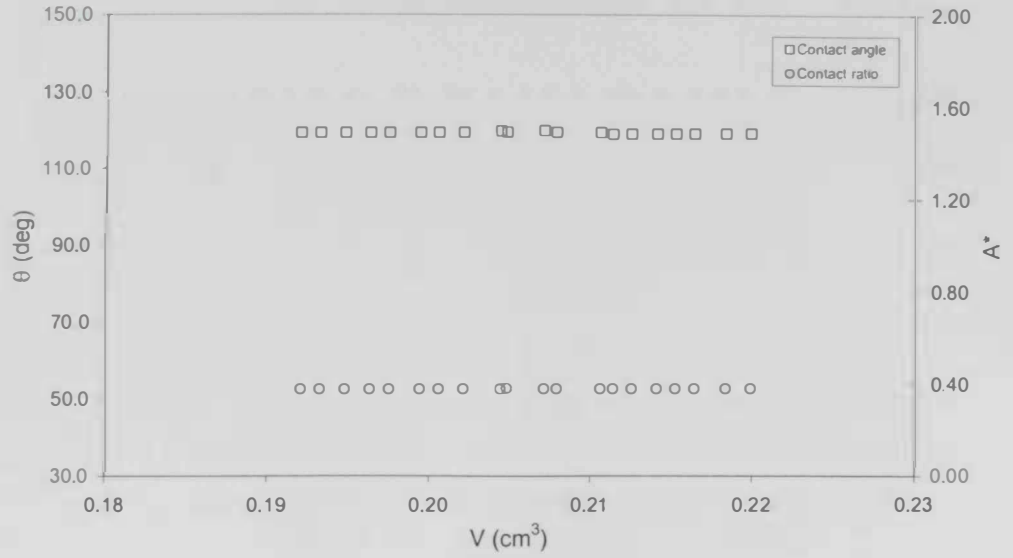

Fig 3.15 Volume against contact angle and contact ratio of water on FC-725-coated silicon wafer. This figure shows that there is only one unique value of contact ratio

Figure 3.16 plots the volumes of formamide (Kwok et al.; 1998b) against the contact angle values and the contact ratio values of formamide on FC-725-coated silicon wafer. It can be seen that the contact ratio values remain constant at the mean value of 0.47 for the same range of volume of the formamide drop (0.17-0.19 cm^3 approximately), where the contact angle values stay constant at the mean value of $106.42^{\circ}\pm0.09^{\circ}$.

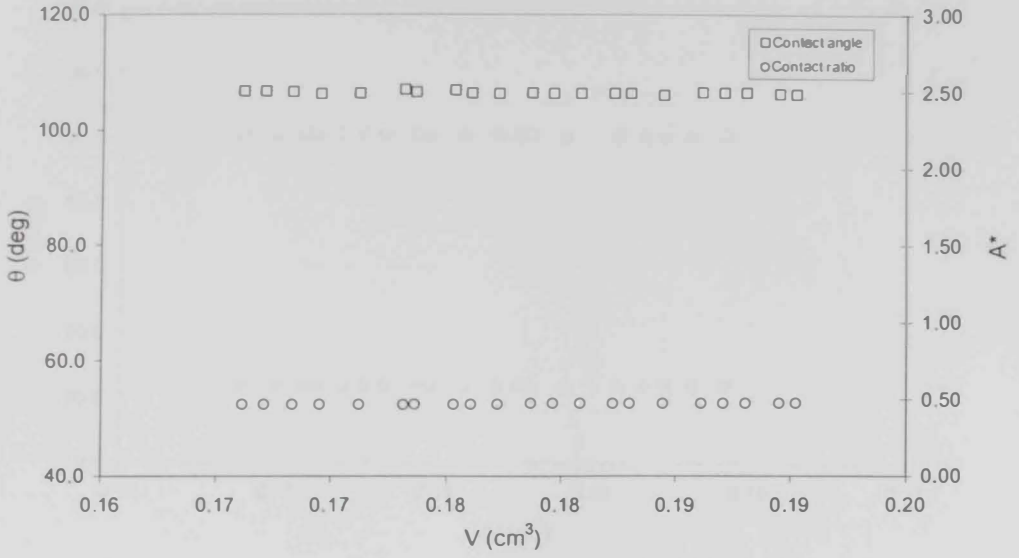

Fig 3.16 Volume against contact angle and contact ratio of formamide on FC-725-coated silicon wafer. This figure shows that there is only one unique value of contact ratio

Figure 3.17 plots the volumes of 2,2-thiodiethanol (Kwok et al.; 1998b) against the contact angle values and the contact ratio values of 2,2-thiodiethanol on FC-725-coated silicon wafer. It can be seen that the contact ratio values remain constant at the mean value of 0.51 for the same range of volume of the 2,2-thiodiethanol drop (0.14-0.16 cm^3 approximately), where the contact angle values stay constant at the mean value of $100.66^{\circ}\pm0.08^{\circ}$.

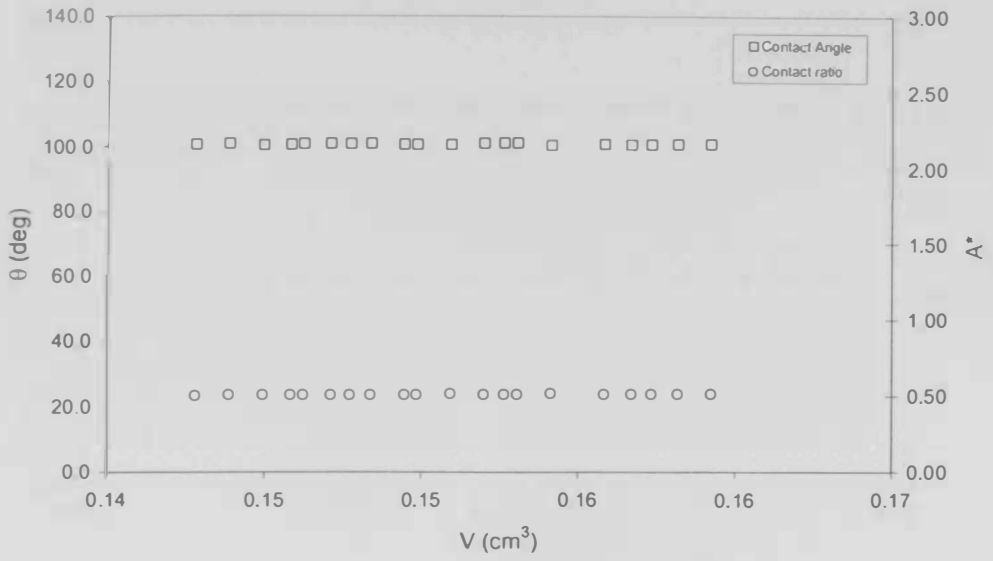

Fig 3.17 Volume against contact angle and contact ratio of 2,2-thiodiethanol on FC-725-coated silicon wafer. This figure shows that there is only one unique value of contact ratio

Figure 3.18 plots the volumes of 3-pyridylcarbinol (Kwok et al., 1999a) against the contact angle values and the contact ratio values of 3-pyridylcarbinol on P(MMA/EMA, 30/70). It can be seen that the contact ratio values remain constant at the mean value of 0.91 for the same range of volume of the 3-pyridylcarbinol drop (0.03-0.05 cm^3 approximately), where the contact angle values stay constant at the mean value of $48.46^{\circ}\pm0.09^{\circ}$.

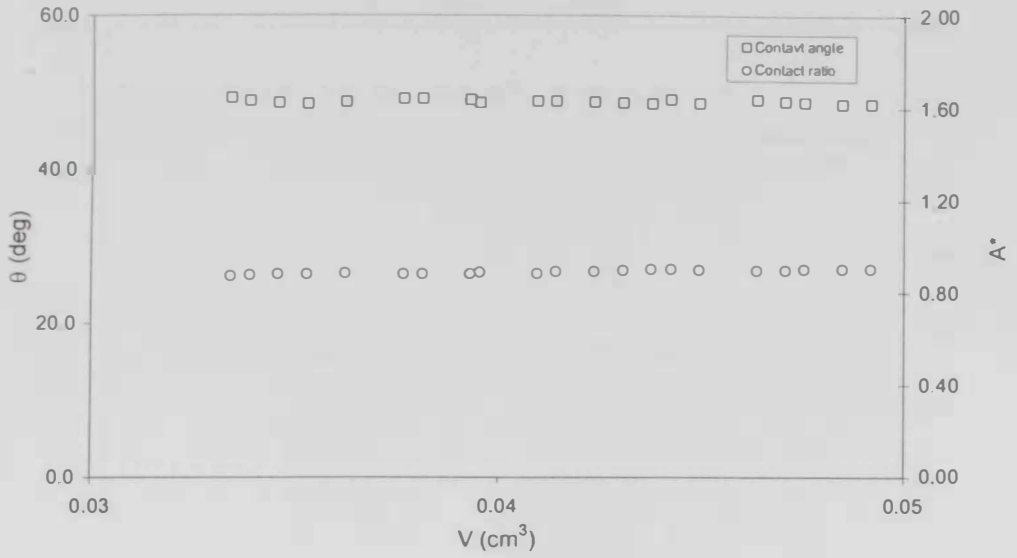

Fig 3.18 Volume against contact angle and contact ratio of 3-pyridylcarbinol on P(MMA/EMA, 30/70). This figure shows that there is only one unique value of contact ration for a system

Figure 3.19 plots the volumes of diethylene glycol (Kwok et al.; 1999b) against the contact angle values and the contact ratio values of diethylene glycol on P[S-(H/CM)]. It can be seen that the contact ratio values remain constant at the mean value of 0.83 for the same range of volume of the diethylene glycol drop (0.01-0.03 cm^3 approximately), where the contact angle values stay constant at the mean value of $50.93^{\circ}\pm0.08^{\circ}$.

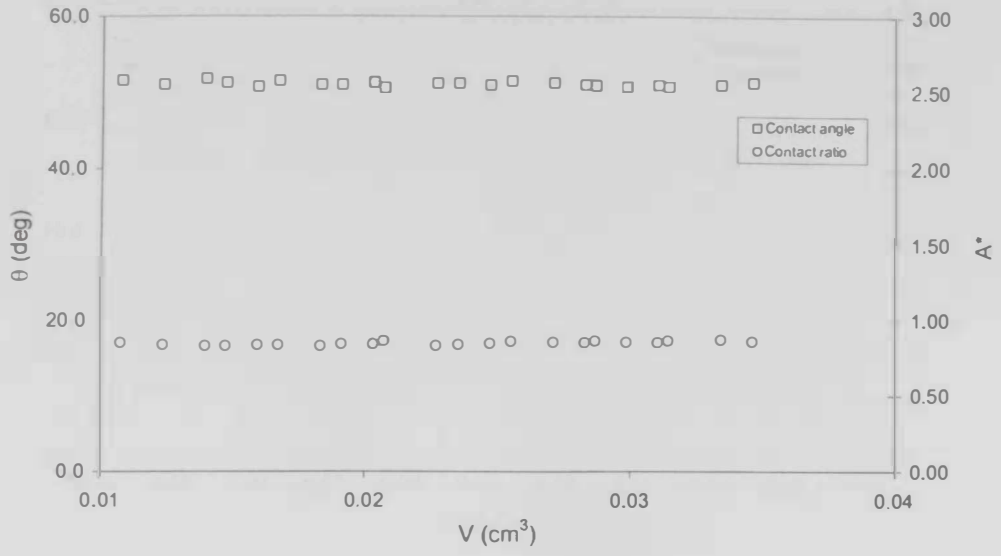

Fig 3.19 Volume against contact angle and contact ratio of diethylene glycol on P[S-(H/CM)]. This figure shows that there is only one unique value of contact ratio

Figure 3.20 plots the volumes of glycerol (Kwok et al.; 1999b) against the contact angle values and the contact ratio values of glycerol on P[S-(H/CM)]. It can be seen that the contact ratio values remain constant at the mean value of 0.61 for the same range of volume of glycerol drop (0.04-0.13 cm^3 approximately), where the contact angle values stay constant at the mean value of $76.47^o \pm 0.07^o$.

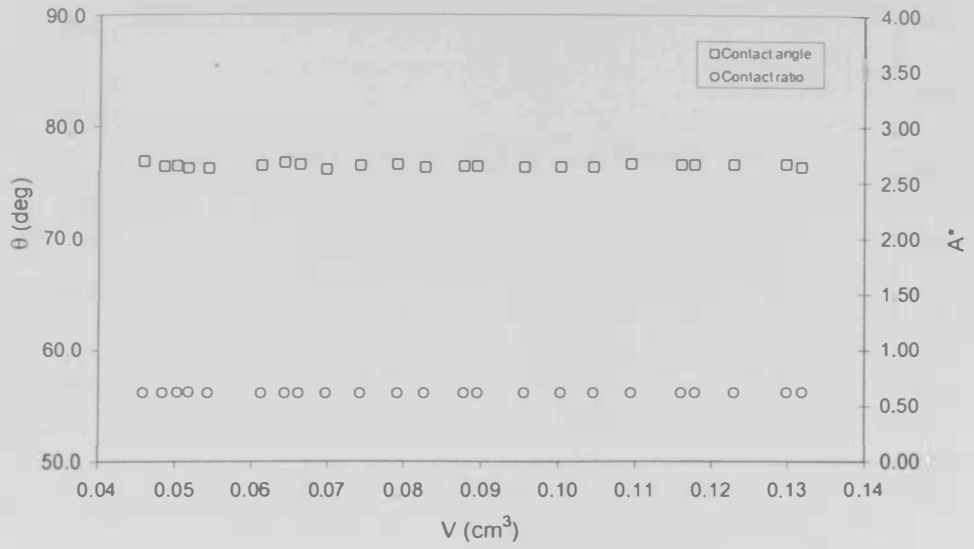

Fig 3.20 Volume against contact angle and contact ratio of glycerol on P[S-(H/CM)]. This figure shows that there is only one unique value of contact ratio

Figure 3.21 plots the volumes of formamide (Kwok et al.; 1999b) against the contact angle values of formamide on P[S-(H/CM)] and the contact ratio values. It can be seen that the contact ratio values remain constant at the mean value of 0.65 for the same range of volume of the formamide drop (0.03-0.09 cm^3 approximately), where the contact angle values stay constant at the mean value of $69.96^o \pm 0.10^o$.

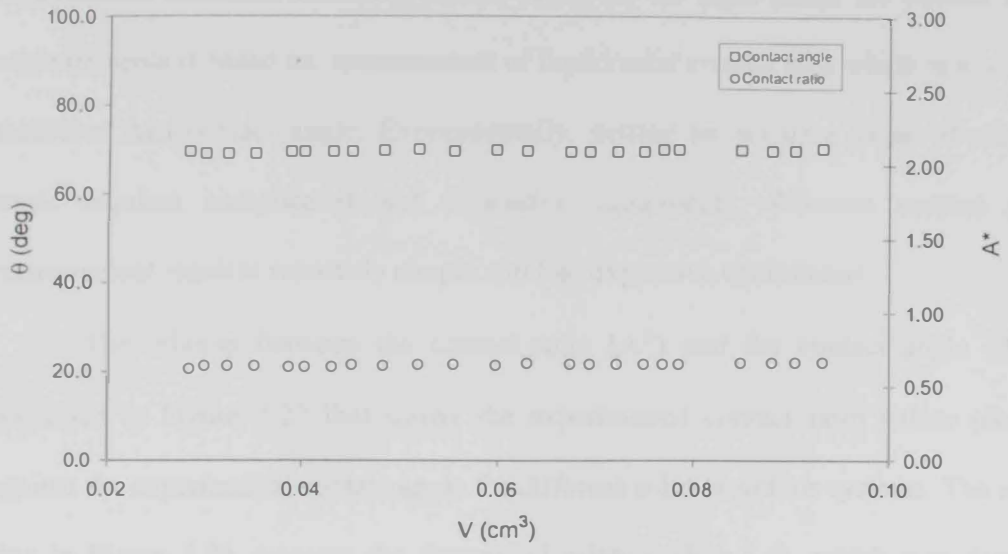

Fig 3.21 Volume against contact angle and contact ratio of formamide on P[S-(H/CM)]. This figure shows that there is only one unique value of contact ratio

3.1.4 Concluding remarks

Contact angle and contact ratio values for the previous different system are summarized in Table 3.1. In conclusion, if it is considered that the contact angle (advance contact angle) of a specific system is a wettability parameter of a wetting system, which is true because the system has only a unique value of the contact angle, contact ratio is also can be considered as a wettability parameter of a wetting system because the system has only one unique value of the contact ratio. Therefore, contact ratio can be presented as a new concept in measuring wettability alternative to contact angle.

Referring to the contact angle problems mentioned in the introduction of this chapter it is fair to say that even the factors which affect contact angle measurement, which may lead to a wrong value for the contact angle, also affect the measurement of the contact ratio. However, the contact angle greatly depends on the curvature of the

drop (Fig 1.2), and the slope of the tangent which is more difficult to get a precise experimental measurements than contact ratio. On the other hand, the contact ratio measurements is based on measurement of liquid/solid contact area which is easier to measurer than contact angle. Experimentally, getting an accurate value of contact angle requires complicated and expensive equipments. Whereas contact area measurement requires relatively simple and less expensive equipments.

The relation between the contact ratio (A*) and the contact angle (θ) is presented in Figure 3.22 that shows the experimental contact ratio values plotted against the experimental contact angle for different solid-liquid-air systems. The solid line in Figure 3.22 presents the theoretical relation (Eqn.3.6), which was derived based on spherical cap approximation (Eqn 3.4), of the contact ratio of a system to its contact angle.

This Figure shows 1) Even at high value of contact angle, there is a good agreement between the theoretical relation (Eqn.3.8) and the experimental and literature values 2) The relation between the contact angle and the contact ratio is power law. As the contact angle decreases, the contact ratio increases and visa versa. 3) The small deviation of the contact angle and the contact ratio values of the system, which have low contact angles, from the theoretical curve can be contributed for most likely to the accuracy of ADSA-P that decreases as contact angle decreases.

Finally, the contact ratio value of the system can be approximately calculated from the system contact angle value by using Equation 3.8.

Table 3.1: Low-rate dynamic contact angles and contact ratios of different systems

Solid	Liquid	Contact Angle θ (deg)	Contact Ratio A^*
PS	Water	95.56±0.80	0.52
	Glycerol	84.54±0.50	0.62
	Formamide	74.35±0.13 [2]	0.65
	Ethylene glycol	59.54±0.06 [2]	0.84
PMMA	Water	83.68±0.70	0.60
	Glycerol	72.66±0.60	0.71
	Diiodomethane	41.98±0.06 [1]	0.81
FC-725-coated silicon wafer	Water	119.21±0.08 [3]	0.38
	Formamide	106.42±0.09 [3]	0.47
	2,2-thiodiethanol	100.66±0.08 [3]	0.51
P(MMA/EMA, 30/70)	3-pyridylcarbinol	48.46±0.09 ° [4]	0.91
P[S-(H/CM)]	Diethylene glycol	50.93±0.08 [5]	0.83
	Glycerol	76.47±0.07 [5]	0.61
	Formamide	69.96±0.10 [5]	0.65

[1] Kwok et al., 1998c
[2] Kwok et al., 1998d
[3] Kwok et al., 1998b
[4] Kwok et al., 1999a
[5] Kwok et al., 1999b

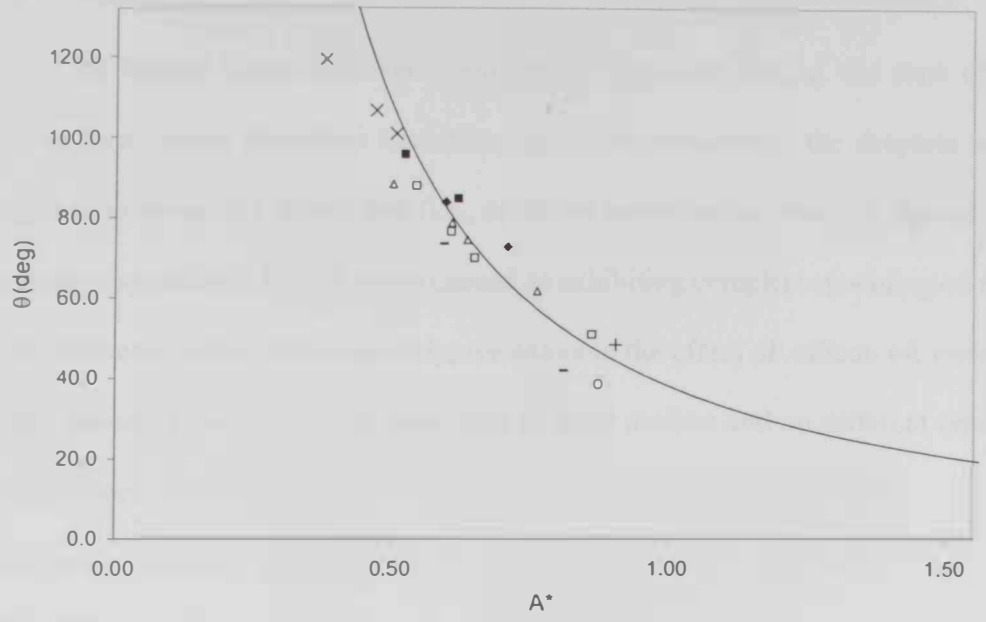

Fig 3.22 Experimental Contact ratio values verses the experimental Contact angle for different systems. The solid curve represents theoretical relation (Eqn 3.6) between the Contact ratio of a system and its Contact angle based on spherical cap approximation (Eqn 3.4). ■ liquids on PS solid surface, ♦ liquids on PMMA solid surface, + liquids on P(MMA/EMA) solid surface (Kwok, 1999a), ○ liquids on Poly(propene-alt-N-(n-alky)malemide) (Kwok, 1998a), □ liquids on P[S-(H/CM)] solid surface (Kwok, 1999c), - liquids on PMMA solid surface (Kwok, 1998c), Δ liquids on PS solid surface (Kwok, 1998d), x liquids on FC-725-coated silicon wafer (Kwok et al., 1998b).

3.2 The effect of viscosity on the kinetics of spreading

All liquids tested exhibited spontaneous spreading rate at the start of the process then passed through a transition zone. After transition, the droplets either continued to spread at a slower rate (i.e., complete spreading) or ceased to spread (i.e., incomplete spreading). PDMS is recognized as exhibiting complete spreading on most of the surfaces. In the following study, we examine the effect of silicon oil viscosity on the spreading kinetics on the same type of solid surface and on different types of solid surfaces.

3.2.1 Thermodynamic framework

It is commonly theorized and experimentally validated (Starov et al., 1994; Chebbi and Selim, 1997, Chebbi, 2000) that viscous force, capillary force, and van der Waals force control the spreading of silicon oil where the gravity and inertia forces are neglected. In the major part of the drop where the curvature of the surface is constant, the capillary force are important and viscous forces are negligible. In the vicinity of the inflexion point, viscous forces come into play, and significant changes of the curvature occur. In the near vicinity of the contact line, van der Waals forces become important and cannot be ignored (Chebbi, 2000). A recent investigation (Alteraifi and Sasa , 2003) has shown that the solid substrate plays a significant role in equilibrial spreading as well as the rate at which it is achieved i.e the intermolecular forces between liquid and solid surface play a role in the spreading kinetics.

3.2.2 The effect of different viscosities of silicon oil on the kinetics of spreading on the same solid surface

Figure 3.23 shows the spreading kinetics of silicon oil with different viscosities (100 cP, 500 cP, 1000 cP, 10,000 cP) on a glass solid surface. The spreading kinetics is presented as the contact ratio (A^*) value of the silicon oil plotted against spreading time. The experimental measurements were interrupted after 1200 seconds for 100 cP, 500 cP, 1000 cP silicon oil and after 2400 seconds for 10,000 cP silicon oil. Having the same solid surface type (glass, PS, or PMMA) and the same liquid surface tension (γ_{lv} = 21.5 dyne/cm for silicon oil) applied in the same conditions for the vapour-liquid-solid system, while varying liquid viscosity. Figure 3.23 demonstrates that the liquid viscosity (viscous dissipation rate) is responsible for the difference spreading kinetics. In other words, the lower the liquid viscosity, the faster the spreading rate. The effect of viscosity is shown on the log-log scale plot in Figure 3.24. Figure 3.24 shows that as viscosity decreases the rate of spreading (dA^*/dt) increases. Similar results are presented for other solid surfaces namely, PMMA and PS in Figures 3.25-3.28.

To theoretically analyze the rate dependence on liquid viscosity, The Tanner law was applied. The general form of the Tanner law is given by

$$A = Ct^n \tag{3.10}$$

where

$$C = \frac{\gamma \kappa}{\mu R_f} \tag{3.11}$$

where R_f is the equilibrium contact radius, κ is a non-dimensional parameter that has to be determined empirically and n is the power factor. Dividing both sides of the Tanner equation by the surface area of the spherical droplet before spreading (surface

area (S) = 6.34 mm^2 for V=1.5 μL), the Tanner law can be represented in terms of contact ratio, A^*, as follows:

$$A^* = C^* t^n \tag{3.12}$$

where

$$C^* = \frac{C}{S} \tag{3.13}$$

Applying the least square fit (using Microsoft Excel) for Equation 3.13 for the experimental data shown in Figures 3.23, 3.25 and 3.27. The C^* and n values of Equation 3.12 are summarized in Table 3.2.

The kinetics behavior characterized by Tanner's exponent, n, in Table 3.2 suggests that for a specific system, such as silicon oil on glass, as the viscosity decreases, Tanner law exponent, n, increases. A Larger n value means a greater spreading rate (dA^*/dt). Therefore, the lower the viscosity the faster the spreading. The same conclusion has been reported by Extrand (1993). He reported that while changing the drop volume or surface made little difference to the spreading rate, changing the viscosity had a more profound effect, the drop with lower viscosity spreads much faster than one with higher viscosity. The spreading time was found proportional to the viscosity (Extrand, 1993).

Table 3.2: Values of C* and power factor n of the for spreading of silicon oil on glass, PS and PMMA

Solid	Silicon oil viscosity (cPoise)	$C^* (s)^{-n}$	n	R^2
Glass	100	1.12	0.26	0.99
	500	0.75	0.25	0.99
	1000	0.66	0.24	0.99
	10,000	0.42	0.23	0.99
PMMA	100	1.1	0.25	0.99
	500	0.76	0.25	0.99
	1000	0.68	0.24	0.99
	10,000	0.42	0.23	0.99
PS	100	1.21	0.26	0.99
	500	0.79	0.25	0.99
	1000	0.69	0.24	0.99
	10,000	0.42	0.23	0.99

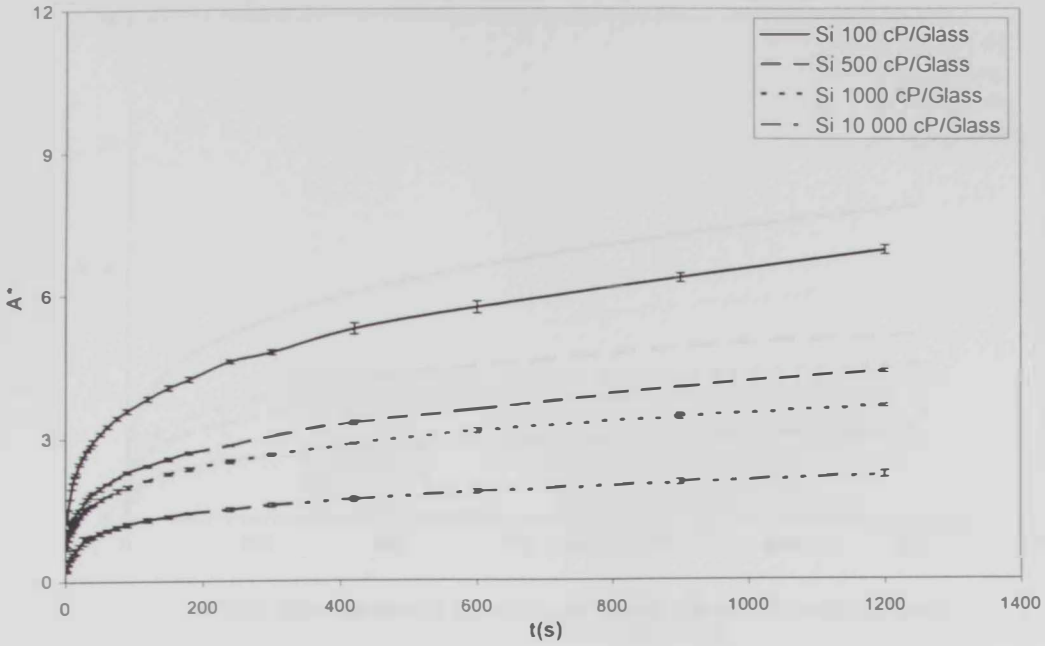

Fig. 3.23 Kinetics of spreading of silicon oils on a glass solid surface

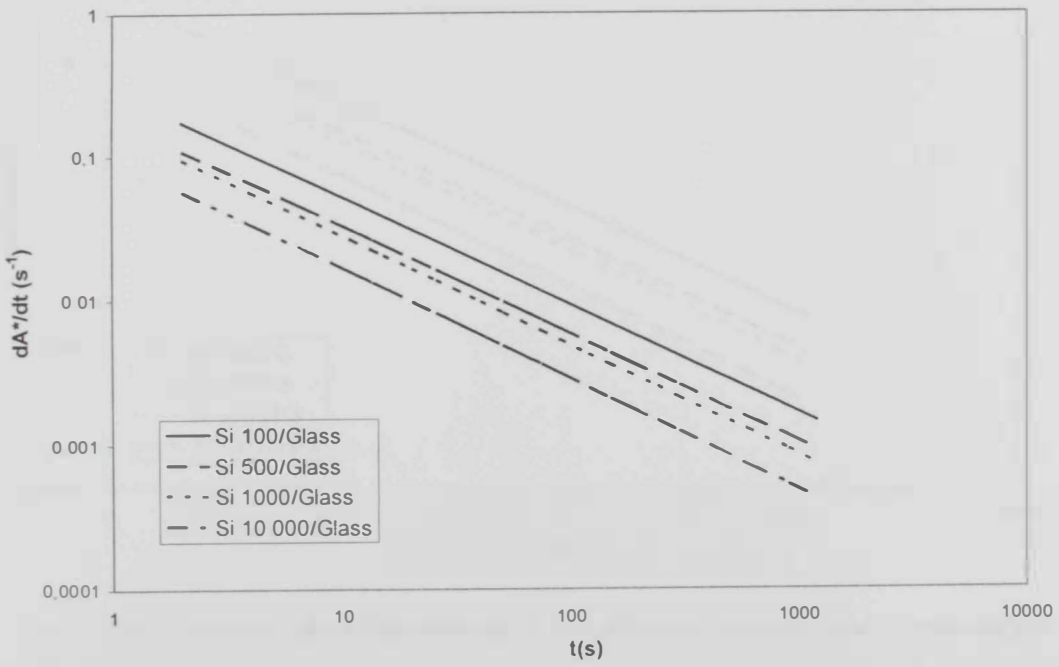

Fig. 3.24 Rate of spreading of silicon oil with different viscosities on a glass solid surface

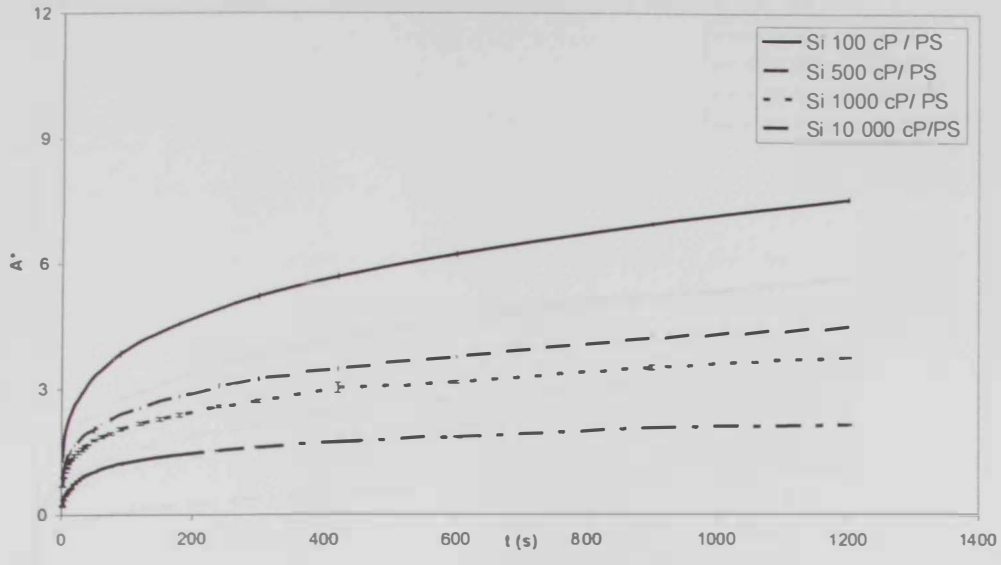

Fig. 3.25 Kinetics of spreading of silicon oils on a PS solid surface

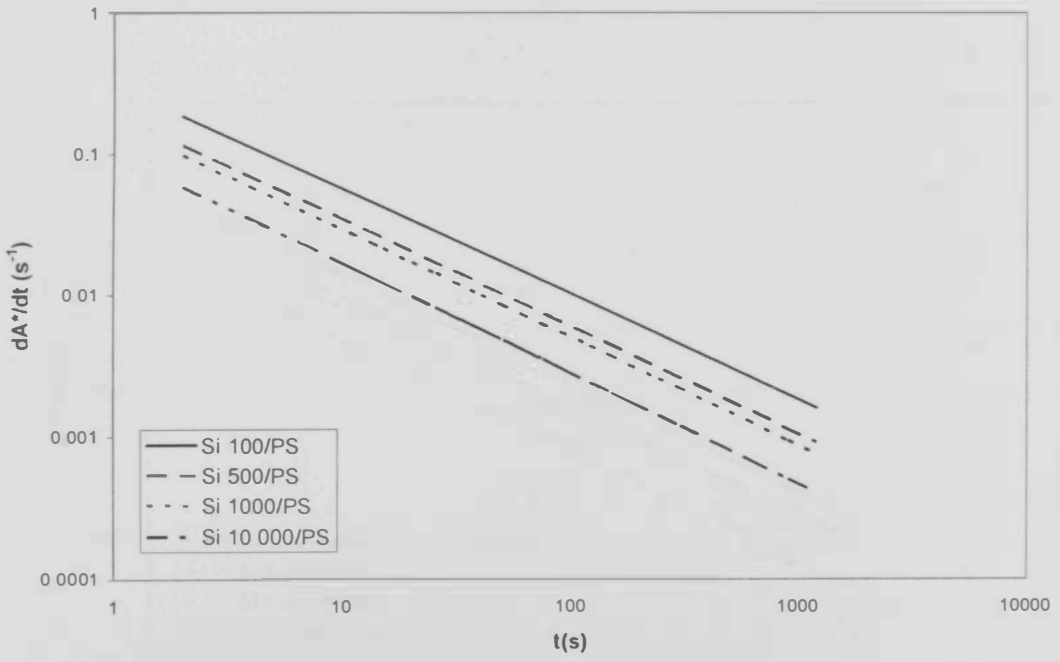

Fig. 3.26 Rate of spreading of silicon oil with different viscosities on a PS solid surface

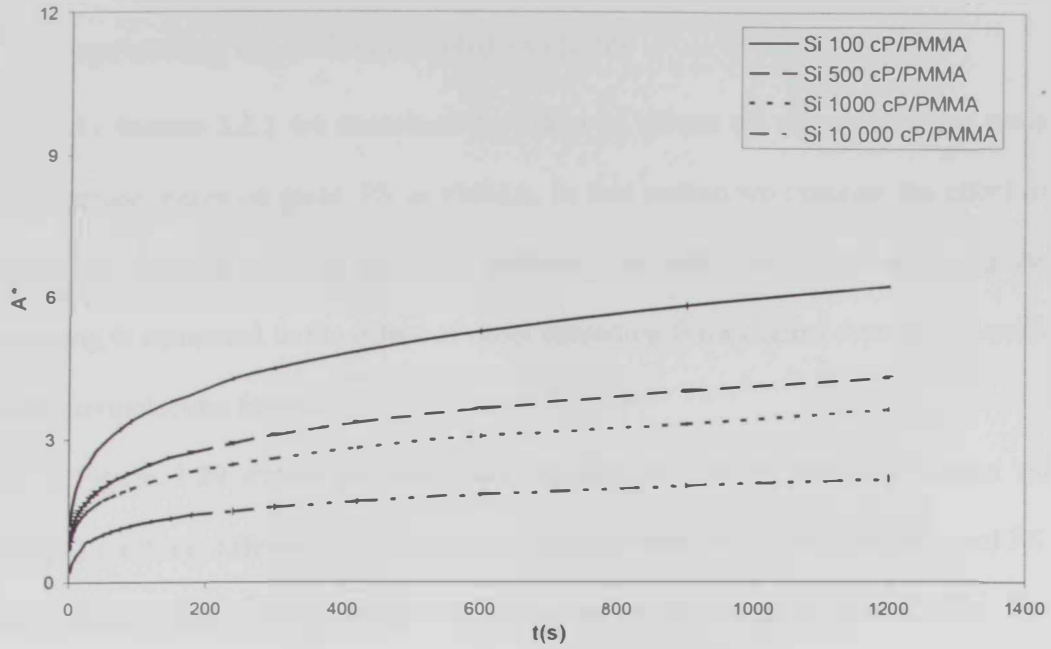

Fig. 3.27 Kinetics of spreading of silicon oils on a PMMA solid surface

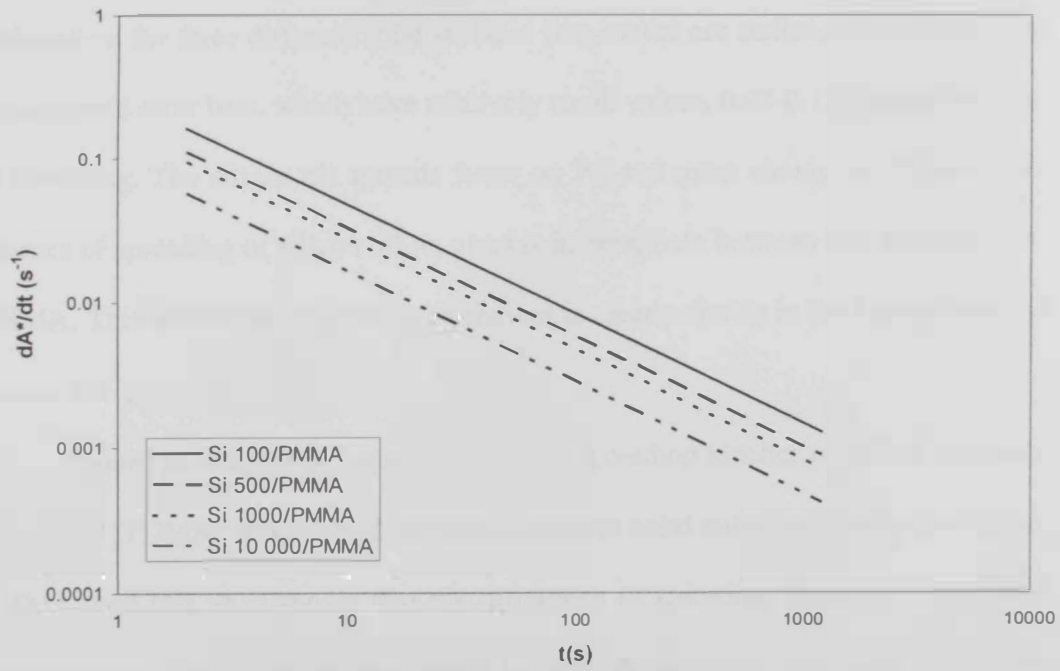

Fig.3.28 Rate of spreading of silicon oil with different viscosities on PMMA solid surface

3.2.3 The effect of different viscosities` of silicon oil on the kinetics of spreading on different solid surfaces

In Section 3.2.1 we examined the effect of silicon oil viscosity on the same solid surface, either on glass, PS or PMMA. In this section we examine the effect of silicon oil viscosity on different solid surfaces. The effect of viscous force on the spreading is compared to the effect of other spreading forces effect especially liquid-solid intermolecular forces.

Figure 3.29 shows the spreading kinetics of 100 cP viscosity silicon oil (PDMS) on three different solid substrates, namely soda-lime glass, PMMA, and PS. The spreading kinetics is presented as the spreading time against contact ratio. The experimental measurements were interrupted after 1200 seconds for 100 cP, 500 cP, 1000 cP silicon oils and after 2400 seconds for 10,000 cP silicon oil. Figure 3.29 shows that the spreading kinetics of 100 cP viscosity silicon oil is significantly different on the three different solid surfaces (the curves are statistically different due to uncrossed error bars, which have relatively small values, 0.08-0.12) during the time of spreading. The silicon oil spreads faster on PS and more slowly on PMMA. The kinetics of spreading of silicon oil on glass is intermediate between that on PS and on PMMA. This difference in spreading behavior is clearly shown in the log-log scale as shown in Figure 3.30.

A similar analysis in Figure 3.31 for the spreading kinetics of 500 cP viscosity silicon oil (PDMS) was applied for three different solid substrates (soda-lime glass, PMMA, and PS). It is shown that the difference in spreading kinetics on the three solid surfaces is less than the one shown for 100 cP silicon oil, especially for PS and glass. The spreading remains faster on PS and slower on PMMA, while it falls in

between for the glass solid surface. Again the difference in spreading behavior is shown in the log-log scale plot in of Figure 3.32.

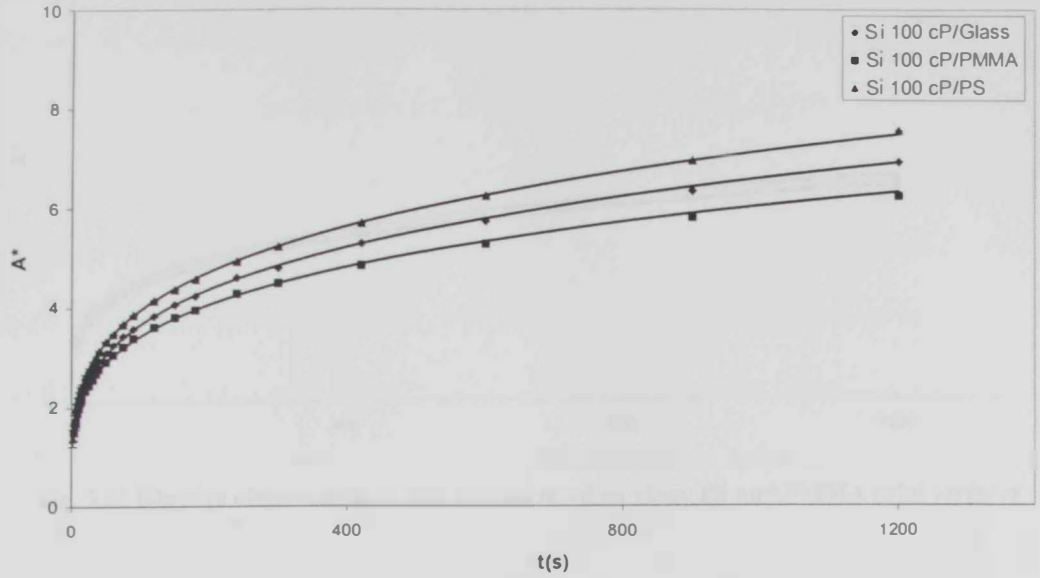

Fig. 3.29 Kinetics of spreading of 100 cP silicon oil on glass, PS and PMMA solid surfaces

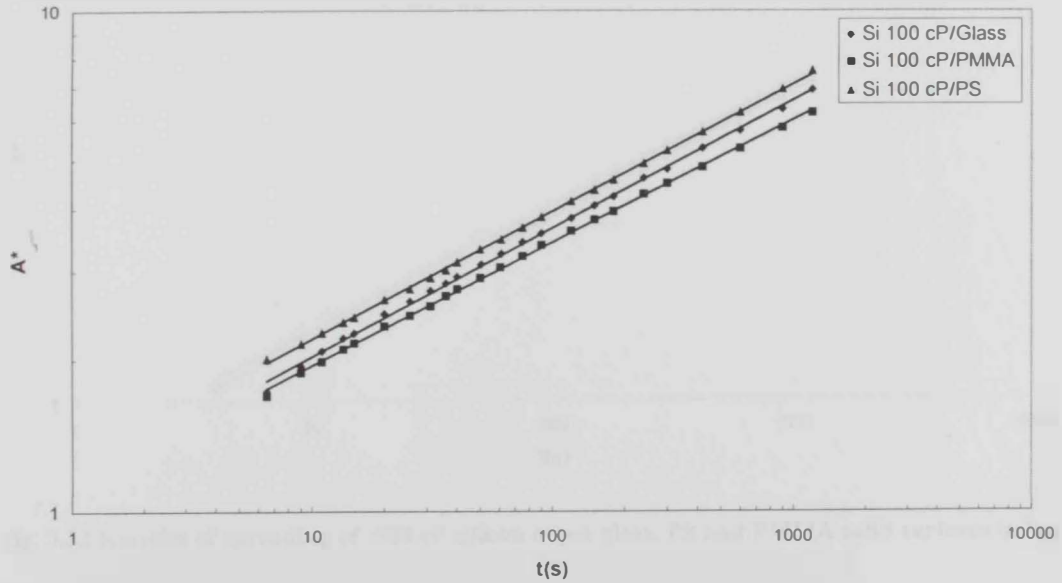

Fig. 3.30 Kinetics of spreading of 100 cP silicon oil on glass, PS and PMMA solid surfaces in log-log scale

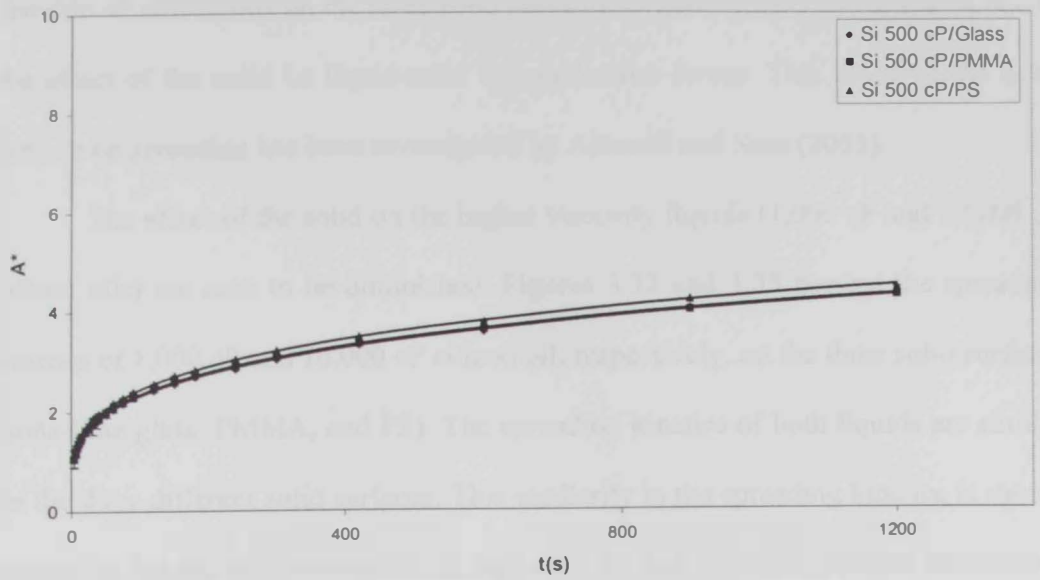

Fig. 3.31 Kinetics of spreading of 500 cP silicon oil on glass, PS and PMMA solid surfaces

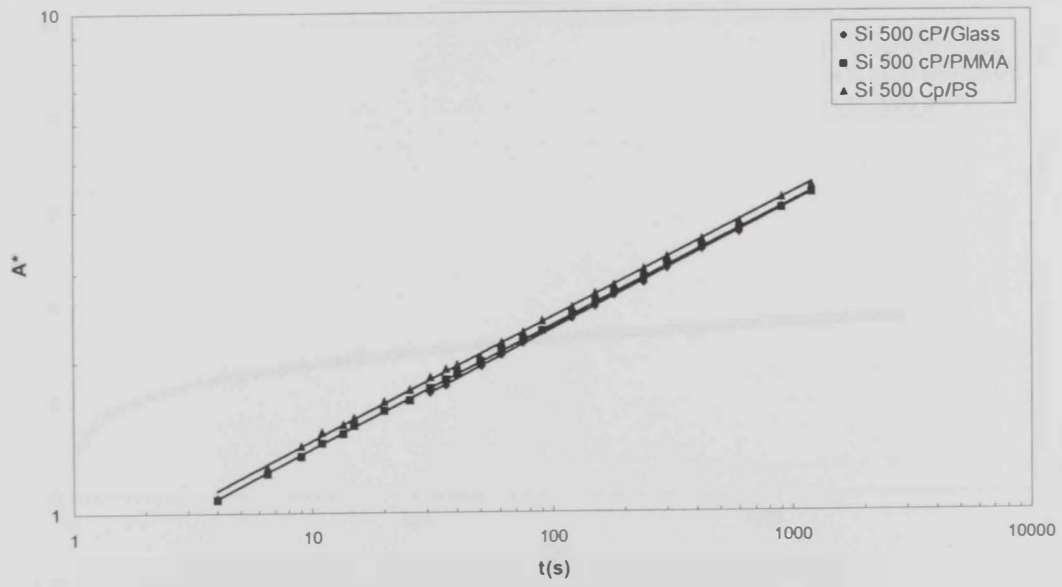

Fig. 3.32 Kinetics of spreading of 500 cP silicon oil on glass, PS and PMMA solid surfaces in log-log scale

From the previous discussion, the difference in spreading kinetics of 100 cP and 500 cP silicon oils on the three solid surfaces (Figures 3.23-3.28) might be due to the effect of the solid i.e liquid-solid intermolecular forces. This effect of the solid surface on spreading has been investigated by Alteraifi and Sasa (2003).

The effect of the solid on the higher viscosity liquids (1,000 cP and 10,000 cP silicon oils) are seen to be diminished. Figures 3.33 and 3.35 present the spreading kinetics of 1,000 cP and 10,000 cP silicon oil, respectively, on the three solid surfaces (soda-lime glass, PMMA, and PS). The spreading kinetics of both liquids are similar on the three different solid surfaces. This similarity in the spreading kinetics is shown clearly on the log-log presentation in Figures 3.34 and 3.36 for 1,000 cP and 10,000 cP silicon oils, respectively.

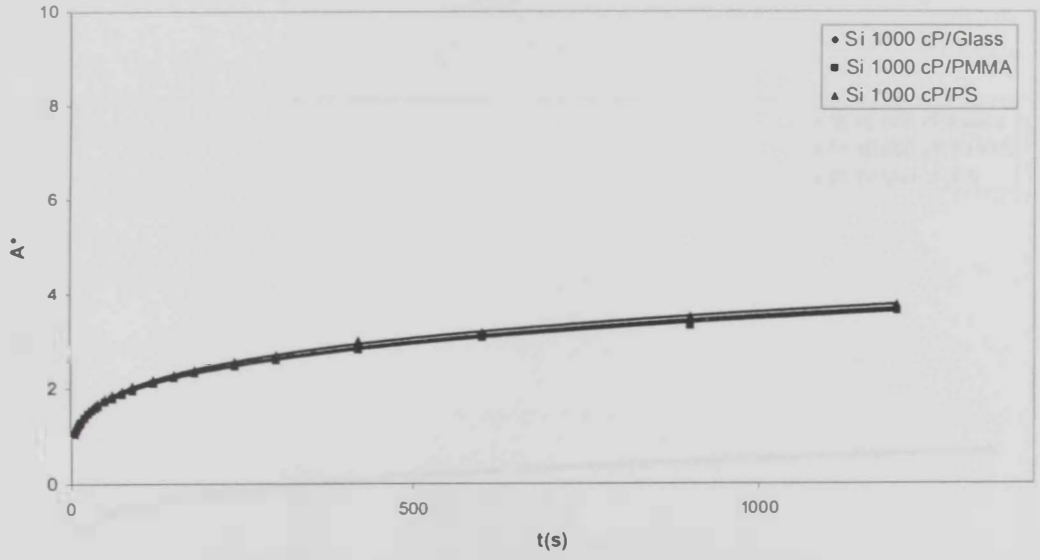

Fig. 3.33 Kinetics of spreading of 1000 cP silicon oil on glass, PS and PMMA solid surfaces

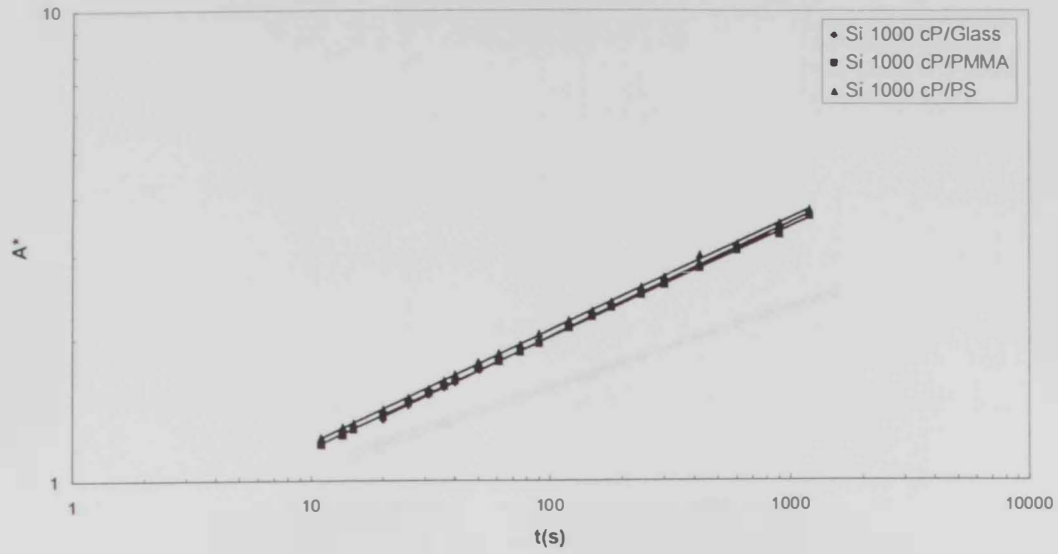

Fig. 3.34 Kinetics of spreading of 1000 cP silicon oil on glass, PS and PMMA solid surfaces in log-log scale

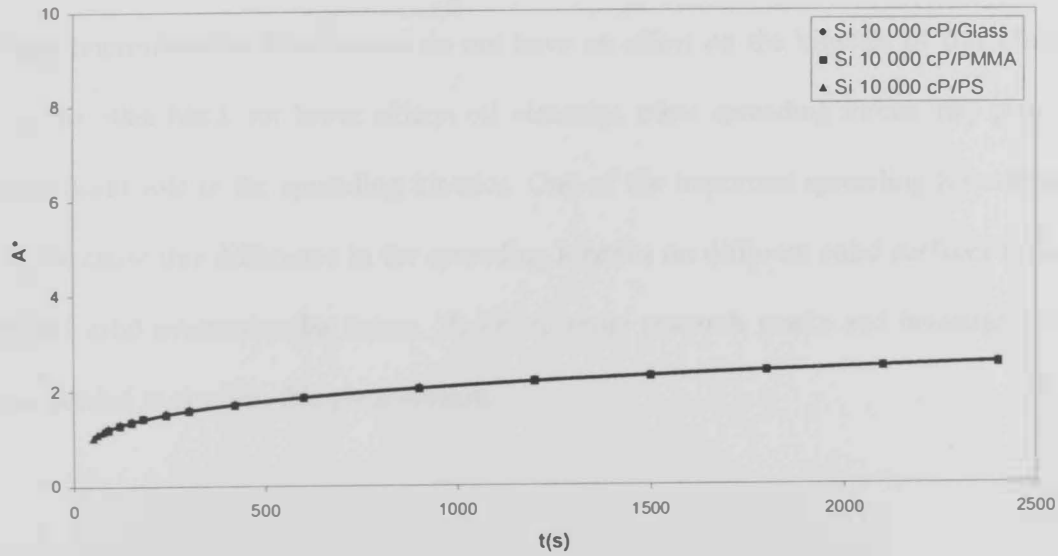

Fig. 3.35 Kinetics of spreading of 10.000 cP silicon oil on glass, PS and PMMA solid surfaces

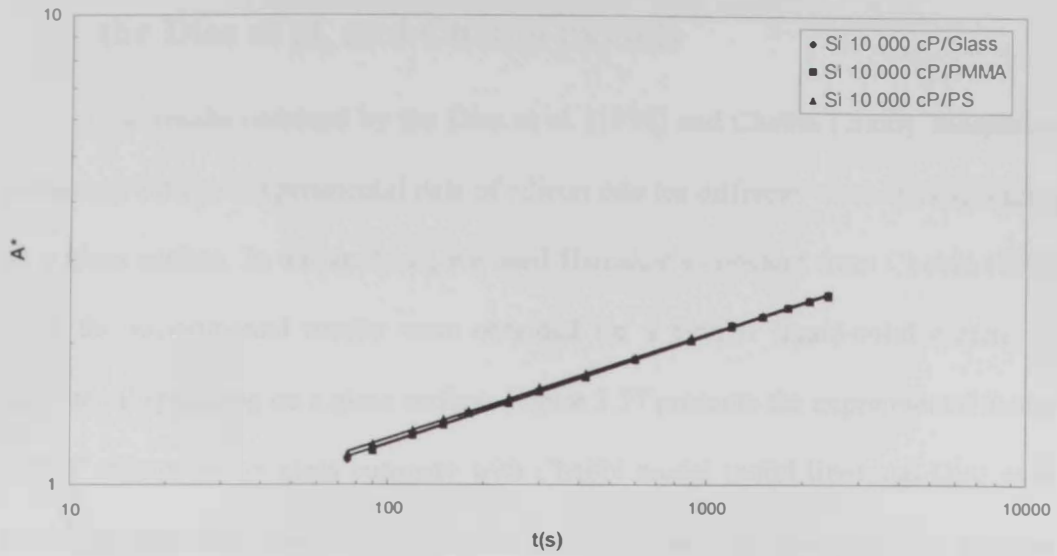

Fig. 3.36 Kinetics of spreading of 10,000 cP silicon oil on glass, PS and PMMA solid surfaces in log-log scale

Therefore, the experimental results show that the higher the silicon oil viscosity, the higher the viscous effect in the kinetics of spreading, where the liquid-solid intermolecular force seems do not have an effect on the kinetics of spreading. On the other hand, for lower silicon oil viscosity, other spreading forces may play a significant role in the spreading kinetics. One of the important spreading forces that might cause this difference in the spreading kinetics on different solid surfaces is the liquid-solid intermolecular forces. However, more research works and investigations are needed to confirm this phenomenon.

3.3 Comparison between the experimental data and model the Diez et al. and Chebbi models

The results obtained by the Diez et al. (1994) and Chebbi (2000) models are compared with our experimental data of silicon oils for different viscosities spreading on a glass surface. In our analysis, we used Hamaker's constant from Chebbi (2000) since the experimental results were obtained for a similar liquid-solid system, i.e silicone oil spreading on a glass surface. Figure 3.37 presents the experimental data of 100 cP silicon oil on glass compare with Chebbi model (solid line) and Diez et al. model (dashed line). The x-axis in Figure 3.37 represents the dimensionless time that is defined by Chebbi (2000) as

$$T = \frac{t\,\gamma}{3\,\mu\,V^{1/3}} \tag{3.14}$$

where t is the spreading time, μ is the liquid viscosity, σ is the liquid surface tension and V is the liquid drop volume. The y-axis in Figures 3.37 represents the dimensionless contact radius of the liquid drop on the solid substrate, which is defined as

$$X = \frac{R}{V^{1/3}} \tag{3.15}$$

where R is the contact radius of the liquid drop on the solid surface.

A similar analysis was carried out for 500 cP, 1000 cP, 10 000 cP silicon oils spreading on glass surface and results are presented in Figures 3.38-3.40, respectively. The comparison between the Chebbi and Diez et al. models is based on the deviation from experimental data defined as

$$\text{Percent Deviation (PD)} = \frac{|X_{model} - X_{exp}|}{X_{exp}} 100\% \tag{3.16}$$

The PD was determined for all data points for each liquid. The average value and the maximum of PD for each liquid are summarized in Table 3.3.

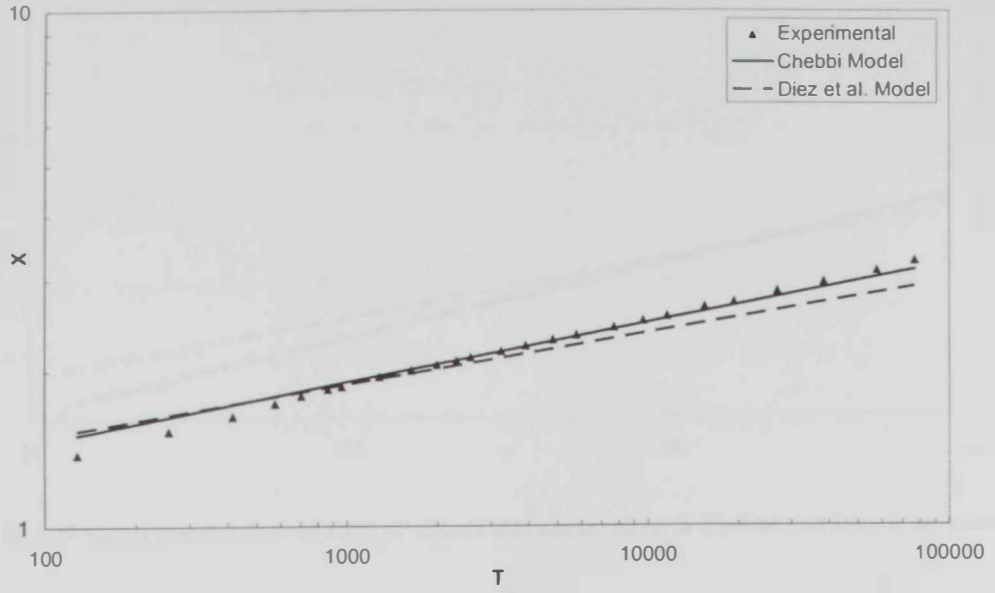

Fig. 3.37 Experimental data of 100 cP silicon oil compared with Chebbi and Diez et al. models

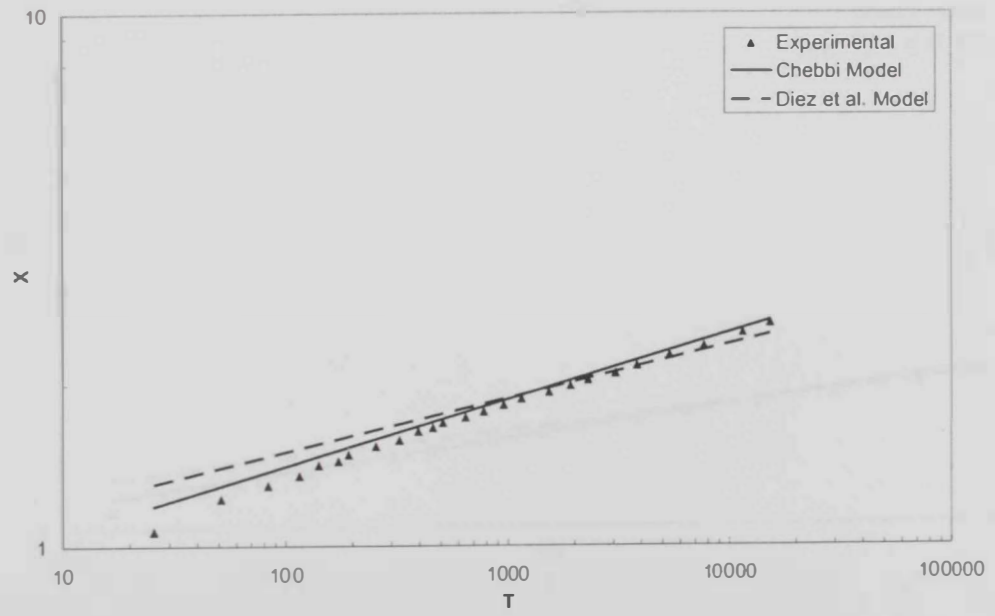

Fig. 3.38 Experimental data of 500 cP silicon oil compared with Chebbi and Diez et al. models

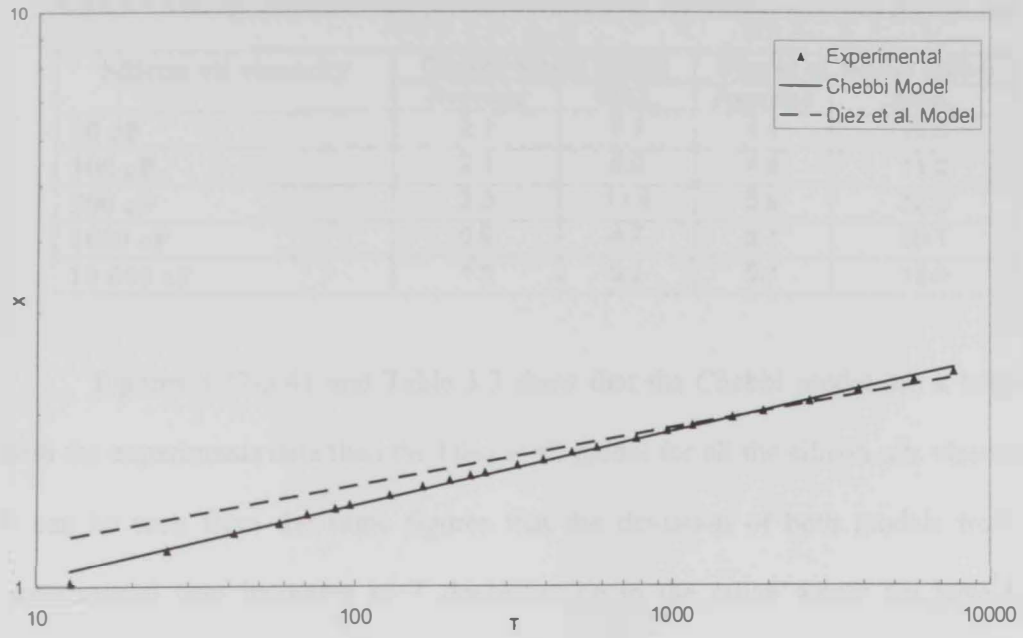

Fig 3.39 Experimental data of 1000 cP silicon oil compared with Chebbi and Diez et al. models

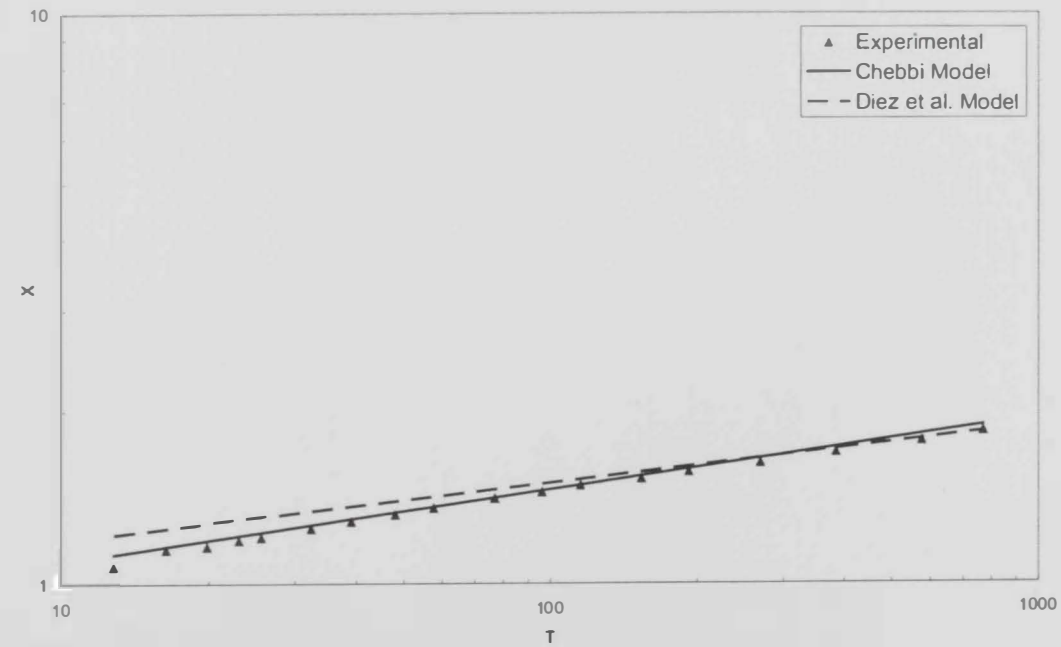

Fig 3.40 Experimental data of 10,000 cP silicon oil compared with Chebbi and Diez et al. models

Table 3.3 Average and maximum percent deviation for the Chebbi and Diez et al. models

Silicon oil viscosity	Chebbi Model (2000)		Diez et al. Model (1994)	
	Average	MAX.	Average	MAX.
50 cP	2.1	8.1	4.4	13.0
100 cP	2.1	9.0	4.8	11.2
500 cP	3.3	11.4	5.9	22.5
1000 cP	0.9	4.7	5.1	20.1
10 000 cP	1.6	5.3	5.1	13.9

Figures 3.37-3.41 and Table 3.3 show that the Chebbi model has a better fit with the experiments data than the Diez et al. model for all the silicon oils viscosities. It can be seen from the same figures that the deviation of both models from the experimental data increases as T decreases i.e in the range where we have large contact angles (first stage of spreading). This is because both models are based on a lubrication theory which is applies for small contact angle value (Deiz et al., 1994; Chebbi, 2000).

Chapter 4

Summary & Conclusions

Since the introduction of Young's equation (1805), contact angle, θ, has remained the main focus of most theoretical and experimental investigations to indicate the state wettability of vapour-liquid-solid systems. In addition, the rate of change in the contact angle has been used as the relevant parameter of spreading kinetics. However, many restrictions and difficulties are associated with contact angle measurements that are well recognized in the literature. This has led to inaccurate measurements of contact angle and interpretation. Although it may seen easy to carry out contact angle measurement, contact angle phenomena are nevertheless complicated.

Considering that the velocity of the contact line is the pertinent quantity, it is therefore reasonable to regard the change in the contact area as the flux of the process. In the first part of this thesis, a new measuring parameter for wettability was introduced based on the liquid/solid contact area. This term is called "contact ratio", A^*. The contact ratio is defined as the ratio between the spreading contact area of the liquid over solid surface to the surface area of the spherical drop before spreading. The measurements of contact areas and low rate dynamic contact angles for various liquid/solid systems were carried out using the ADSA-P technique. Liquid drop volume and solid/liquid radius were also measured by ADSA-P. Subsequently, the contact ratio was determined.

In addition to the experimental results, the published data show that there is a unique contact ratio value for a specific vapour-liquid-solid system. Furthermore, the relation between the contact angle and the contact ratio is strictly a power law relation. The theoretical relation between the contact ratio and the contact angle is based on spherical cap approximation. The results presented in this thesis show that

even at high values of contact angle, there is a good agreement between the theoretical relation and the experimental results.

Therefore it can be concluded that if the contact angle is a wettability parameter because of its unique value, hence the contact ratio may also be considered as a wettability parameter for its unique value of a specific system. Therefore, contact ratio can be presented as a new concept in measuring wettability alternative to contact angle. Moreover, contact ratio may provide a more precise measure of wettability than contact angle. In fact, experimentally, contact ratio is easier to measure and most probably more accurate than the contact angle. However further investigations for this issue are needed.

The second part of this thesis investigated the effect of viscosity on the spreading kinetics by studying the spreading kinetics of silicone oil (PDMS) liquid with various viscosities (100 cP, 500 cP, 1,000 cP, 10,000 cP) on three different types of solid surfaces namely glass, PMMA and PS. the spreading kinetics is represented by measuring the rate of change of the contact ratio. The results of the study suggest the following.

1. The lower the viscosity of the liquid, the faster the spreading. Numerically, based on the modified Tanner law, the rate of spreading was characterized by the power factor of Tanner law, n. The values of the power factor, n, for the tested systems were summarized in Table 3.2

2. The higher the silicon oil viscosity, the higher the viscous effect in the kinetics of spreading, where the liquid-solid intermolecular force seems don't have effect on the kinetics of spreading. On the other hand, for lower silicon oil

viscosity, other spreading forces might play a significant role in the spreading kinetics. One of the important spreading forces that may cause this difference in the spreading kinetics on different solid surfaces is the liquid-solid intermolecular forces. However further investigations are needed to validate this phenomenon.

3. The kinetics measurements of silicon oils with various viscosities were compared with the theoretical models of Diez et al. (1994) and Chebbi (2000). The results show that the Chebbi model fit the experimental data better than the Diez et al. model

Chapter 5

Future Work

The subject of wettability had been intensively investigated during the past century. However, the phenomena still remain ambiguous, and many fundamental issues of wettability is still questionable and require clarification. We have attempt to address some of these issue in this thesis. However, further investigation is needed to better understand the concept of contact ratio. Future work may cover some of the following issues:

1. Explore the effect of different system parameters affecting the contact angle measurements on the contact ratio. These parameters include the line tension and drop size, surface roughness and surface heterogeneity...etc. Are their effect on the contact ratio comparable to their effect on the contact angle?
2. Modify the existing theoretical models to consider contact ratio instead of contact angle.
3. Further investigations are suggested to validate the contact ratio measurements as an alternative measure of wettability to contact angle. This may include the study of different liquid/solid systems such as polymer liquids spreading on polymer solids, and other solid geometry such as powder.
4. Further investigation are suggested to validate the effect of viscosity forces compare with other forces. Develop a thermodynamic model that describes the framework of driving and resisting forces in the spreading kinetics; and test this model by applying different liquid/solid systems or specially coated solids that may have chemical resistance to the spreading kinetics.

References

1. A. R Balkenende, H. J. A. P., van de Boogaard, M Scholten and N. P. Willard, (1998), "Evaluation of Different Approaches To Assess the Surface Tension of Low-Energy Solids by Means of Contact Angle Measurements", Langmuir, 14, 5907.

2. Adamson W., (1997), "Physical Chemistry of Surfaces", 6th Ed, New York, Wiley-Interscience.

3. Alteraifi A.M and Moet A, (2004), "Is "complete spreading really complete?", Proceeding of HTFED04, ASME Heat Transfer/Fluid Engineering Summer Conference, Charlotte, North Carolina, USA.

4. Alteraifi A.M and Sasa B.J, (2003), "The role of solid substrate on the spreading kinetics of liquid droplet", Computational Method in Multiphase Flow, Santa Fe, New Mexico, USA.

5. Alteraifi A.M, Sherif D. and Moet A., (2003), "Interfacial effects in the spreading kinetics of liquid droplets on solid substrates", Journal of Colloid and Interface Science, 264, Issue 1, 221-227.

6. Amirfazli A., (2001), "Drop Size Dependence of Contact Angles and Line Temsion", PhD Thesis, University of Toronto.

7. Amirfazli A., and Neumann A.W., (2004), "Status of the Three-Phase Line Tension: a Review", Advance Colloid Interface Science, 110, 121-141.

8. Amirfazli A., Kwok D.Y., Gaydos J., Neumann A.W., J. Colloid Interface Sci. 205 1998 1.

9. Ashleya K, Meredithb J, Eric A, Raghavana D and Karnic A, (2003), "Combinatorial investigation of dewetting: polystyrene thin films on gradient hydrophilic surfaces", Polymer, 44, 769–772.

10. Barthlott W and Neinhuis C, (1997) B, "Purity of the sacred lotus, or escape from contamination in biological surfaces, Annals of Botany, 79, 667-677.

11. Berg J.C, (1993), "Wettability", Surfactant Science Series, 49, Marcel Dekker Inc., New York.

12. Boruvka, L. and Neumann, A.W., (1977), "Generalization of the Classical Theory of Capillarity", Journal of Chemical Physics . 66, 5464-5476.

13. Brochard-Wyart F. and de Gennes P. G., (1992), "Dynamics of partial wetting", Advances in Colloid and Interface Science, 39, 1-11.

14. Cassie A.B.D., Baxter S., (1944), "Wettability of porous surfaces", Transactions of the Faraday Society, 40, 546 – 551.

15. Cassie, A. B. D., (1948), "Contact Angels", Discussions of the Faraday Society, 3, 11-16.

16. Lam C.N., (2001), "A study of advancing & receding contact angles and contact angle hysteresis", Master thesis, University of Toronto.

17. Chandra S, di Marzo M, Qiao Y and Tartarini P, (1996), " Effect of Liquid – Solid Contact Angle on Droplet Evaporation", Fire Ssafety Journal, 27, 141-158.

18. Chao D and Zhang N, (2001), " New Method Developed to Measure Contact angle of Sessile Drop", R&T 2001 Research and Technology, 188-189.

19. Chebbi R. and Selim M. S., (1997), "Capillary Spreading of Liquid Drops on Solid Surfaces", Journal of Colloid and Interface Science, 195, Issue 1, 66-76.

20. Chebbi R., (2000), "Dynamics of Wetting", Journal of Colloid and Interface Science, 229, Issue 1, 155-164.

21. Chen J. and Wada N., (1992), "Edge profiles and dynamic contact angles of a spreading drop", Journal of Colloid and Interface Science, 148, Issue 1, 207-222.

22. Chen K.H. and Wilcox W.R., (1977) "Anomalous influence of body force on trapping of foreign particles during solidification", Journal of Crystal Growth, 40, Issue 2, 214-220.

23. Cheng P., (1990), PhD Tthesis, University of Toronto.

24. Cheng P., Li D., Boruvka L, Rotenberg Y. and Neumann A. W., (1990), " Automation of axisymmetric drop shape analysis for measurements of interfacial tensions and contact angles", Colloids and Surfaces, 43, Issue 2, 151-167.

25. Crafton E. F. and Black W. Z., (2004), "Heat transfer and evaporation rates of small liquid droplets on heated horizontal surfaces.", International Journal of Heat and Mass Transfer, 47, Issues 6-7, 1187-1200.

26. de Coninck J., de Ruijter M. J. and Voué M, (2001), "Dynamics of wetting" Current Opinion in Colloid and Interface Science, 6, Issue 1, February 2001, 49-53.

27. de Gennes P.G, (1985), "Wetting: static and dynamics", Review of Modern Physics, 57, (3), Part I, 827-863.

28. de Ruijter M , Kolsch P, Voue M, De Coninck J and Rabe J, (1998), "Effect of temperature on the dynamic contact angle", Colloids and Surfaces -A, 144, 235-243.

29. Decker E. L. and Garoff S, (1996), "Using vibrational noise to probe energy barriers producing contact angle hysteresis", Langmuir, 12, 2100-2110.

30. Derjaguin B., Muller V. and Toporov Yu., (1980), "On different approaches to the contact mechanics", Journal of Colloid and Interface Science, 73, Issue 1, 293-294.

31. Diez J. A., Gratton R., Thomas L. P. and Marino B., (1994) "Laplace pressure driven drop spreading", Phys. Fluids 6, 24.

32. Drummond C. and Israelachvili J, (2002), "Surface forces and wettability", Journal of Petroleum Scince & Engineering, 33, 123-133.

33. Duncan D., Li D., Gaydos J., Neumann A.W., J. Colloid Interface Sci. 169 1995 256.

34. Dussan V. EB., (1979), "On the spreading of liquids on solid surfaces: static and dynamic contact lines.", Annual Review of Fluid Mechanics. 11:371-400.

35. Elschenbroich C and Salzer A, (1992), Organometallics A Concise Introduction, 2nd Ed, 101-111, New York: VCH.

36. Extrand C. W., (1993), "Spontaneous Spreading of Viscous Liquid Drops", Journal of Colloid and Interface Science, 157, Issue 1, 72-76.

37. Fay J.A., (1969), "The spread of Oil Slicks on a Calm Sea." In: Oil on the Sea, (Hoult, D.P., ed.), Plenum Press, NY, 53-63.

38. Fogden A. and White L. R., (1990), "Contact elasticity in the presence of capillary condensation : I. The nonadhesive Hertz problem", Journal of Colloid and Interface Science, 138, Issue 2, 414-430.

39. Fowkes F. M., (1964), "Attractive forces at interfaces.", Industrial Engineering Chemistry. 56:40-52.

40. Frohn A. and Roth N, (2000), "Dynamics of Droplets", Berlin: Norbert-Roth.

41. Fuerstenau D.W., Diao J. and Hanson J. S., (1990), "Estimation of the Distribution of Surface Sites and Contact Angles on Coal Particles from Film Flotation Data.", Energy and& Fuels, 4, 34-37.

42. Gu Y. and Li D., (1998), "A model for a liquid drop spreading on a solid", surface Colloids and Surfaces A: Physicochemical and Engineering Aspects, 142, Issues 2-3, 243-256.

43. Guermeur R., Biquard F. and Jacolin C., (1985), "Density profiles and surface tension of spherical interfaces. Numerical results for nitrogen drops and bubbles", The Journal of Chemical Physics, 82, Issue 4, 2040-2051.

44. Hall R. O. A., Mortimer M. J., and Mortimer D. A., (1987), "Surface Energy Measurements on UO2", A Critical Review, J. Nucl Mater. 148, 237-256.

45. Hardy W.B, (1919), "Spreading of liquids on glass", Phil. Magazine, 38, 49.

46. He B., Lee J. and Patankar N. A., (2004), "Contact angle hysteresis on rough hydrophobic surfaces", Colloids and Surfaces A: Physicochemical and Engineering Aspects, 248, Issues 1-3, 101-104.

47. Hervet, H. and de Gennes, P. G., (1984), "The dynamics of wetting: precursor films in the wetting of 'dry' solids", C. R. Acad. Science, 299 II, 499.

48. Hoffman R., (1975), "A study of the advancing interfaces", J. Colloid and Interface Science, 50, pp. 228-241.

49. Kasemo B, (2002), "Biological Surface Science", Surface Science, Issues 1-3, 500, 656-677.

50. Kwok D. Y. H., (1998), "Contact Angels and Surfaces Energetics", PhD Thesis, University of Toronto.

51. Kwok D. Y., Lam C. N. C., Li A., Leung A., Wu R., Mok E. and Neumann A. W., (1998b), "Measuring and interpreting contact angles: a complex issue", Colloids Surfaces A: Physicochem. Eng. Aspects, 142, 219-235.

52. Kwok D. Y., Lam C. N. C., Li A., Zhu K., Wu R. and Neumann A. W., (1998d), "Low-rate dynamic contact angles on polystyrene and the determination of solid surface tensions", Polymer Engineering and Science., 38, 1675-1684.

53. Kwok D. Y., Leung A., Lam C. N. C., Wu R. and Neumann A. W., (1998c), "Low-rate dynamic contact angles on poly(methyl methacrylate) and the determination of solid surface tensions", J. Colloid Interface Sci., 206, 44-51.

54. Kwok D. Y., Li A. and Neumann A. W., (1999a), "Low-rate dynamic contact angles on poly(methyl methacrylate/ethyl methacrylate, 30/70) and the determination of solid surface tensions", J. Polym. Sci. B: Polym. Phys., 37(16), 2039-2051.

55. Kwok D. Y., Li A., Lam C. N. C., Leung A. and Neumann A. W., (1998a), "Low-rate dynamic contact angles on non-inert poly(propene-alt-N-(n-alkyl)maleimide) copolymers by axisymmetric drop shape analysis", Langmuir, 14, 2221-2224.

56. Kwok D. Y., Li A., Lam C. N. C., Wu R., Zschoche S., Pöschel K., Gietzelt T., Grundke K., Jacobasch H.-J. and Neumann A. W., (1999b), "Low-rate dynamic contact angles on poly(styrene-(hexyl/10-carboxydecyl 90:10)maleimide) and the determination of solid surface tensions", Macro. Chem. Phys., 200(5), 1121-1133.

57. Lelah M and Marmur A, (1981), "Spreading of kinetics of drops on glass", J. Colloid and Interface Science, 82, 518-525.

58. Li D. and Neumann A. W., (1992), "Contact angles on hydrophobic solid surfaces and their interpretation", Journal of Colloid and Interface Science, 148, Issue 1, 190-200.

59. Li D., (1991), PhD Thesis, University of Toronto.

60. Li D., Xie M. and Neumann A. W., (1993), "Vapour Adsorption and Contact Angles on Hydrophobic Solid Surfaces". Colloid and Polymer Science, 271, 573-580.

61. Lopez, J., Miller, C. A., and Ruckenstein, E., (1976), "Spreading kinetics of liquid drops on solids", J. Colloid Interface Science. 56, 460.

62. Marmur A., (1983). "Equilibrium and spreading of liquids on solid surfaces", J. Colloid and Interface Science, 19, 75-102.

63. Marmur A., (1994), "Contact Angle Hysteresis on Heterogeneous Smooth Surfaces", Journal of Colloid and Interface Science, 168, Issue 1,40-46

64. Marmur A., (1996), "Equilibrium contact angles: theory and measurement", Colloids and Surfaces A: Physicochemical and Engineering Aspects, 116, Issues 1-2, 55-61.

65. Matijevic E., (1969), "Surface and Colloid Science", John Wiley & Sons, USA.

66. Matyushov D. V. and Schmid R., (1996), "Calculation of Lennard-Jones energies of molecular fluids", Journal of Chemical Physics. 104, 8627-8638.

67. Miracle-Solé S., (2002), "Rigorous results on wetting, rough and heterogeneous substrates, Physica A: Statistical Mechanics and its Applications, 314, Issues 1-4, 299-303.

68. Myers D, (1999), "Surface Interfaces and Colloids", John Wiley & Sons, USA

69. Neumann A. W. and Good R. J., (1972), "Thermodynamics of contact angles. I. Heterogeneous solid surfaces ", Journal of Colloid and Interface Science, 38, Issue 2, 341-358.

70. Neumann A. W., (1962), Thesis, Mainz.

71. Neumann A. W., (1974), "Contact angles and their temperature dependence: thermodynamic status, measurement, interpretation and application", Advances in Colloid and Interface Science, 4, Issues 2-3, 105-191.

72. Neumann A. W., Good R. J., Hope C. J. and Sejpal M., (1974), "An equation-of-state approach to determine surface tensions of low-energy solids from contact angles ", Journal of Colloid and Interface Science, 49, Issue 2, 291-304

73. Ogarev V; Timonina T; Arslanov V and Trapeznikov A, (1974), "Spreading of polydimethylsiloxane drops on solid horizontal surfaces", Journal of Adhesion, 6, 337-355

74. Oliver J. F. , Mason S. G., (1980), "Liquid spreading on rough metal surface", J. Mater. Science, 59, 431 – 437.

75. Oliver J.F., Huh C., Mason S.G., J. Colloid Interface Sci. 93 1983 169.

76. Pashley R. M., McGuiggan P. M., Horn R. G. and Ninham B. W., (1988), "Forces between bilayers of cetyltrimethylammonium bromide in micellar solutions", Journal of Colloid and Interface Science, 126, Issue 2, 569-578.

77. Reid R, Prausnitz J and Poling B, (1987), "The properties of gases and liquids", 4th edition, McGraw-Hill Inc.

78. Rotenberg Y., (1983), PhD Thesis, Unversity of Toronto.

79. Rotenberg Y., Boruvka L. and Neumann A. W., (1983), "Determination of surface tension and contact angle from the shapes of axisymmetric fluid interfaces", Journal of Colloid and Interface Science, 93, Issue 1, 169-183.

80. Sasa B. J., (2003), "The Role of the Solid Substrate on the Sspreading Kkinetics of a Liquid Ddroplet.", Master Tthesis, United Arab Emirates University.

81. Schlangen Luc J, (1996), "Adsorption and wetting: experiments, thermodynamics and molecular aspects", PhD Thesis, The Wageshningen University

82. Schonhorn H, Frisch H , and Kwei T, (1966), "Kinetics of wetting of surfaces by polymer melts" , J. Appl. Physics, 37, Pg. 4967-4973.

83. Seaver, A, and Berg, J, (1994), "Spreading of droplet on solid surface", J. Applied Polymer Science, 52, 431-435.

84. Shaw D, (1992), Colloid & surface Chemistry, Butterworth- Heinemann OXFORD

85. Skinner F. K., Rotenberg Y. and Neumann A. W., (1989), "Contact angle measurements from the contact diameter of sessile drops by means of a modified axisymmetric drop shape analysis", Journal of Colloid and Interface Science, 130, Issue 1, 25-34.

86. Spelt, J. K., (1985), PhD Thesis, University of Toronto.

87. Starov V. M., Kalinin V. V. and Jing-Den Chen, (1994), "Spreading of liquid drops over dry surfaces", Advances in Colloid and Interface Science, 50, 13, 187-221.

88. Sullivan D. E., (1981), "Surface tension and contact angle of a liquid–solid interface.", J. Chem. Phys. 74, 4, 2604.

89. Tanner L. H, (1979), "The spreading of silicone oil drops on horizontal surfaces", J. Applied Physics, 12, 1473-1484.

90. Turunen M., (2004), "Interfacial Compatibility of Polymer-Based Structure in Electronics.", PhD Thesis, Helsinki University of Technology.

91. Valignat M, Voue M, Oshanin G and Cazabat A.M., (1999), "Structure and dynamics of thin liquid films on solid substrates", Colloids and Surfaces A: Physicochem. Eng. Aspects, 154, 25–31.

92. van den Doel L.R., Young I.T., and Van Vliet L.J, (1999). "Monitoring the evaporation process of liquid samples in sub-nanoliter vials" ASCI'99, Proc. 5th Annual Conference of the Advanced School for Computing and Imaging (Heijen, NL, June 15-17), ASCI, Delft, 58-64.

93. van Giessen A. E., Bukman D. J and Widom B., (1997), "Contact Angles of Liquid Drops on Low-Energy Solid Surfaces", Journal of Colloid and Interface Science, 192, Issue 1, 257-265.

94. van Oss C. J. , Chaudhury M. K. , Good R. J., (1988), "Interfacial Lifschitz-van der Waals and polar interactions in macroscopic systems", Chem. Rev., 88, 927–941.

95. Van Remoortere P., and Joos B., (1993), "About the Kinetics of Partial Wetting", Journal of Colloid and Interface Science, 160, Issue 2, 387-396.

96. Vargha-Butler E. I., Moy E. and Neumann A. W., (1987), "Sedimentation behaviour of low surface energy powders in different non-polar liquid systems.", Colloids and Surfaces, 24, Issue 4, 315-324.

97. Website 1. http://www.chemfinder.com.

98. Website 2. http://www.sabreen.com/surface_wetting.htm.

99. Website 3. http://www.solgel.com/articles/June00/Birch/cleaning4.htm.

100. Wenzel, R. N. (1936), "Resistance of solid surfaces to wetting by water", Industrial and Engineering Chemistry, 28, 988-994.

101. Yang L.J, Yao T.J, Huang Y.L, Xu.Y and Yu-Chong Tai, (2002), "Marching Arching Velocity of Capillary Meniscuses in Microchannels", Fifteenth IEEE

International Conference on Micro Electro Mechanical Systems (MEMS '02), Las Vegas, USA, Jan. 20-24.

102. Young T., (1805), "An Essay on the Cohesion of Fluids", Philosophical Transactions of the Royal Society of London, 95, 65-87.

103. Zhang N and Chao D, (2001), "Flow Visualization in Evaporating Liquid Drops and Measurement of Dynamic Contact Angles and Spreading Rate". Journal of Flow Visualization and Image Processing, vol. 8, issue 3, Nov, Pg. 303–312.

104. Zhao Q., Liu Y. and Abel E.W., (2004), "Effect of temperature on the surface free energy of amorphous carbon films", Journal of Colloid and Interface Science, 280, Issue 1, 174-183.

105. Zisman W, (1964), "Contact angle, wettability and adhesion", Advances in Chemistry Series, No. 43, ACS, Washington D.C., 1.

106. Zografi G. and Johnson B. A., (1984), "Effects of surface roughness on advancing and receding contact angles", International Journal of Pharmaceutics, 22, Issues 2-3, 159-176.

كيناتيكية الانتشار لسائل يدعى"silicon oils" باستخدام قيم مختلفة للزوجة (500cP,100cP 1000 cP, 10,00 cP). لقد تم دراسة الانتشار على ثلاثة أنواع من السطوح الصلبة و هي glass, PS, PMMA. استخدم في هذه الدراسة حجم ثابت للسائل قيمته 1.5 ميكروليتر. و تمت مقارنة النتائج بنموذجين نظريين و هما نموذج Chebbi و نموذج .Diez et al. النتائج أظهرت انه كلما قلت قيمة لزوجة السائل زادت سرعة الانتشار. كلما زادت قيمة لزوجة السائل قوى الزوجة تصبح أكثر فعالية و ان القوى البين الجزئيان يبدو أنها ليس لها تأثير على كيناتيكية الانتشار. و أظهرت النتائج أيضا أن نموذج Chebbi أفضل من نموذج .Diez et al. و أخيرا أن موضوع هذا البحث مهم لكثير من التطبيقات مثل المواد المركبة و الطلاء المواد الطبية و تطبيقات كثيرة أخرى.

دراسة العمليات العمليات الكيناتيكية للقطرة على السطوح الصلبة باستخدام أسلوب جديد: النسب السطحية

الخلاصة

بالرجوع إلى معادلة "ينغ", فان زاوية التماس و الشد السطحي للسائل هما العاملين الوحيدين الذي يمكن قياسهما بواسطة التجارب العملية. زاوية التماس تعتبر خاصية ديناميحرارية لذا زاوية التماس استخدمت و ما زالت تستخدم في كل الدراسات المتعلقة في انتشار السوائل على السطوح الصلبة. معدل التغير في زاوية التماس استخدم في دراسة ديناميكية الانتشار على الرغم من الصعوبات المرافقة لقياس زاوية التماس. اذا اعتبرنا سرعة خط التماس عامل مهم في عملية الانتشار فمن المنطقي اعتبار التغير في مساحة التماس كعامل يعبر عن عملية الانتشار. لقد تم حديثا إيجاد علاقة بين مساحة التماس و زاوية التماس باستخدام علاقة تقريبية تسمى "سفيريكال كاب". لقد قمنا بإيجاد معامل جديد لقياس عملية الانتشار و هو يعتمد على المساحة التلامسية بين السائل و الصلب و يسمى النسب التلامسية أو النسب السطحية. النسب السطحية عبارة النسبة بين المساحة السطحية بين السائل و الصلب و المساحة السطحية للقطرة الكروية للسائل قبل الانتشار. قياس نصف القطر التلامسي و زاوية التلامس تم بواسطة تكنيك يسمى ADSA. باستخدام قيمة النصف القطر التلامسي يمكن إيجاد قيمة النسبة التلامسية. العلاقة بين النسبة التلامسية و زاوية التماس التي تعتمد على العلاقة التقريبية " سفيريكال كاب" أظهرت تطابق جيد بين القيم النظرية و القيم الماسة عمليا حتى للقيم الكبيرة لزاوية التماس. نظرا زاوية التماس تعتبر أداة قياس لعملية الانتشار لنظام معين لان لها قيمة واحدة لهذا لنظام. و على هذا الأساس يمكن اعتبار النسبة التلامسية أداة قياس لعملية الانتشار لنظام معين لان لها قيمة واحدة لهذا لنظام. لقد تم أيضا دراسة

جامعة الإمارات العربية المتحدة
عمادة الدراسات العليا
برنامج ماجستير علوم المواد

دراسة العمليات الكيناتيكية للقطرة على السطوح الصلبة باستخدام أسلوب جديد: النسب السطحية

رسالة مقدمة من الطالب:

عبدالحفيظ "محمد عدنان" الحرباوي

الى جامعة الإمارات العربية المتحدة
استكمالا لمتطلبات الحصول على درجة الماجستير في علوم و هندسة المواد

2004 - 2005